El Niño amplified food insecurity in early modern Europe

Emile Esmaili*[1], Michael J. Puma†[1,2], Francis Ludlow[3], Eva Jobbová[3], Janavi Kumar[1], Poul Holm[3], Fredrik Charpentier Ljungqvist[4,5], John Alphonsus Matthews[6], Johannes Rom Dahl[3], and Andrea Seim[7,8,9]

[1]Center for Climate Systems Research, Columbia Climate School, Columbia University, United States
[2]NASA Goddard Institute for Space Studies, United States
[3]Trinity Centre for Environmental Humanities, Trinity College, Dublin, Ireland
[4]Department of History, Stockholm University, Stockholm, Sweden
[5]Bolin Centre for Climate Research, Stockholm University, Stockholm, Sweden
[6]Institute of History and Archaeology, University of Tartu, Estonia
[7]Chair of Forest Growth and Dendroecology and Chair of Forest History, Institute of Forest Sciences, University of Freiburg, Germany
[8]Department of Botany, University of Innsbruck, Austria
[9]Regional Climate Group, Department of Earth Science, University of Gothenburg, Sweden

The El Niño–Southern Oscillation (ENSO) is a dominant source of global inter-annual climate variability, yet its long-term influence on food security remains poorly understood. Drawing on a recently compiled dataset of 160 European famines and a new high-resolution ENSO reconstruction, we show a robust correspondence between positive ENSO anomalies (El Niño events) and subsistence crises during the early modern period (1500–1800). These anomalies increased the probability of famine onset in Central Europe – the European region that we find most teleconnected with ENSO variability – where we estimate that more than 40% of famine onsets are associated with El Niño events. To explain this finding, we establish a pathway in which positive ENSO anomalies are revealed (1) to be associated with excessive summer wetness and (2) consequently reduced grain harvests. We further show that ENSO effects on famine duration were even more widespread: El Niño events increased the annual likelihood of famine persistence by 24% in all nine European regions for which data are available. To explain this finding, we study grain price data and show that ENSO-induced climate variability drove grain prices up by 6.5% after one year – even in non-teleconnected locations. We posit that this outcome is consistent with significant market integration that allowed climate-related shocks to propagate across the continent. We further show that these grain price shocks spilled over to other subsistence goods, such as fish, an effect we attribute to demand substitution given the lack of apparent ENSO influence on European and North Atlantic marine environments. Collectively, these results provide novel and robust evidence for the influence of mechanisms of global climate variability on regional food security during the early modern period in Europe.

This is a non-peer-reviewed preprint submitted to EarthArXiv. It has been submitted to a peer-reviewed journal, but has yet to be formally accepted.

*Corresponding author: ee4561@princeton.edu – Current affiliation: Center for Policy Research on Energy and the Environment, Princeton University
†Corresponding author: mjp38@columbia.edu

1 Introduction

Early modern Europe (c. 1500–1800) experienced large-scale political, socioeconomic, and cultural transformations[1] that occurred in tandem with the climatic cooling of the Little Ice Age[2, 3]. In particular during the late 16th century and throughout much of the 17th century, many parts of Europe endured repeated famines[4, 5, 6]. These subsistence crises occurred despite advances in agriculture and food trade networks that should (in theory) have bolstered food security[7], although frequent large-scale wars likely weakened the effects of this progress (see Parker [8]). While social and political events, not least warfare, can credibly explain some of these famines, it is clear that consecutive years of adverse climatic conditions for agriculture also played an important role in famine causation in strongly grain-dependent pre-industrial Europe[9, 10]. Cold and late springs followed by excessively wet and cold summers constituted the major climatic threat to food production in Northern and Central Europe, whereas droughts posed a relatively greater threat in the Mediterranean region[11, 2, 10]. While the proximate meteorological contributions to European famines have been documented[4], there is a significant knowledge gap on the ultimate causal role of global-scale modes of climatic variability on the onset and duration of these famine episodes. The role of the El Niño–Southern Oscillation (ENSO) has been particularly overlooked in analyses of European food security and famine history.

ENSO is a main driver of global inter-annual climate variability, with profound effects on weather patterns that influence socio-economic conditions across diverse regions globally[12, 13]. Its contemporary impacts have been extensively studied in tropical and subtropical regions, where it modulates precipitation and temperature patterns, promoting droughts, floods, and other extreme weather events[14, 15]. These events have significantly affected economies[16], agriculture and food security[17, 18, 19, 20], and potentially increased civil conflict probability[21]. ENSO effects on temperature and precipitation patterns are particularly pronounced in large parts of Africa, Australia, North and South America, but its influence also extends globally through long-distance climatic “teleconnections" [22] (significant links between weather phenomena at widely separated locations on Earth)[23]. For Europe, the contemporary influence of ENSO on precipitation is subject to ongoing study[24], and recent work shows that ENSO strongly modulates the leading mode of European summer rainfall variability, producing a dipole pattern with drier (wetter) conditions in northern (southern) Europe[25]. The influence of ENSO teleconnections on pre-industrial European climate remains, however, largely unexplored.

The effects of ENSO on pre-industrial food security also remain understudied, despite dramatic examples of how particular historical El Niño events disrupted harvests. For instance, the El Niño anomaly of 1788–1793 weakened monsoon rainfall in India, promoting widespread crop failures and triggering a series of notable and far-reaching societal disruptions across multiple world regions, including conjectured links to the French Revolution (1789)[26, 27]. Qualitative studies have also documented links between extreme El

Niño events and catastrophic 19th-century famines in South Asia, East Asia, and South America, while also highlighting the mediating role of governance failures and exploitative trade systems that restricted access to locally grown grain by the poor[20]. However, there is a notable lack of quantitative research examining whether ENSO acted as a more systemic influence in societal and economic disruptions over longer time periods.

This study presents novel quantitative evidence of ENSO impacts on food security in early modern Europe. Using extensive data compiled by historians since the late 19th century, we demonstrate that positive ENSO anomalies (including major El Niño events) increased the probability of famine onsets in Central Europe, where we estimate it contributed to the onset of over 40% of the famine episodes, whereas elsewhere in Europe the influence of ENSO can be seen in extending the duration of existing famines. To explain these findings, we establish a plausible causal pathway along which ENSO impacted food security. Specifically, we show that ENSO variability can be detected in (1) European soil moisture and precipitation patterns, (2) grain harvests and, ultimately, (3) grain and fish prices.

Research on the early modern climate–food security nexus has focused primarily on grain harvests and trade, often overlooking other climate-sensitive components of the food system, such as marine food sources, which have been historically integral to subsistence and trade[28]. Thus, we also explore the effects of ENSO on fish prices and observe a notable response that suggests a demand-side substitution effect on fish prices driven by terrestrial crop failures, rather than a supply-side response in which fish prices are driven by catch variation under the influence of ENSO. By delineating these pathways of effect, we advance understandings of how global-scale modes of climate variability shaped food systems and livelihoods in early modern Europe.

2 Results

To examine the role of ENSO in early modern European subsistence crises, we treat it as an exogenous and unpredictable source of short-term climate fluctuations. Rather than confine our attention to severe El Niño events, we focus on how continuous and plausibly random ENSO variability influenced European climate, harvests, and prices, thereby contributing to subsistence crises. For this, we use a novel tree-ring-based reconstruction of sea surface temperatures across the equatorial Pacific by Cook and Cane [29]. From this reconstruction, we capture ENSO by deriving the NINO3.4 index, defined as the average sea surface temperature (SST) anomaly in region 5°N–5°S, 170°W–120°W, relative to a 1801–1900 reference period. NINO3.4 is the most widely used proxy for identifying El Niño conditions, conventionally defined as positive SST anomalies that lie above a given threshold. In our analysis, we use "El Niño" and "positive ENSO anomalies" interchangeably, while noting that the standard threshold-based definition may be less relevant in a

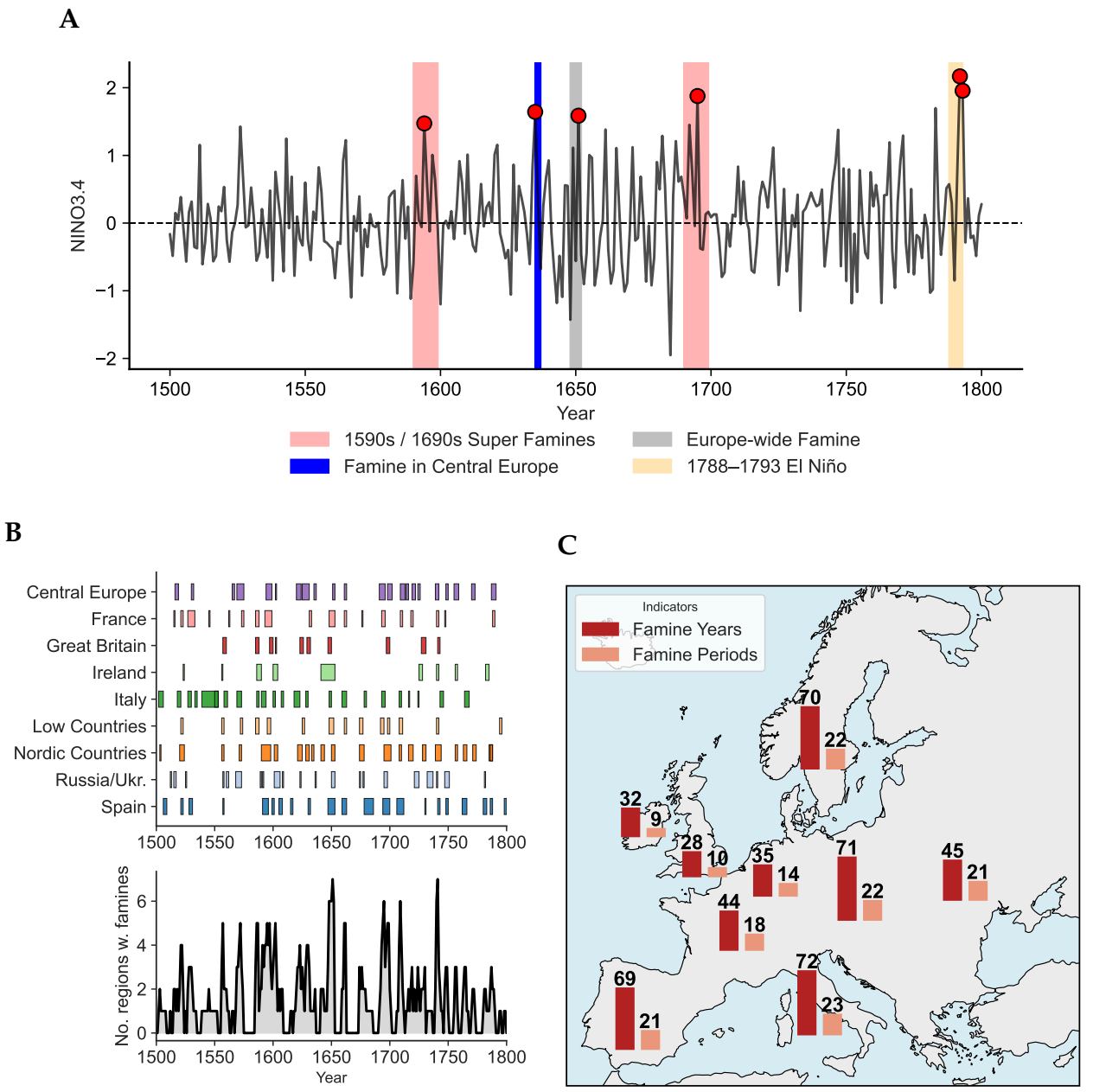

Figure 1: **ENSO and famines in early modern europe. (A)** ENSO index (NINO3.4 Region SST anomalies relative to the 1801–1900 mean), with extreme values (red dots) linked to key societal crises (pink: 1590s and 1690s Super Famines; blue: 1635–36 Famine in Central Europe; grey: 1647–1652 Europe-wide Famines). Additionally, the strongest El Niño events from the 1500–1800 period (yellow shading) are highlighted. **(B)** The top panel presents famine periods across different regions. Each horizontal bar represents a continuous famine episode within a given region, spanning from the estimated onset year to its termination. The bottom panel shows the annual number of concurrent famine years aggregated across all regions. **(C)** Map of all nine regions covered by the Ljungqvist et al. [6] famine data. Number of famine periods (red bars) and total years spent in famines (orange bars) within each region (bars located in the center of each region).

long-term historical context. Alternative ENSO indices are explored in robustness checks (Supplementary I).

We first pair this ENSO reconstruction with a compilation of famine years across nine European regions published in Ljungqvist et al. [6]. Figure 1 highlights the main variables of interest by depicting famine onset (timing) and duration in relation to ENSO anomalies. This suggests that peak El Niño events closely coincided with many famine periods.

2.1 ENSO Linked to the Onset of Famine Periods in Teleconnected Regions

We find that El Niño events were statistically significantly associated with famine onsets in Central Europe (Figure 2A,B), where we estimate that a $+1\,^{\circ}\mathrm{C}$ ENSO anomaly was on average associated with a 6.9 percentage point (95% confidence interval [CI]: [1.7, 12.0]) increase in the probability of famine onsets. We derive our estimate from a linear probability model with region and decade fixed effects that isolates the plausibly causal impact of ENSO, removing the influence of region and decade-specific unobservables. This approach, motivated by the recent climate impacts literature (see [30] for a review), rests on the assumption that year-to-year climate variability is "as good as randomly assigned" once decade- and region-specific factors are removed–an assumption particularly well justified for ENSO, whose onset remains unpredictable at annual scales [31].

Our estimate remains largely unchanged when controlling for other potential influences on famine onset, namely European conflict severity and regional climate conditions. Specifically, we extend the model to condition on the yearly number of ongoing wars and conflict-related fatalities from the Conflict Catalog [32], which provides a comprehensive record of armed conflicts since antiquity; seasonal temperature and precipitation (November-–February and April-–July) from the ModE-RA reanalysis [33], a global state-of-the-art reanalysis of monthly climate variables; and June-–August soil moisture from the Old World Drought Atlas [34], a tree-ring-based reconstruction of the self-calibrating Palmer Drought Severity Index (scPDSI), used to infer past hydroclimate variability in Europe.

Despite the strong association between ENSO and famine for Central Europe, we do not find any statistically significant association for other specific regions or for Europe when treated as a single entity (see additional results in Supplementary C). To further assess whether the observed association for Central Europe is spurious, we therefore use a falsification approach (Supplementary I.4) in which we replace the observed ENSO values with fully randomized, false ENSO histories. No systematic relationship with famine onsets in Central Europe emerges: only 0.2% of our 10,000 false histories yield an equally or more extreme estimate, ruling out a spurious correlation with Central European famine onsets.

Machine Learning Attribution of ENSO-related Famines We next aim to identify which Central European famines were triggered by ENSO conditions. Our fixed-effects regression framework (above), while establishing robust associations between ENSO and famine onsets, is able to predict only one of the 22 historical famine events in-sample. This limited predictive power diminishes its usefulness for robust attribution. To address this gap, and in line with recent calls to integrate causal inference with predictive approaches [35], we employ a machine learning classifier (see Methods 4.2). The model conditions on ENSO alongside conflict, temperature, precipitation, and soil moisture (scPDSI) to classify each year as a famine onset or not. The classifier not only perfectly predicts famine onsets in-sample (100% accuracy) but also maintains near-perfect performance under cross-validation (Figure 2E), supporting its relevance for attribution.

We then leverage the model to perform a counterfactual simulation, allowing us to directly quantify the contribution of ENSO to historical famines in Central Europe. Specifically, by comparing the famine onsets under the observed ENSO conditions with counterfactual famine onsets under a scenario in which positive ENSO anomalies during such onset years are manually set to neutral (Figure 2C), we can identify which famines are attributable to ENSO variability. This counterfactual analysis suggests that nine of the 22 recorded famine periods in Central Europe for the study period can be directly linked to ENSO variability, representing over 40% of the famines for the period. This shows that while El Niño events were certainly not the sole cause, just under half of recorded famine events were associated with (at least partially triggered by) ENSO.

To assess the sensitivity of our estimate to different predictor choices, we re-tune the algorithm on restricted predictor sets. Across these specifications, the estimated attribution of El Niño ranges from five to nine famine onsets, corresponding to 23–40% of all observed Central European famine events (Supplementary C). The feature importance scores (Figure 2D), used to estimate which predictors were the most influential in the model's predictions, highlight ENSO and June–August soil moisture (scPDSI) as the most important predictors, confirming ENSO's importance in predicting onsets accurately and pointing to possible soil-moisture teleconnections.

Impact of ENSO on European climate and grain harvests While ENSO's contemporary global climatic impacts are well-documented [36][37][38], its historical association with European hydroclimate (precipitation and soil moisture) is underexplored. We identify potential teleconnections by correlating (Pearson's r) the ENSO time-series with grid-point-level time series of April–July precipitation and scPDSI (data described earlier). These analyses reveal that positive ENSO anomalies were associated with higher April–July (AMJJ) precipitation and higher June–August (JJA) soil moisture in many European regions. Notably, however, we observe the strongest correlations (statistically significant at the 10% level) between positive ENSO anomalies and anomalously wet conditions in Central Europe and the Balkans (see Fig. 3).

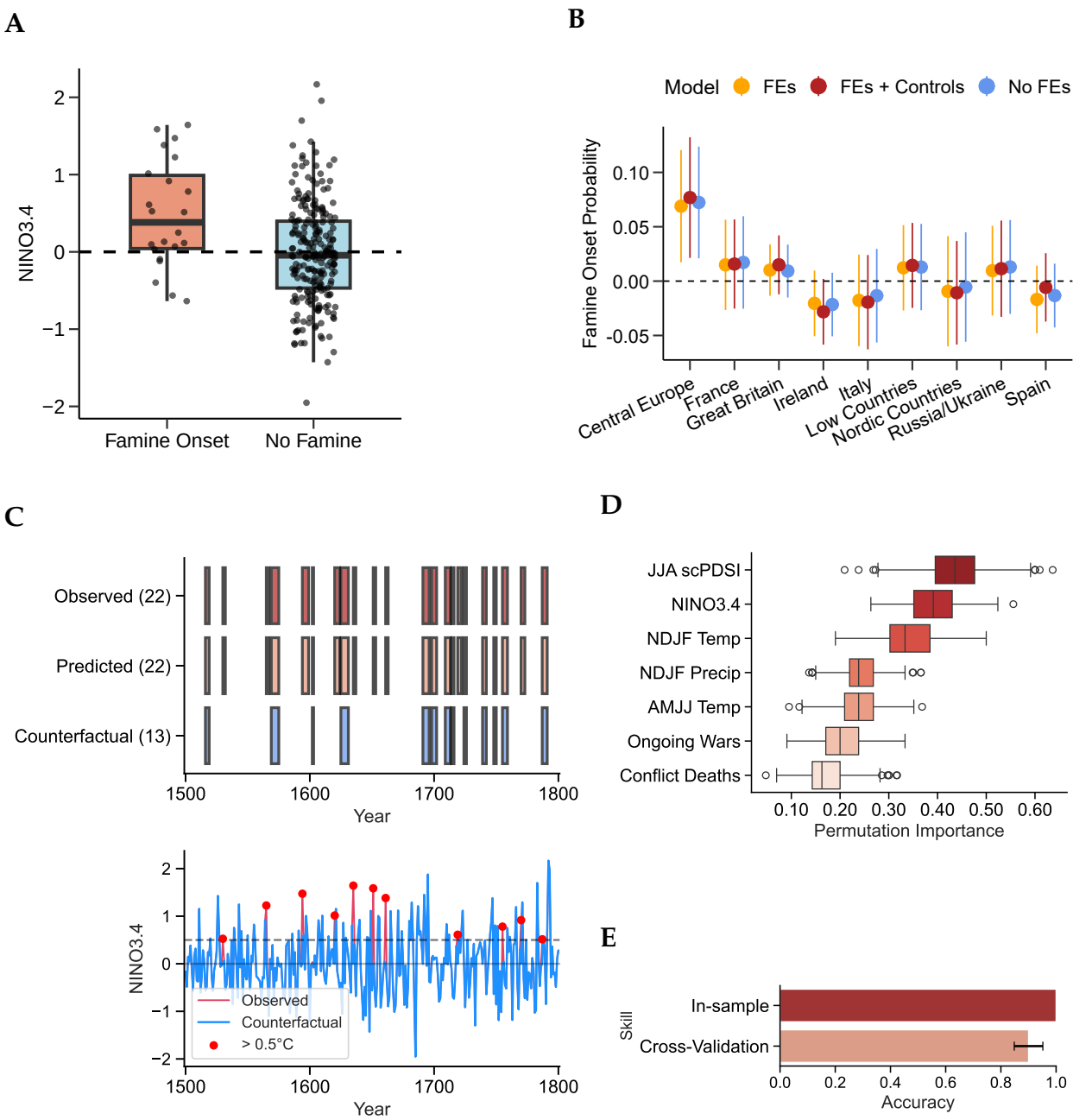

Figure 2: **ENSO and the onset of famine periods.** **(A)** Distribution of ENSO (NINO3.4) anomalies (annual values relative to the 1500–1800 mean) at famine onset in Central Europe. **(B)** Estimated effect of a $+1\,°C$ ENSO (NINO3.4) anomaly on the probability of famine onset, using a Linear Probability Model (LPM) with region-specific impacts. Yellow whiskers include Fixed-Effects (FEs), whereas red whiskers include FEs and the following controls: annual count of conflict-related deaths and ongoing wars, November–February (NDJF) temperature and precipitation, April–July (AMJJ) temperature and precipitation and June–August (JJA) scPDSI ([34]). 95% confidence intervals with robust standard errors: Newey–West for models without FEs and Driscoll–Kraay for those with FEs. **(C)** Predicted, observed, and counterfactual chronologies of central European famine onsets from the Gradient Boosting classifier fine-tuned via a grid search performed via 10-fold cross-validation. The counterfactual represents a scenario in which positive ENSO anomalies are held at neutral conditions (NINO3.4 = 0) during historical onset years. **(D)** Permutation importance of the tuned Gradient Boosting classifier used to classify years into famine onsets, based on $N = 50$ permutations. Predictors include ENSO (NINO3.4), June–August (JJA) scPDSI, November–February (NDJF) temperature and precipitation, April–July (AMJJ) temperature, the annual number of ongoing conflicts and estimated conflict-related deaths. **(E)** Model performance in famine onset attribution. The cross-validation score reflects the mean accuracy over 10 folds.

The areas of strongest ENSO influence on European hydroclimate thus closely match the Central European region where famine onsets were statistically significantly associated with ENSO. This correspondence suggests that excessively wet early summers were particularly disruptive to food security in Central Europe. Many studies [11, 9, 2, 3, 39] have documented the adverse effect of wet summers on harvest outcomes in this region. Our findings suggest the existence of an active causal pathway where ENSO teleconnections in Central Europe repeatedly produced adverse weather that depressed grain harvests to levels capable of triggering famines, given the prevailing socioeconomic context (including food access characteristics, and storage and distribution capabilities) of early modern Central Europe.

To further establish this, we assess the dynamic causal effects of ENSO anomalies on grain harvests. Our primary focus is on rye and wheat, with a secondary focus on other grains. As the two primary bread grains in much of Europe [10], and the most susceptible to damage from excessive wetness [2], rye and wheat were the main price-driving crops, making them particularly relevant to our analysis. Our extensive compilation of harvest data includes tithes (a percentage tax based on the annual harvest) as well as yield ratio records (the proportion of yield in relation to seed) and some yield per unit records[39]. All these harvest records reflect the size of year to year harvest variations. We estimate impulse response functions to a $+1\,^{\circ}$C ENSO shock on harvest data using panel local projections [40], which flexibly incorporate fixed effects for decade, location, and grain type to account for unobserved drivers in harvests fluctuations. Our impulse response functions thus isolate the contribution of a positive ENSO shock to inter-annual harvest variations, holding all other sources of variability constant, and allow us to determine the direction (or sign), magnitude and temporal persistence of harvest responses.

Based on the consistency of observed teleconnections between ENSO and soil moisture (as measured via the June–August scPDSI[34]), we also partition our harvest time-series into 'Teleconnected' and 'Weakly affected' groups. In teleconnected regions, rye and wheat harvests declined by an average of 6.4% (CI [1.9%, 10.9%]) following a $+1\,^{\circ}$C ENSO shock (Figure 3A). Moreover, we observe a persistent effect that remains statistically significant even after three years, with an average decline of 6.5 % (CI [1.4%, 11.6%]). This may partly reflect the impact of genuine multi-year climate responses to ENSO forcing. However, because much of our harvest data derive from grain tithes, this persistence will also reflect a "memory" effect embedded in the tithe records: following a poor harvest, reduced availability of seed grain could depress the next year's yields, which in turn affected subsequent tithes[39]. Although the observed responses are statistically significant, the estimates carry large standard errors, reflecting both the limited number of apparently teleconnected regions with available harvest records and their geographical clustering[39]. We also find that other grains types, including barley and oats, which are more resilient to wet conditions[2], showed weaker responses to positive ENSO shocks in teleconnected regions than rye and wheat, further confirming the important role of soil moisture teleconnections (Figure 3D).

We observe similar behavior, with even larger impulse responses in rye/wheat harvests, and a similar

multi-year persistence, when we modulate our partition of the available harvest data based on observed ENSO teleconnections to April–July (AMJJ) precipitation anomalies (see Supplementary E). Our findings on grain harvests remain robust to alternative model specifications for capturing the persistent effects of ENSO shocks (Supplementary I.1). Placebo ENSO shocks that use fully randomized ENSO histories produce no detectable harvest response, with estimates tightly centered around zero, while our baseline effects lie well outside the resulting null distributions (Supplementary I.4). Using the yield ratio compilation from Slicher van Bath [41], as alternative harvest data, we obtain an even larger effect, presumably because a higher proportion of this dataset derives from Central Europe (Supplementary I.2). Finally, we confirm that our statistical inferences are not biased by spatial or temporal autocorrelations (Supplementary I.7).

2.2 ENSO Prolonged Famines Across all European Regions

Beyond the dates of famine onset, famine duration is of great interest in influencing the scale of mortality and other impacts such as mass population displacement. We find that ENSO is associated with the duration of early modern European famines, across all nine regions in our compilation. Using a time-dependent Cox proportional hazards model stratified by region, we estimate that, on average across all nine regions, a $+1$°C ENSO anomaly occurring during an already ongoing famine reduced its likelihood (technically, instantaneous hazard) of ending by approximately 24% (hazard ratio $= 0.76$, CI [0.58, 0.99]), relative to the case if ENSO conditions had been neutral.

In testing the robustness of this finding, we note that estimates remain similar across further models that control for the influence of climate-related and conflict-related observables as well as model specifications that account for unobserved heterogeneity in the assembled panel data (Figure 4A). Our results are also robust to other alternative model specifications and falsification exercises (Supplementary I.1 and I.4). We additionally confirm that the proportional hazards assumption holds for all models in Figure 4A. Global tests of proportional hazards [42] thus yield p-values consistently above 0.1 (Supplementary F), supporting our use of the proportional hazards framework.

We also note that while hazard ratios capture relative differences in instantaneous risk, survival curves convey the cumulative effect on famine duration for different counterfactual scenarios. For example, as shown in Figure 4B, a $+2\,$°C ENSO anomaly (a severe El Niño) increases the modeled probability that a famine would persist beyond three years by roughly 28 percentage points compared with a $-1\,$°C ENSO anomaly (a La Niña event).

Finally, we find that ENSO emerges as a key out-of-sample predictor of famine persistence, reinforcing the claim that it was strongly linked to prolonged famines, as evidenced by linear and non-linear machine learning approaches to survival analysis, through a robust cross-validation procedure (see Figure 4C; more

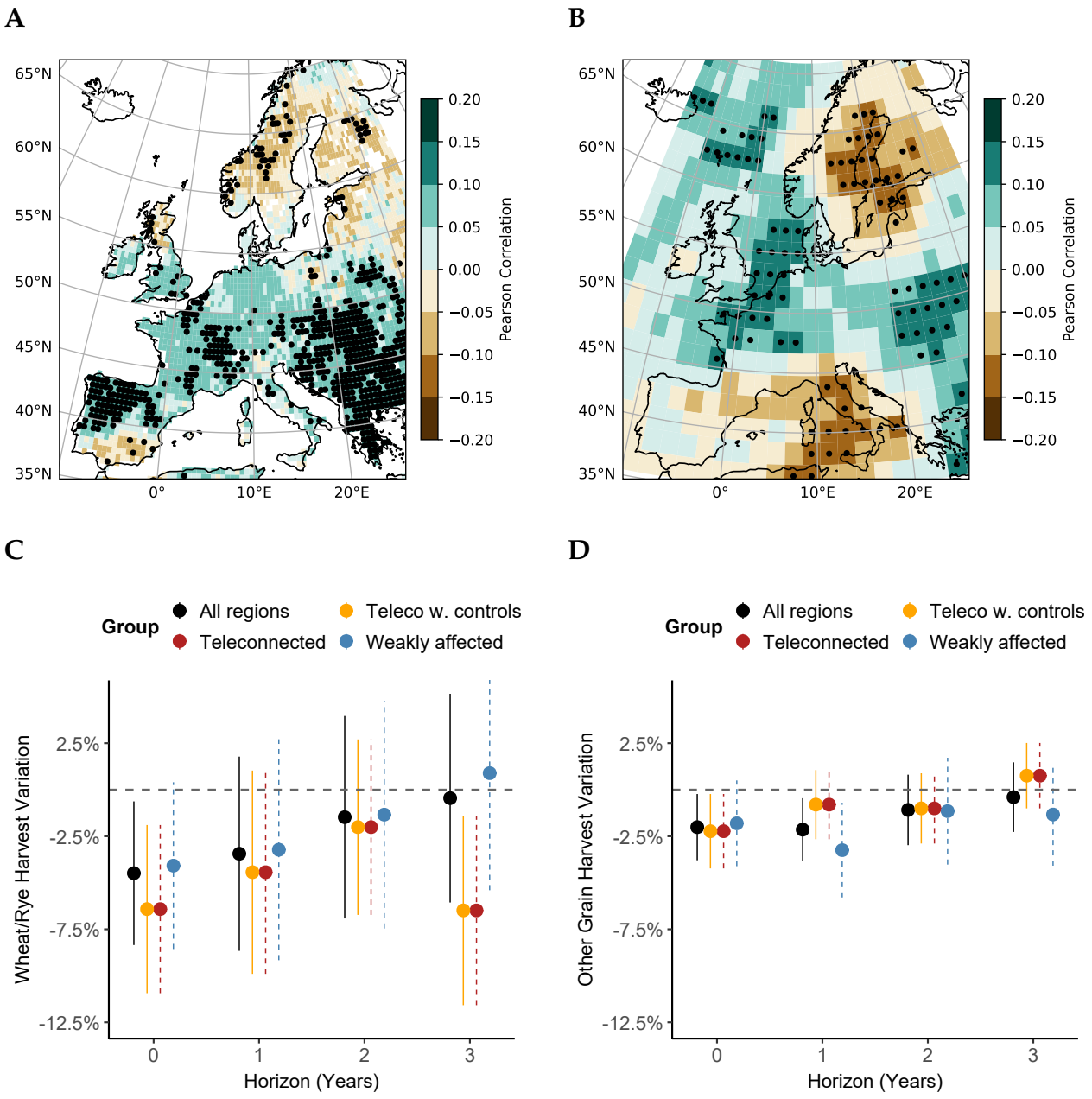

Figure 3: **ENSO teleconnections and grain harvest responses.** Correlation map of ENSO (NINO3.4 index) and **(A)** June–August scPDSI ([34]) and **(B)** April to July precipitation ([33]) over the entire period (1500–1800). Dotted grid-points show significant Pearson correlations at the 10% level. **(C)** Impulse response functions to a +1 °C ENSO shock on rye and wheat grain harvests, and **(D)** on other grain harvests (see legend for colors). Impulse response functions (IRFs) are estimated using 'location-grain-record' fixed-effects (location of the harvest, the record type, e.g., tithe, yield ratio, and yield per unit, and the grain type) and decade fixed-effects. Whiskers correspond to the 95% confidence interval with Driscoll-Kraay standard errors. The groups include 'Teleconnected' IRFs estimated only on the sample of time-series whose scPDSI is correlated with ENSO at 10% significance and 'Weakly affected' IRFs, estimated on the records that exhibit no significant scPDSI correlation. 'Teleco w. controls' IRFs are estimated on teleconnected locations and include (as controls) local April–July and November–February temperature and precipitation, June–August soil moisture (scPDSI), and the number of ongoing wars and estimated conflict fatalities per year.

details in Methods 4.4). Across all models, ENSO stands out as the only consistently essential predictor, as reflected by its high permutation importance (4D), quantifying the loss in predictive skill when ENSO is removed from the model. Similar patterns of importance are observed when evaluating in-sample performance over the full period (Supplementary G).

Market integration and price shock propagation Whereas the role of ENSO in triggering famine onset in teleconnected regions is explicable via a direct pathway from climate impact to diminished harvests, the role of ENSO in prolonging famine duration across Europe (including regions without notable teleconnections) requires further explanation. One plausible mechanism involves the transmission of price shocks from teleconnected regions to other markets, including those already experiencing famines, contributing to their extension. This is consistent with the fact that Central Europe, with constituent territories such as Poland being known as the 'granary of Europe'[43], was among the few regions of the continent that regularly produced grain surpluses for export [44]. Shortfalls here could thus impact food access and propagate price increases more widely[10]. To test this hypothesis, we exploit grain price data alongside fish prices as comparator.

ENSO impact on grain and fish prices The available grain price series are identified according to 46 major European cities, while the fish price series cover 8 cities (see Methods 4.1 for details on the sources). We find that ENSO triggered a broad-based rise in prices across cities, even in weakly teleconnected locations (which comprise the majority of our grain series for the period). This suggests a pan-European market response to regional harvest failures that is understandable in the context of the extensive market integration and associated grain trade in early modern Europe [45, 46, 47, 48, 10]. We estimate that a $+1$ °C ENSO shock led to a cumulative increase in grain prices of up to 6.5% (CI [3.8%, 9.3%]) after one year, with prices gradually returning to baseline over an eight-year horizon (Figure 5A). As per our harvest results, these impulse responses are designed to isolate the impact of an ENSO shock on inter-annual price fluctuations, controlling for other sources of variability.

The impacts of climate variability on contemporary and future marine food sources are of increasing concern, as is the role of fish in past subsistence strategies. In contrast to the immediate effects observed in grain prices, we find that marine fish prices started rising approximately two years following a $+1$ °C ENSO shock, peaking (approximately) at a 3.4% (CI [1.0%, 5.7%]) increase after three years (Figure 5B). However, we see no strong evidence of a corresponding post-ENSO-shock response in historical fish catches from North Atlantic or European waters (herring and cod; see Supplementary H). We thus posit that the observed price response largely reflects a demand substitution effect arising from ENSO-related grain scarcity, rather than an impact on the marine environment affecting marine productivity that limited the supply of catchable herring and cod. This is consistent with documentation of a minimal ENSO impact on present

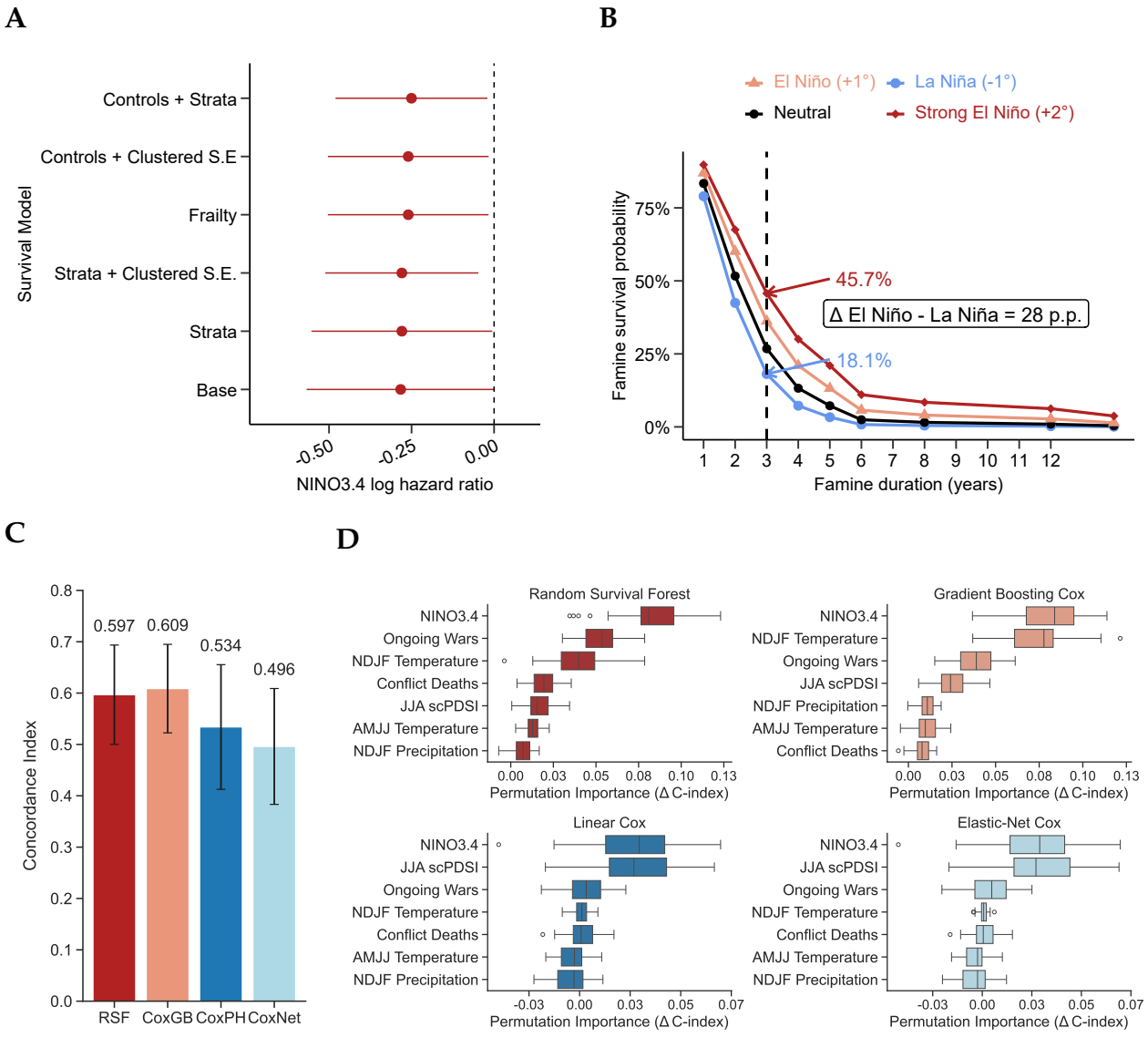

Figure 4: **ENSO anomalies and famine duration. (A)** Estimated log-hazard ratios for the ENSO index across various model specifications and controls. "Clustered S.E." denotes models with standard errors clustered at the famine level. "Controls" include November–February temperature, precipitation, June–August soil moisture, and armed conflict exposure. "Strata" indicates Cox models stratified by region. "Frailty" incorporates a random effect to account for unobserved heterogeneity or dependencies within a population. Error bars represent 95% confidence intervals. **(B)** Modeled survival curves for famine duration under varying ENSO anomaly scenarios using the "base" Cox Proportional Hazards model without region-level stratification. $\Delta = 28$ p.p. indicates that the probability of a famine persisting after 3 years is higher by 28 percentage points in the 3°C increase from La Niña to El Niño. **(C)** Cross-validation performance measured by concordance indices of four survival models: Standard Cox Proportional Hazards (CoxPH), Cox regression with elastic net regularization (CoxNet), Random Survival Forest (RSF), and Gradient Boosted Cox Regression (CoxGB). All models are fine-tuned using a grid search with 10-fold cross-validation, nested within an outer 10-fold cross-validation loop to evaluate out-of-sample performance. Error bars reflect the variation in concordance indices across folds. **(D)** Permutation Importance scores for each fine-tuned models, based on the decrease in Concordance Index (Δ C-Index) for $N = 50$ permutations.

North Atlantic fisheries (see Bertrand et al. [49]).

The delayed (post-ENSO shock) increase in historical fish prices suggests that dietary substitution to fish occurred gradually following poor grain harvests. Households may at first have preferentially relied upon alternative strategies such as stored grains, substitute crops, or increased reliance on imported grains before meaningfully shifting consumption to fish[5, 6]. We also observe differential responses between fish types: cod prices increased by roughly 5.6% (CI [2.0%, 9.3%]) for a $+1\,^{\circ}\mathrm{C}$ ENSO shock, whereas herring prices increased by 1.9% (CI [-1.0%, 4.1%]). Both responses peaked three years post-shock, although cod prices began to respond (one year) earlier. These different responses suggest that market accessibility and value influenced substitution patterns. Cod, being more affordable and widely available, may have served as a more immediate grain substitute. The notion of cod as so-called 'food for the poor' (or, in reality, a staple for the working population) has been discussed by Hitzbleck [50] for Germany and by Grafe [51] for Spain, and is further supported by our analysis. In contrast, herring, particularly influenced by the higher-value Dutch herring trade, was relatively more expensive, potentially explaining its more delayed and muted price response to ENSO shocks (for more, see Allaire and Holm [52]).

As before, we verify that our results for grain and fish price responses are robust to alternative model specifications, and find this to be so (Supplementary I.1). Placebo regressions with fully randomized ENSO histories thus generate no systematic price responses, with estimates centered near zero. In contrast, the observed effects (using the true, observed ENSO history) do not intersect these null distributions (Supplementary I.4). Using alternative grain price compilations to that of Ljungqvist and Seim [10] yields similar estimates (Supplementary I.2), and we further show that spatial and temporal autocorrelation do not drive our statistical inferences (Supplementary I.7).

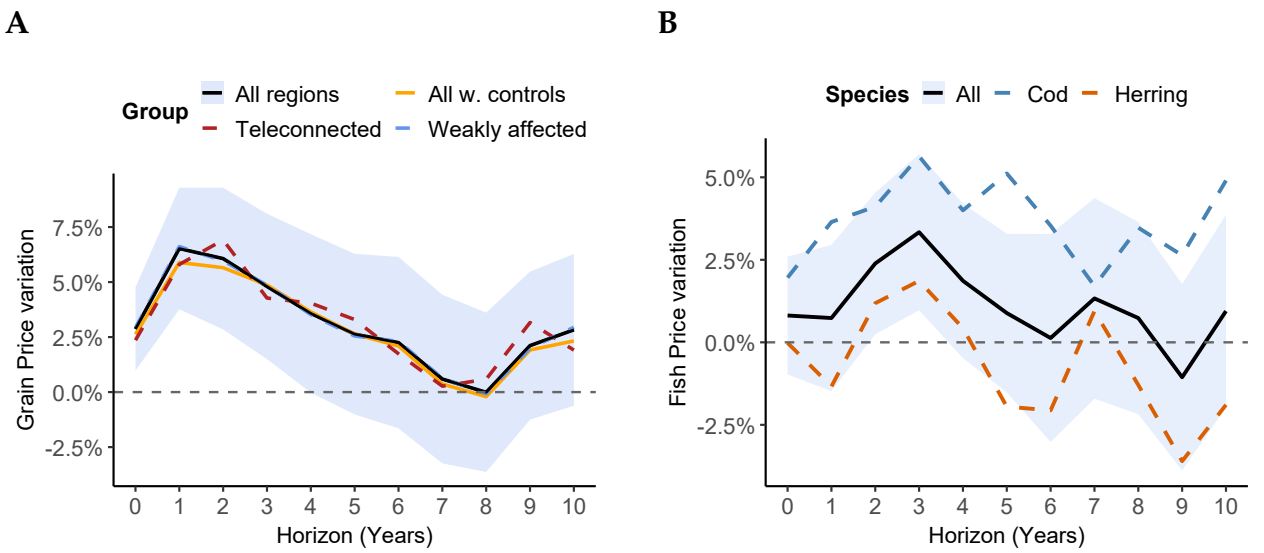

Figure 5: **ENSO shocks broadly raised staple food prices. (A)** Impulse response functions (IRFs) to a +1 °C ENSO shock on grain prices. The groups include 'Teleconnected' IRFs estimated only on the sample of cities whose scPDSI is correlated with ENSO at 10% significance and 'Weakly affected' IRFs, estimated on the records that exhibit no significant scPDSI correlation. 'All w. controls' IRFs include local April–July and November–February temperature and precipitation, June–August soil moisture (scPDSI), and the number of ongoing wars and estimated conflict fatalities per year. **(B)** Impulse response functions of a +1 °C ENSO shock on fish prices, differentiated by species (Cod and Herring). Shaded areas correspond to the 95% confidence interval of the baseline models (black lines) with Driscoll-Kraay standard errors. All Impulse response functions (IRFs) are estimated using 'city-species' fixed-effects and decade fixed-effects.

3 Discussion

We provide the first robust evidence that ENSO – more typically associated with tropical and subtropical impacts – was statistically significantly associated with the onset of regionally specific Central European famines. To explain this we offer quantitative evidence of an active causal pathway by which ENSO repeatedly induced (1) excessive summer wetness in Central Europe, (2) reduced harvest yields and (3) elevated grain prices. Moreover, we show that positive ENSO anomalies increased year-to-year famine persistence across all European regions studied, even if not acting as a direct trigger in regions with limited or no obvious ENSO climate teleconnections. We posit that this reflects (at least in part) the substantial grain market integration known for the period. Given this, Central European grain deficits may not only have restricted supplies ordinarily traded to other European regions, but created reverse demand on the local grain supplies of these regions, as well as potentially motivating deleterious behaviors including grain hoarding and price speculation. To assess the general plausibility of these indirect market-mediated pathways, we employ available European grain price data and show that prices rose following positive ENSO anomalies even in regions for which no convincing teleconnections were observed, nor clear harvest deficits.

Grain prices have long been central to the analysis of food shortages and famines [53, 54], often serving as key indicators for their timing and intensity[55]. We note that recent scholarship cautions against directly inferring famine conditions from high prices, even if grain prices generally reflect the broader food supply. [6, 56]. For example, state-level interventions such as emergency relief measures might prevent famine conditions while prices remain high. While acknowledging this, we nonetheless argue that the notable and consistent increases in grain prices following positive ENSO shocks provide compelling evidence that ENSO played an indirect role in extending famine durations broadly across Europe, beyond the core strongly teleconnected region of Central Europe, in the context of integrated grain markets.

Our findings contribute to longstanding debates over the relative roles of climatic, socioeconomic and political factors in explaining early modern famines[57]. While some scholarship has emphasized direct climate impacts on past societies, other studies privilege the role of markets, institutions, and entitlements in determining famine onsets and outcomes[58, 5, 59, 2, 6]. Our analyses provides quantitative evidence for both environmental causation and market-mediated amplification mechanisms [60, 44]. The pronounced effects on famine persistence further highlight the importance of sociopolitical and socioeconomic factors in prolonging subsistence crises beyond initial climate triggers [57, 4, 6]. These results support the view that early modern European famines emerged through complex interactions between climate variability, harvest failures and integrated grain markets, challenging both simple climate determinism and purely societal explanations [9].

We also note limitations in the principal data underlying our analyses. The ENSO reconstruction for the

1500–1800 period is based on 242 chronologies – fewer than half the number available after 1800 – which reduces reconstruction skill. Nonetheless, Cook and Cane [29] emphasize that their indices effectively capture the remote impacts of tropical Pacific SST on rainfall, rather than relying on *in situ* ENSO-sensitive tree-ring chronologies. Because they only include tree-ring records that strongly reflect these teleconnections, the resulting indices may serve as reliable indicators of ENSO impacts. Our study assesses teleconnections between ENSO and the European climate using multiple climate reconstructions, each with their own uncertainties. For example, the tree-ring-based JJA scPDSI reconstruction (also known as the Old World Drought Atlas) that we use to infer soil moisture conditions is less skilled for some regions, such as Eastern Europe[61]. To address this, we compared several reconstructions and saw recurring patterns, such as robust soil moisture and precipitation teleconnections in Central and Eastern Europe. Finally, the famine year compilation by Ljungqvist et al. [6] offers a comprehensive list of major European famines for the entire early modern period. However, assembling a representative chronology of famines across different European regions is challenging. Many events were localized or sub-regional in nature[5], and their full geographic extent is often uncertain due to limitations of the historical data[4]. Furthermore, distinguishing between outright famines and more moderate food shortages – based on contemporary definitions – is similarly complicated by the inconsistent nature of available historical sources[62].

Our findings advance knowledge of how large-scale climate variability propagates through interconnected socioeconomic systems. This mechanism of climate impact transmission may help explain historical patterns of widespread societal disruption following major agriculturally adverse climate shocks, providing insights relevant to understanding climate vulnerability in interconnected modern food systems. Future work should address the question of adaptation to famines across centuries. Economists have begun to account for human adaptation in their estimates of climate impacts[63][64] and further insights may arise in assessing how adaptation affects our estimates of ENSO's impact on food security, especially in relation to the progress (plus advantages and disadvantages) of European food market integration. Our results should encourage broader investigation into teleconnections between ENSO and the early modern European climate, a period coinciding with the main phase of the Little Ice Age[3]. Future studies can offer insights into how ENSO teleconnections have evolved over time, and how their triggering of climatic extremes may have impacted societies (not only in food security) both economically and socially.

4 Methods

4.1 Data

4.1.1 Famine chronology

We use the most recent compilation of famines in early modern Europe from Ljungqvist et al. [6], who revised and updated the lists from Alfani and Ó Gráda [4] [65] to provide a comprehensive chronology of famine years. The following European regions from 1250 to 1800 CE were included: Central Europe, France, Great Britain, Ireland, Italy, the Low Countries, the Nordic countries, Spain, and Ukraine/Russia. The famine year list only indicates the presence of famine conditions within a region, but does not inform us about neither the severity nor the geographical extent of the famine within the given region. For most pre-19th-century European famines, such information is unavailable because of source limitations.

4.1.2 Climate reconstructions

We use a tree-ring–based ENSO reconstruction from Cook and Cane [29]. This climate field reconstruction [66] of tropical Pacific sea surface temperatures (HadISST[67]) for boreal winter (December–February) is based on a circum-Pacific tree-ring network from regions known to be affected by El Niño rainfall. Our baseline metric for ENSO is the NINO3.4 region (5°N–5°S, 170°W–120°W). We also compute Niño 1+2 (0–10°S, 90°W–80°W), Niño 3 (5°N–5°S, 150°W–90°W) and Niño 4 (5°N–5°S, 160°E–150°W). We use the anomaly in degree Celsius sea surface temperature (SST) for each region, measured as the deviation from the 1801–1900 mean SST.

Our climate analysis focuses on late spring and early summer temperature and precipitation (average of April–July, AMJJ), winter temperature and precipitation (average of November–February, NDJF) and June–August (JJA) soil moisture.

For temperature and precipitation, we use the ensemble mean 2-meter air temperature and total precipitation from the Modern Era Reanalysis (ModE-RA) [33]. ModE-RA is a global monthly paleo-reanalysis covering the period 1421 to 2008. To reconstruct past climate fields, an offline data assimilation approach is used, blending together information from an ensemble of transient atmospheric model simulations and instrumental observations. In the early period, ModE-RA utilizes natural proxy data and documentary data, while from the 17th century onward, instrumental measurements are also assimilated[68]. ModE-RA is systematically assessed through comparisons with independent time series, gridded instrumental observations, and other climate reconstructions. Unlike most paleo-reanalyses, which rely on non-transient priors from climate simulations with low-frequency variability driven by the assimilated proxy data, ModE-RA de-

rives its centennial-scale variability from the model's response to external forcings. As a result, this dataset is particularly well-suited for investigating variability from intra-annual to multi-decadal timescales. We take advantage of ModE-RA's monthly temporal resolution – compared to earlier reconstructions by Luterbacher et al. [69] and Pauling et al. [70] – to flexibly construct temperature and precipitation maps for April–July (AMJJ) and November–February (NDJF).

For soil moisture, we use the Old World Drought Atlas (OWDA) [34]. The OWDA is a gridded, annually resolved reconstruction of summer (June–August, JJA) hydroclimatic variability across Europe and North Africa over the past millennium. It is based on an extensive network of tree-ring chronologies from living, archaeological, and sub-fossil material, standardized to preserve long-term variability. The applied climate field reconstruction method was the point-by-point regression with ensemble weighting against the self-calibrating Palmer Drought Severity Index (scPDSI). The OWDA provides year-to-year maps of drought and pluvial conditions on a 5,414-point 0.5°$\times$ 0.5°longitude–latitude grid, which enables detailed characterization of hydroclimatic variability during the early modern period in Europe.

For our panel of famine periods, we assign every region a unique scPDSI/temperature/precipitation value every year based on the spatial average over that region. For subsequent analyses conducted at the sub-regional level (i.e. city, district or estate), we geocode each location and assign the grid-cell(s) closest to its latitude and longitude coordinates to extract local climate values. The temperature and precipitation data are provided at a spatial resolution of 1.8°$\times$ 1.8°, while the scPDSI data are at a finer resolution of 0.5°$\times$ 0.5°. We use a 1°$\times$ 1° radius around the coordinates for the scPDSI in order to match the coarser temperature resolution. This larger radius also smooths our ENSO–scPDSI teleconnection partitions. Note that, in order to weight the scPDSI, temperature and precipitation fields according to their area on a sphere, each grid point is multiplied by $\sqrt{\cos\phi}$ where ϕ is the latitude.

4.1.3 Commodity prices and grain harvests

We use annual grain price time-series published by Ljungqvist and Seim [10], for a given city and year. We show our results are similar when using other grain price compilations in Supplementary I.2. For fish prices, we use a compilation that spans eight European cities (Amsterdam, Antwerp, Barcelona, Gdansk (Danzig), London, Munich and Vienna), with both cod and herring prices, deriving from Matthews [71], Allaire and Holm [52] and the Allen-Unger Global Commodity Prices Database[72].

We included an extensive compilation of quantitative harvest data from the published literature (much of which was also included in Ljungqvist et al. [39]). The dataset includes harvest data from present-day France, Germany, Hungary, Spain, Switzerland, and Sweden. We utilized three main types of harvest data: (1) tithe records from regions where tithes reflected actual fluctuations in harvest size, (2) yield ratios –

measuring the quantity harvested relative to the amount sown – from individual farms and estates, and, more rarely, (3) total yield quantities recorded for individual farms, estates, or larger districts.

A detailed list of references for the grain harvest and price data is provided in Supplementary A.

4.1.4 Conflict measures

To estimate the annual number of conflict fatalities in Europe as a whole, we use the Conflict Catalog, a taxonomy of the most severe recorded violent conflicts [32]. To calculate the yearly fatalities from events spanning multiple years, the total fatalities for each event are evenly distributed across all the years of its duration. This method aggregates overlapping events by summing their contributions within each year. Although the assumption of even distribution across years may be less accurate for protracted conflicts such as the Thirty Years' War, no reliable source provides annualized fatality estimates for such multi-year events, to our knowledge.

Similarly we compute the number of ongoing wars in a given year, and the number of wars started in a given year, which we use as our main measure of conflict onset.

4.2 ENSO and the Onset of Famine Periods

Causal Inference We examine the causal impact of ENSO on the start of famine periods by using the following fixed-effects linear probability model:

$$\text{Onset}_{i,t} = \alpha_i + \gamma_{\text{Decade(t)}} + ENSO_t \times \delta_i + \mathbf{x_{i,t}}\beta + \epsilon_{i,t} \tag{1}$$

where $\text{Onset}_{i,t}$ is an indicator equal to 1 if region i experiences a famine in year t but not in year $t-1$, and 0 otherwise. α_i denotes region fixed effects; $\gamma_{\text{Decade}(t)}$ captures decade fixed effects; $ENSO_t \times \delta_i$ represents the interaction between the ENSO index (NINO3.4) in year t and region-specific sensitivity to ENSO anomalies; $\mathbf{x}_{i,t}$ is a vector of time-varying control variables, including April–July and November–February temperature and precipitation anomalies, the self-calibrating Palmer Drought Severity Index (scPDSI), and the number of ongoing wars in Europe in year t; and $\epsilon_{i,t}$ is the idiosyncratic error term. Standard errors are corrected for autocorrelation and heteroskedasticity using Driscoll–Kraay standard errors. The fixed effects in Equation 1 are central to our identification strategy. By absorbing location-specific and time-trending influences on famine onset non-parametrically, they isolate the contribution of ENSO from both observed and unobserved confounders. This approach is more robust than attempting to enumerate and control for the other possible drivers of famine directly. In effect, the specification attributes variation in famine onset to idiosyncratic

ENSO shocks within a region and year, supporting a causal interpretation of the parameter δ_i. We also report results of these regressions in table form, as well as a similar logistic regression model in Supplementary C.

Machine Learning Attribution To quantify the contribution of ENSO and other predictors (regional temperature, precipitation, soil moisture, and conflict) to famine onsets in Central Europe, we trained a Gradient Boosting classifier[73]. Formally, the fitted model defines a nonlinear mapping f:

$$\text{Onset}_t = f(\mathbf{x_t}, ENSO_t)$$

where $\mathbf{x_t}$ is the vector of covariates at time t and $ENSO_t$ is the NINO3.4 index anomaly.

Model hyperparameters were tuned via 10-fold cross-validation to maximize predictive accuracy for classifying each year as a famine onset or non-onset (see Table 1 for the grid). Using this fine-tuned model, we generated two scenarios: the model's predictions under observed conditions ($\text{Onset}^{\text{OBS}}$) and a counterfactual scenario (Onset^{CF}) in which positive ENSO anomalies during historical famine onsets were set to 0 ($ENSO^{\text{CF}}$):

$$\text{Onset}_t^{\text{OBS}} = f(\mathbf{x_t}, ENSO_t); \quad \text{Onset}_t^{\text{CF}} = f(\mathbf{x_t}, ENSO_t^{CF})$$

True positive famine counts were then aggregated from the model predictions under observed and counterfactual conditions. This allows us to estimate the number of historical famines attributable to ENSO given by

$$\sum_t \text{Onset}_t^{\text{OBS}} - \text{Onset}_t^{\text{CF}}$$

where t denotes each year in the early modern period.

Model performance was evaluated both in-sample and out-of-sample via cross-validation, providing a robust assessment of the classifier's predictive skill. We show that using different subsets of predictors yields comparable results in Supplementary C.

Table 1: Hyperparameter grid used for tuning the Gradient Boosting Classifier via cross-validation.

Model	Hyperparameters
Gradient Boosting Classifier	Maximum depth $\in \{1, 3, 5, 10\}$
	Number of estimators $\in \{3, 5, 10, 50\}$
	Learning rate $\in \{0.01, 0.05, 0.1, 0.2, 0.3, 0.4, 0.5\}$
	Subsample $\in \{0.7, 0.9\}$
	Maximum features $\in \{\sqrt{}, 0.5\}$
	Minimum samples per leaf $\in \{2, 5\}$
	Minimum samples per split $\in \{5, 10\}$

4.3 Dynamic Causal Effect of ENSO on Prices and Harvests

We estimate the dynamic causal effects of global temperature shocks using panel local projections [40], which extends the approach of Òscar Jordà [74] to panel data. Specifically, for each horizon $h = 0, \ldots, H$, we estimate the following regressions:

For grain prices:

$$\ln(\text{GrainPrice}_{i,t+h}) - \ln(\text{GrainPrice}_{i,t-1}) = \theta_h^G \, \text{ENSO}_t + \mathbf{x}'_{i,t}\boldsymbol{\beta}_h^G + \delta_{i,h}^G + \gamma_{h,\text{Decade}(t)}^G + \varepsilon_{i,t+h}^G, \tag{2}$$

where $\text{GrainPrice}_{i,t}$ is the price of grain in city i at time t, $\delta_{i,h}^G$ represents city fixed effects.

For fish prices, which vary by species:

$$\ln(\text{FishPrice}_{i,s,t+h}) - \ln(\text{FishPrice}_{i,s,t-1}) = \theta_h^F \, \text{ENSO}_t + \mathbf{x}'_{i,t}\boldsymbol{\beta}_h^F + \delta_{i,s,h}^F + \gamma_{h,\text{Decade}(t)}^F + \varepsilon_{i,s,t+h}^F, \tag{3}$$

where s indexes fish species, and $\delta_{i,s,h}^F$ represents city-species fixed effects.

For grain harvests:

$$\ln(\text{GrainHarvest}_{i,g,r,t+h}) - \ln(\text{GrainHarvest}_{i,g,r,t-1}) = \theta_h^Y \, \text{ENSO}_t + \mathbf{x}'_{i,t}\boldsymbol{\beta}_h^Y + \delta_{i,g,r,h}^Y + \gamma_{h,\text{Decade}(t)}^Y + \varepsilon_{i,g,r,t+h}^Y, \tag{4}$$

where g indexes grain type, r indexes the harvest proxy (tithe, yield or yield ratio), i indexes the location of the record and $\delta_{i,g,r,h}^Y$ represents location-grain-record fixed effects.

θ_h captures the dynamic causal effect of interest at horizon h, which we interpret as the impulse response function. $\mathbf{x}_{i,t}$ is a vector of potential control variables, and $\gamma_{\text{Decade}(t)}$ are decade fixed effects that control for common long-run trends across locations. The error term $\varepsilon_{i,t+h}$ may be serially correlated. The inclusion of fixed effects is essential for the causal interpretation of θ_h, as they absorb location-specific factors and decadal trends, isolating the effect of ENSO shocks from confounding factors, just as the fixed-effects specification in Equation 1. Our main findings remain robust across an alternative model specification, as discussed in Supplementary I.1. Because the ENSO shock does not vary by location, the error term is potentially serially and cross-sectionally correlated. For inference, we rely on Driscoll and Kraay [75] standard errors that are robust to such cross-sectional and serial dependence. We set $H = 4$ for grain harvests and a longer horizon of $H = 10$ for prices, as price responses to climatic shocks are likely to exhibit greater persistence than harvests.

4.4 Survival Analyses of Famines

Inference To evaluate how ENSO influences the hazard of famine occurrence, we use a Cox Proportional Hazards model [76]. We estimate the effect of time-varying ENSO conditions on the hazard of event occurrence using a time-dependent Cox Proportional Hazards model with stratification by region, which allows the baseline hazard to vary across regions. The hazard function for famine i in region r at time t is specified as:

$$h_i(t \mid \text{ENSO}_i(t), \mathbf{X}(t), r) = h_{0r}(t) \exp\left(\beta \cdot \text{ENSO}_i(t) + \boldsymbol{\gamma}^\top \mathbf{X}(t)\right), \tag{5}$$

where: $h_i(t \mid \cdot)$ is the hazard rate for famine i at time t; $h_{0r}(t)$ is an unspecified *region-specific* baseline hazard for region r; $\text{ENSO}_i(t)$ is a time-varying covariate capturing ENSO conditions (NINO3.4 index) at time t for famine i; β is the coefficient capturing the sensitivity of the hazard with respect to ENSO; $\mathbf{X}(t)$ is a vector of time-varying control covariates; and $\boldsymbol{\gamma}$ is the corresponding vector of coefficients.

In the Cox Proportional Hazards framework, coefficients are estimated on the log-hazard scale. The coefficient β corresponds to a hazard ratio (HR) of $\exp(\beta)$. This hazard ratio represents the multiplicative change in the hazard of famine termination associated with a +1°C increase in ENSO, holding other variables constant. The percentage change in hazard can then be computed as $(\exp(\beta) - 1)$.

By stratifying the baseline hazard across regions, the model flexibly accounts for unobserved regional heterogeneity in baseline famine risks while still estimating a common effect of ENSO and other covariates. We verify the robustness of our estimates by including additional time-varying controls, such as temperature and precipitation anomalies and the number of wars in a given year, and by comparing specifications

with clustered standard errors and region-level frailty terms. Incorporating these controls and modeling choices is important for causal interpretation, as they help account for potential confounding factors and unobserved heterogeneity that could otherwise bias the estimated effect of ENSO on famine duration.

Machine Learning Prediction For our predictive exercise, we use four different survival models: a standard Cox Proportional Hazards regression, an Elastic-Net Cox Regression [77], a Random Survival Forest [78] and a Gradient Boosting Survival Analysis, i.e. a Gradient-boosted Cox proportional hazard loss with regression trees as base learner ([79]). All models use the average values of the selected predictors (NINO3.4, temperature and precipitation indices, spring–summer scPDSI, and conflict measures) over the famine period, with famine duration as the outcome variable.

We employ a cross-validation (CV) approach to estimate out-of-sample performance. The nested cross-validation procedure ensures that hyper-parameter tuning does not bias the estimate of out-of-sample performance. By performing an inner CV to select the best hyper-parameters and an outer CV to evaluate model performance, we obtain an unbiased estimate of the concordance index for unseen data.

The training and evaluation procedure for each model is as follows:

1. Define an outer $k = 10$ fold cross-validation split to evaluate model performance on unseen data.
   (a) Within each outer training fold, perform an inner $k = 10$ fold cross-validation to tune hyper-parameters via a grid search. Select the hyperparameter combination that maximizes the mean concordance index (*C*-index) across the inner folds. The specific hyperparameter grids used in this search are detailed in Supplementary G.
   (b) Refit the model with the selected hyperparameters on the entire outer training fold and evaluate its predictive performance (concordance index) on the corresponding outer test fold.
2. Aggregate the performance estimates across all outer folds to obtain the model's out-of-sample concordance index (mean and standard deviation).
3. After completing the nested cross-validation, refit each model on the full dataset using the best hyperparameters identified in the inner loops, and compute permutation feature importances to assess variable contributions to predictive performance.

4.5 Robustness Checks

We conduct a series of robustness checks to test the sensitivity of our findings on famine onsets, duration, grain and fish prices, and agricultural yields to modeling assumptions, data sources, and inference methods.

A summary is provided in Table 12.

Permutation Tests We assess the robustness of our results by randomly permuting the ENSO sequences across years in the panel datasets and re-estimating the models. The observed effects consistently fall well outside the 95% confidence intervals of the resulting placebo distributions (Figs. 24, 25).

Alternative Data Sources Using the grain price dataset from Federico et al. [46] and Allen [80] results in impulse responses nearly identical to our main analyses using Ljungqvist and Seim [10] (Figs. 21a, 21b). Using the earlier, less extensive, compilation of yield ratio time-series of Slicher van Bath [41], we again find a strong ENSO effect, if anything larger than in our estimates (Fig. 22). This result likely reflects the narrower coverage of the Slicher van Bath [41] dataset, which includes a high share of Central European time series.

Alternative Model Specifications We re-estimate the effects of ENSO on famine duration using parametric hazard models (Weibull, log-logistic, Tobit), which consistently indicate significant positive effects of ENSO anomalies on famine duration (Table 13). Additionally, we use fixed-effects regressions to model famine duration, grain prices, and harvests. These models, including contemporaneous and lagged ENSO shocks, confirm strong and persistent effects (Tables 14–18).

Sample Composition We show that our main results are robust to alternative samples and exclusion tests. The dynamic effects of ENSO on prices and harvests are largely insensitive to excluding one location at a time or to dropping 20-year blocks, leaving the impulse responses unchanged (Figs. 27–32). Similarly, our famine onset and duration results are robust to excluding individual famine episodes, with baseline estimates remaining well within the range of leave-one-out re-estimates (Fig. 26).

Inference and Standard Errors Our results are robust to alternative standard error corrections, including Conley spatial clustering and two-way clustering (Tables 19–21).

Reverse Causality Granger causality tests reject the possibility that grain prices or harvests predict ENSO anomalies, alleviating concerns of reverse causality (Table 22).

Choice of ENSO Index We confirm robustness to the choice of ENSO index: results hold across NINO1+2, NINO3, NINO3.4, and NINO4 reconstructions (Fig. 23).

Acknowledgments

This project was funded by the European Research Council (ERC) under the European Union's Horizon 2020 research and innovation programme (4-OCEANS, grant no. 951649). F.C.L. was supported by the Swedish Research Council (Vetenskapsrådet, grant no. 2023-00605) and the Marianne and Marcus Wallenberg Foundation (grant no. MMW 2022-0114). A.S. was supported by the Swedish Research Council (Vetenskapsrådet, grant no. 2023-00605). We thank Maria Waldinger for sharing the grain yield data she processed from Slicher van Bath [41] and Enrique Llopis for the Spanish yield data published in Llopis et al. [81]. Maria Wallenberg Bondesson and Folke Lundström helped with digitizing grain harvest data from publications.

The authors declare no competing interests.

Author Contributions

Conceptualization: E.E., M.J.P., F.L., P.H., E.J., F.C.L.

Data curation: F.L., F.C.L.

Formal analysis: E.E., J.K.

Writing - original draft: All authors

Writing - review & editing: All authors

Data availability

All the codes and datasets used for this study can be found at https://github.com/emileDesmaili/enso-famine-paper

References

[1] Merry E Wiesner. *Early Modern Europe, 1450–1789*. Cambridge: Cambridge University Press, 2006.

[2] Christian Pfister and Heinz Wanner. *Climate and Society in Europe: The Last Thousand Years*. Bern: Haupt Verlag, 2021.

[3] Heinz Wanner, Christian Pfister, and Raphael Neukom. The variable European Little Ice Age. *Quaternary Science Reviews*, 287:107531, 2022. doi: 10.1016/j.quascirev.2022.107531.

[4] Guido Alfani and Cormac Ó Gráda. *Famine in European history*. Cambridge University Press, 2017. doi: 10.1017/9781316841235.

[5] Dominik Collet and Maximilian Schuh. *Famines During the 'Little Ice Age' (1300–1800): Socio-natural Entanglements in Premodern Societies*. Springer, Berlin/Heidelberg, 2018. doi: 10.1007/978-3-319-54337-6.

[6] Fredrik Charpentier Ljungqvist, Andrea Seim, and Dominik Collet. Famines in medieval and early modern Europe – Connecting climate and society. *WIREs Climate Change*, 15(1):e859, 2024. doi: https://doi.org/10.1002/wcc.859.

[7] Stephen Broadberry, Bruce M. S. Campbell, Alexander Klein, Mark Overton, and Bas van Leeuwen. *British Economic Growth, 1270–1870*. Cambridge University Press, Cambridge, 2015. doi: 10.1017/CBO9781107707603.

[8] Geoffrey Parker. *Global crisis: War, climate change and catastrophe in the seventeenth century*. Yale University Press, New Haven, 2013.

[9] Fredrik Charpentier Ljungqvist. Climate and society in European history. *WIREs Climate Change*, 12 (2):e691, 2021. doi: 10.1002/wcc.691.

[10] Fredrik Charpentier Ljungqvist and Andrea Seim. Reassessing grain price variability in early modern Europe (c. 1500–1800). *European Economic Review*, 170:104852, 2024. doi: 10.1016/j.euroecorev.2024.104852.

[11] Sam White, John Brooke, and Christian Pfister. Climate, weather, agriculture, and food. In Sam White, Christian Pfister, and Franz Mauelshagen, editors, *The Palgrave Handbook of Climate History*, pages 331–353. Springer, Berlin/Heidelberg, 2018. doi: 10.1057/978-1-137-43020-5_27.

[12] Edward S Sarachik and Mark A Cane. *The El Niño–Southern Oscillation phenomenon*. Cambridge University Press, 2010. doi: 10.1017/CBO9780511817496.

[13] Michael J. McPhaden, Stephen E. Zebiak, and Michael H. Glantz. ENSO as an integrating concept in earth science. *Science*, 314(5806):1740–1745, 2006. doi: 10.1126/science.1132588.

[14] Simon J Mason and Lisa Goddard. Probabilistic precipitation anomalies associated with ENSO. *Bulletin of the American Meteorological Society*, 82(4):619–638, 2001. doi: 10.1175/1520-0477(2001)082<0619:PPAAWE>2.3.CO;20.

[15] Jitendra Singh, Moetasim Ashfaq, Christopher B Skinner, Weston B Anderson, Vimal Mishra, and Deepti Singh. Enhanced risk of concurrent regional droughts with increased ENSO variability and warming. *Nature Climate Change*, 12(2):163–170, 2022. doi: 10.1038/s41558-021-01276-3.

[16] Christopher W. Callahan and Justin S. Mankin. Persistent effect of El Niño on global economic growth. *Science*, 380(6649):1064–1069, 2023. doi: 10.1126/science.adf2983.

[17] Toshichika Iizumi, Jing-Jia Luo, Andrew J Challinor, Gen Sakurai, Masayuki Yokozawa, Hirofumi Sakuma, Molly E Brown, and Toshio Yamagata. Impacts of El Niño Southern Oscillation on the global yields of major crops. *Nature Communications*, 5(1):3712, 2014. doi: 10.1038/ncomms4712.

[18] Yi Liu, Wenju Cai, Xiaopei Lin, Ziguang Li, and Ying Zhang. Nonlinear El Niño impacts on the global economy under climate change. *Nature Communications*, 14(1):5887, 2023. doi: 10.1038/s41467-023-41551-9.

[19] Matias Heino, Michael J Puma, Philip J Ward, Dieter Gerten, Vera Heck, Stefan Siebert, and Matti Kummu. Two-thirds of global cropland area impacted by climate oscillations. *Nature Communications*, 9(1):1257, 2018. doi: 10.1038/s41467-017-02071-5.

[20] Mike Davis. *Late Victorian Holocausts: El Niño Famines and the Making of the Third World*. Verso, London; New York, 2001.

[21] Solomon Hsiang, Kyle Meng, and Mark Cane. Civil conflicts are associated with the global climate. *Nature*, 476(7361):438–441, 2011. doi: 10.1038/nature10311.

[22] Jakob Bjerknes. Atmospheric teleconnections from the equatorial pacific. *Monthly weather review*, 97 (3):163–172, 1969.

[23] C. F. Ropelewski and M. S. Halpert. Global and regional scale precipitation patterns associated with the El Niño/Southern Oscillation. *Monthly Weather Review*, 115:1606–1626, 1987. doi: 10.1175/1520-0493(1987)115<1606:GARSPP>2.0.CO;2.

[24] Jeffrey Shaman. The seasonal effects of ENSO on European precipitation: Observational analysis. *Journal of Climate*, 27(17):6423–6438, 2014. doi: 10.1175/JCLI-D-14-00008.1.

[25] M. Martija-Díez, J. López-Parages, B. Rodríguez-Fonseca, et al. The stationarity of the ENSO teleconnection in European summer rainfall. *Climate Dynamics*, 61:489–506, 2023. doi: 10.1007/s00382-022-06596-4.

[26] Richard H. Grove. Global impact of the 1789–93 El Niño. *Nature*, 393:318–319, 1998. doi: 10.1038/30674.

[27] Richard H Grove. The great El Niño of 1789–93 and its global consequences: Reconstructing an extreme climate event in world environmental history. *The Medieval History Journal*, 10(1-2):75–98, 2006. doi: 10.1177/09719458070100020.

[28] Poul Holm, Francis Ludlow, Cordula Scherer, Charles Travis, Bernard Allaire, Cristina Brito, Patrick W. Hayes, J. Al Matthews, Kieran J. Rankin, Richard J. Breen, and et al. The North Atlantic Fish Revolution (ca. AD 1500). *Quaternary Research*, 108:92–106, 2022. doi: 10.1017/qua.2018.153.

[29] Edward R. Cook and Mark A. Cane. Tree rings reveal ENSO in the last millennium. *Geophysical Research Letters*, 51(19):e2024GL109759, 2024. doi: https://doi.org/10.1029/2024GL109759.

[30] Dylan Hogan and Wolfram Schlenker. Chapter 2 – Empirical approaches to climate change impact quantification. volume 1 of *Handbook of the Economics of Climate Change*, pages 53–111. North-Holland, 2024. doi: https://doi.org/10.1016/bs.hesecc.2024.10.006.

[31] Axel Timmermann, Soon-Il An, Jong-Seong Kug, Fei-Fei Jin, Wenju Cai, Antonietta Capotondi, Kim M Cobb, Matthieu Lengaigne, Michael J McPhaden, Malte F Stuecker, et al. El niño–southern oscillation complexity. *Nature*, 559(7715):535–545, 2018.

[32] Peter Brecke. Violent conflicts 1400 AD to the present in different regions of the world. In *1999 Meeting of the Peace Science Society*. Ann Arbor, Michigan, 1999.

[33] Veronika Valler, Jörg Franke, Yuri Brugnara, Eric Samakinwa, Ralf Hand, Elin Lundstad, Angela-Maria Burgdorf, Laura Lipfert, Andrew Friedman, and S. Brönnimann. ModE-RA: a global monthly paleo-reanalysis of the modern era 1421 to 2008. *Scientific Data*, 11:36, 01 2024. doi: 10.1038/s41597-023-02733-8.

[34] Edward R. Cook, Richard Seager, Yochanan Kushnir, Keith R. Briffa, Ulf Büntgen, David Frank, Paul J. Krusic, Willy Tegel, Gerard van der Schrier, Laia Andreu-Hayles, Mike Baillie, Claudia Baittinger, Niels Bleicher, Niels Bonde, David Brown, Marco Carrer, Richard Cooper, Katarina Čufar, Christoph Dittmar, Jan Esper, Carol Griggs, Björn Gunnarson, Björn Günther, Emilia Gutierrez, Kristof Haneca, Samuli Helama, Franz Herzig, Karl-Uwe Heussner, Jutta Hofmann, Pavel Janda, Raymond Kontic, Nesibe Köse, Tomáš Kyncl, Tom Levanič, Hans Linderholm, Sturt Manning, Thomas M. Melvin, Daniel Miles, Burkhard Neuwirth, Kurt Nicolussi, Paola Nola, Momchil Panayotov, Ionel Popa, Andreas Rothe, Kristina Seftigen, Andrea Seim, Helene Svarva, Miroslav Svoboda, Terje Thun, Mauri Timonen, Ramzi Touchan, Volodymyr Trotsiuk, Valerie Trouet, Felix Walder, Tomasz Ważny, Rob Wilson, and Christian Zang. Old World megadroughts and pluvials during the Common Era. *Science Advances*, 1(10):e1500561, 2015. doi: 10.1126/sciadv.1500561.

[35] Jake M. Hofman, Duncan J. Watts, Susan Athey, et al. Integrating explanation and prediction in computational social science. *Nature*, 595(7866):181–188, 2021. doi: 10.1038/s41586-021-03659-0.

[36] D. Zanchettin, S. W. Franks, P. Traverso, and M. Tomasino. On ENSO impacts on European wintertime rainfalls and their modulation by the NAO and the Pacific multi-decadal variability described through the PDO index. *The International Journal of Climatology*, 28:995–1006, 2008. doi: 10.1002/joc.1601.

[37] A. Wu and W. W. Hsieh. The nonlinear association between ENSO and the Euro-Atlantic winter sea level pressure. *Climate Dynamics*, 23:859–868, 2004. doi: 10.1007/s00382-004-0470-5.

[38] H. van Loon and R. A. Madden. The Southern Oscillation. Part I: Global associations with pressure and temperature in northern winter. *Mon. Wea. Rev.*, 109:1150–1162, 1981. doi: 10.1175/1520-0493(1981)109<1150:TSOPIG>2.0.CO;2.

[39] F. C. Ljungqvist, B. Christiansen, J. Esper, H. Huhtamaa, L. Leijonhufvud, C. Pfister, A. Seim, M. K. Skoglund, and P. Thejll. Climatic signatures in early modern European grain harvest yields. *Climate of the Past*, 19(12):2463–2491, 2023. doi: 10.5194/cp-19-2463-2023.

[40] Òscar Jordà, Moritz Schularick, and Alan M. Taylor. The effects of quasi-random monetary experiments. *Journal of Monetary Economics*, 112:22–40, 2020. doi: https://doi.org/10.1016/j.jmoneco.2019.01.021.

[41] BH Slicher van Bath. *Yield ratios, 810–1820*. Afdeling Agrarische Geschiedenis, Landbouwhogeschool, 1963.

[42] Patricia M. Grambsch and Terry M. Therneau. Proportional hazards tests and diagnostics based on weighted residuals. *Biometrika*, 81(3):515–526, 1994. ISSN 00063444. URL http://www.jstor.org/stable/2337123.

[43] T. Związek, P. Guzowski, R. Poniat, M. T. Radomski, M. Kozłowska-Szyc, T. Panecki, S. Słowińska, B. Kruczkowska, M. Targowski, and D. Adamska. On the economic impact of droughts in central europe: the decade from 1531 to 1540 from the polish perspective. *Climate of the Past*, 18(7):1541–1561, 2022. doi: 10.5194/cp-18-1541-2022. URL https://cp.copernicus.org/articles/18/1541/2022/.

[44] Karl Gunnar Persson. *Grain Markets in Europe, 1500–1900: Integration and Deregulation*. Cambridge University Press, Cambridge, 1999. doi: 10.1017/CBO9780511496820.

[45] Giovanni Federico. Market integration. In *Handbook of Cliometrics*, pages 899–924. Springer, 2024. doi: 10.1007/978-3-642-40458-0_68-1.

[46] Giovanni Federico, Max-Stephan Schulze, and Oliver Volckart. European goods market integration in the very long run: From the Black Death to the First World War. *The Journal of Economic History*, 81 (1):276–308, 2021. doi: 10.1017/S0022050720000637.

[47] Giovanni Federico. How much do we know about market integration in Europe? *The Economic History Review*, 65(2):470–497, 2012. doi: 10.1111/j.1468-0289.2011.00608.x.

[48] Fredrik Ljungqvist, Peter Thejll, Bo Christiansen, Andrea Seim, Claudia Hartl, and Jan Esper. The significance of climate variability on early modern European grain prices. *Cliometrica*, 16:29–77, 2022. doi: 10.1007/s11698-021-00224-7.

[49] Arnaud Bertrand, Matthieu Lengaigne, Ken Takahashi, Angel Avadi, Florence Poulain, and Chris Harrod. *El Niño Southern Oscillation (ENSO) Effects on Fisheries and Aquaculture*. The Food and Agriculture Organization (FAO), 2020. doi: 10.4060/ca8348en.

[50] Herbert Hitzbleck. *Die Bedeutung des Fisches für die Ernährungswirtschaft Mitteleuropas in vorindustrieller Zeit unter besonderer Berücksichtigung Niedersachsens*. Göttingen, 1971.

[51] Regina Grafe. *Bacalao: A New Consumer Good Takes on the Peninsula*, pages 52–79. Princeton University Press, 2012. ISBN 9780691144849.

[52] Bernard Allaire and Poul Holm. The price of fish in French supply contracts (1538–1751). A quantitative approach to the early modern French fish market. *Food & History*, 20:41–66, 2022. doi: 10.1484/J.FOOD.5.129871.

[53] Ernest Labrousse. *La crise de l'économie française à la fin de l'Ancien Régime et au début de la Révolution*. Presses Universitaires de France, 1944.

[54] Jean Meuvret. Les crises de subsistances et la démographie de la France d'Ancien Régime. *Population*, pages 643–650, 1946.

[55] Hakon Albers and Ulrich Pfister. Food crises in Germany, 1500–1871. *Jahrbuch für Wirtschaftsgeschichte/Economic History Yearbook*, 66:267–309, 2025. doi: 10.1515/jbwg-2025-0010.

[56] Cormac Ó Gráda. "The last, the most dreadful resource of nature": Economic-historical reflections on famine. *Atlantic Economic Journal*, 44:225–241, 2016. doi: 10.1007/s11293-016-9494-6.

[57] Philip Slavin. Climate and famines: a historical reassessment. *WIREs Climate Change*, 7(4):433–447, 2016. doi: doi.org/10.1002/wcc.395.

[58] John Walter and Roger Schofield, editors. *Famine, Disease and the Social Order in Early Modern Society*. Cambridge University Press, Cambridge, 1989. doi: 10.1017/CBO9780511599637.

[59] Dominik Collet. *Die doppelte Katastrophe: Klima und Kultur in der europäischen Hungerkrise 1770–1772*. Vandenhoeck & Ruprecht, Göttingen, 2019.

[60] Walter Bauernfeind and Ulrich Woitek. The influence of climatic change on price fluctuations in Germany during the 16th century price revolution. *Explorations in Economic History*, 36(3):303–321, 1999. doi: 10.1023/A:1005502518695.

[61] E. R. Cook, O. Solomina, V. Matskovsky, B. I. Cook, L. Agafonov, A. Berdnikova, E. Dolgova, A. Karpukhin, N. Knysh, M. Kulakova, V. Kuznetsova, T. Kyncl, J. Kyncl, O. Maximova, I. Panyushkina, A. Seim, D. Tishin, T. Ważny, and M. Yermokhin. The European Russia Drought Atlas (1400–2016 CE). *Climate Dynamics*, 54(3–4):2317–2335, 2020. doi: 10.1007/s00382-019-05115-2.

[62] Tommy Bengtsson, Cameron Campbell, and James Z. Lee, editors. *Life under Pressure: Mortality and Living Standards in Europe and Asia*. MIT Press, Cambridge, MA, 2004.

[63] Andrew Hultgren, Tamma Carleton, Michael Delgado, Diana R. Gergel, Michael Greenstone, Trevor Houser, Solomon Hsiang, Amir Jina, Robert E. Kopp, Steven B. Malevich, Kelly E. McCusker, Terin Mayer, Ishan Nath, James Rising, Ashwin Rode, and Jiacan Yuan. Impacts of climate change on global agriculture accounting for adaptation. *Nature*, 642:644–652, 2025. doi: 10.1038/s41586-025-09085-w.

[64] Tamma Carleton, Amir Jina, Michael Delgado, Michael Greenstone, Trevor Houser, Solomon Hsiang, Andrew Hultgren, Robert E Kopp, Kelly E McCusker, Ishan Nath, James Rising, Ashwin Rode, Hee Kwon Seo, Arvid Viaene, Jiacan Yuan, and Alice Tianbo Zhang. Valuing the global mortality consequences of climate change accounting for adaptation costs and benefits. *The Quarterly Journal of Economics*, 137(4):2037–2105, 04 2022. doi: 10.1093/qje/qjac020.

[65] Guido Alfani and Cormac Ó Gráda. The timing and causes of famines in Europe. *Nature Sustainability*, 1(6):283–288, 2018. doi: 10.1038/s41893-018-0078-0.

[66] Jason E Smerdon, Edward R Cook, and Nathan J Steiger. The historical development of large-scale paleoclimate field reconstructions over the Common Era. *Reviews of Geophysics*, 61(4):e2022RG000782, 2023. doi: 10.1029/2022RG000782.

[67] N. A. Rayner, D. E. Parker, E. B. Horton, C. K. Folland, L. V. Alexander, D. P. Rowell, E. C. Kent, and A. Kaplan. Global analyses of sea surface temperature, sea ice, and night marine air temperature since the late nineteenth century. *Journal of Geophysical Research*, 108:4407, 2003. doi: 10.1029/2002JD002670.

[68] Richard Warren, Niklaus Emanuel Bartlome, Noémie Wellinger, Jörg Franke, Ralf Hand, Stefan Brönnimann, and Heli Huhtamaa. ClimeApp: data processing tool for monthly, global climate data from the ModE-RA palaeo-reanalysis, 1422 to 2008 CE. *Climate of the Past*, 20:2645–2662, 2024. doi: 10.5194/cp-20-2645-2024.

[69] Jürg Luterbacher, Daniel Dietrich, Elena Xoplaki, Martin Grosjean, and Heinz Wanner. European seasonal and annual temperature variability, trends and extremes since 1500. *Science*, 303(5663):1499–1503, 2004. doi: 10.1126/science.1093877.

[70] Andreas Pauling, Jürg Luterbacher, Christoph Casty, and Heinz Wanner. Five hundred years of gridded high-resolution precipitation reconstructions over Europe and the connection to large-scale circulation. *Climate Dynamics*, 26(4):387–405, 2006. doi: 10.1007/s00382-005-0090-8.

[71] John Matthews. *European Marine Fish Market Dynamics, 1500 to 1800 CE*. PhD thesis, 10 2021.

[72] R. C. Allen and R. W. Unger. The Allen-Unger Global Commodity Prices Database. *Research Data Journal for the Humanities and Social Sciences*, 4:81–90, 2019. doi: doi.org/10.1163/24523666-00401006.

[73] Jerome H. Friedman. Greedy function approximation: A gradient boosting machine. *The Annals of Statistics*, 29(5):1189–1232, 2001. doi: 10.1214/aos/1013203451.

[74] Òscar Jordà. Estimation and inference of impulse responses by local projections. *American Economic Review*, 95(1):161–182, 2005. doi: 10.1257/0002828053828518.

[75] John C. Driscoll and Aart C. Kraay. Consistent covariance matrix estimation with spatially dependent panel data. *The Review of Economics and Statistics*, 80(4):549–560, 1998. doi: 10.1162/003465398557825.

[76] D. R. Cox. Regression models and life-tables. *Journal of the Royal Statistical Society B*, 34(2):187–220, 1972. doi: 10.1111/j.2517-6161.1972.tb00899.x.

[77] Noah Simon, Jerome Friedman, Trevor Hastie, and Robert Tibshirani. Regularization paths for Cox's proportional hazards model via coordinate descent. *Journal of Statistical Software*, 39(5):1–13, 2011. doi: 10.18637/jss.v039.i05.

[78] Hemant Ishwaran, Udaya B. Kogalur, Eugene H. Blackstone, and Michael S. Lauer. Random survival forests. *The Annals of Applied Statistics*, 2(3):841–860, 2008. doi: 10.1214/08-AOAS169.

[79] Greg Ridgeway. The state of boosting. *Computing Sciences and Statistics*, 31:172–181, 1999.

[80] Robert C Allen. The great divergence in European wages and prices from the Middle Ages to the First World War. *Explorations in Economic History*, 38(4):411–447, 2001. doi: 10.1006/exeh.2001.0775.

[81] Enrique Llopis, Elvira Alonso, Paloma Fontanillo, Sara Méndez, Javier Ramos, and Ana Toyos. The severity of wheat yield crises on eight Spanish farms, 1700–1774. *Historia Agraria*, 82:1–34, 2020. doi: 10.26882/histagrar.082e01t.

[82] Moritz John Elsas. *Umriss einer geschichte der preise und löhne in Deutschland: vom ausgehenden mittelalter bis zum beginn des neunzehnten jahrhunderts*. AW Sijthoff, Leiden, 1936–1949.

[83] Nuno Palma and Jaime Reis. From convergence to divergence: Portuguese economic growth, 1527–1850. *The Journal of Economic History*, 79:477–506, 2019. doi: 10.1017/S0022050719000056.

[84] JE Thorold Rogers. *Agriculture and Prices in England*. Clarendon Press, Oxford, 1887.

[85] Tadeusz Furtak. *Ceny w Gdańsku w latach 1701–1815*. Slkł. gł.: Kasa im. J. Mianowskiego, 1935.

[86] Earl Jefferson Hamilton. *American Treasure and the Price Revolution in Spain, 1501–1650*. Harvard University Press, Cambridge, MA, 1934.

[87] Philip T Hoffman. *Growth in a Traditional Society: The French Countryside, 1450–1815*. Princeton University Press, Princeton, 1996.

[88] Auguste Hanauer. *Études économiques sur l'Alsace ancienne et moderne*. A. Durand & Pédone-Lauriel, Paris, 1878.

[89] Alfred Francis Pribram. *Materialien zur Geschichte der Preise und Löhne in Österreich*. Carl Ueberreuters Verlag, Vienna, 1938.

[90] Paolo Malanima. Aspetti di mercato e prezzi del grano e della segale a Pisa dal 1548 al 1818. In M. Mirri, editor, *Ricerche di storia moderna*, pages 288–327. Pacini, Pisa, 1976.

[91] Thomas Rahlf. *Getreide in der Sozial- und Wirtschaftsgeschichte vom 16. bis 18. Jahrhundert, Das Beispiel Köln im regionalen Vergleich*. Auenthal Verlag, Trier, 1996.

[92] David S Jacks. Market integration in the North and Baltic Seas, 1500–1800. *Journal of European Economic History*, 33:285–329, 2004.

[93] Rainer Metz. *Geld, Währung und Preisentwicklung: Der Niederrheinraum im europäischen Vergleich 1350–1800*. Schriftenreihe des Instituts für bankhistorische Forschung, Frankfurt am Main, 1990.

[94] Julian Pelc. *Ceny w Gdańsku w XVI i XVII wieku*. skł. gł. Kasa im. Mianowskiego-Instytut Popierania Polskiej Twórczości Naukowej, Lwów, 1937.

[95] H Hauser. *Recherches et documents sur l'histoire des prix en France depuis 1500 à 1800*. Les Presses modernes, Paris, 1936.

[96] Georges Frêche and Geneviève Frêche. *Les prix des grains des vins et des legumes a Toulouse, 1486–1868*. Presses universitaires de France, Paris, 1967.

[97] CA Verrijn Stuart. Overzicht van marktprijzen van granen te Arnhem in de jaren 1544–1901. *Bijdragen tot de Statistiek van Nederland*, 26:19–23, 1903.

[98] René Baehrel. *Une croissance: La basse provence rurale de la fin du XVIe siècle a 1789*. Éditions de l'École des Hautes Études en Sciences sociales, Paris, 1961.

[99] Gaspar Feliu. *Precios y salarios en la Cataluña moderna*. Banco de España, Madrid, 1991.

[100] Gabriele Lombardini. *Pane e denaro a Bassano*. Neri Pozza, Bassano del Grappa, 1963.

[101] Dietrich Ebeling and Franz Irsigler. *Getreideumsatz, Getreide- und Brotpreise in Köln, 1368–1797*. Böhlau-Verlag, Cologne, 1976.

[102] Brian R Mitchell. *Abstract of British Historical Statistics*. Cambridge University Press, Cambridge, 1971.

[103] Nicolaas Wilhelmus Posthumus. *Inquiry into the History of Prices in Holland*. E.J. Brill, Leiden, 1946–1964.

[104] Nunzio Federigo Faraglia. *Storia dei prezzi in Napoli dal 1131 al 1860*. A. Forni, Naples, 1878.

[105] G. Parenti. *Prezzi e mercato del grano a Siena 1546–1765*. c. Cya, Florence, 1942.

[106] Jérome Alexandre Sillem. *Tabellen van Marktprijzen van Granen te Utrecht in de Jaren 1393 tot 1644, uit de rekeningen en weeklijsten der Domprossdij*. J. Müller, Amsterdam, 1901.

[107] Earl Jefferson Hamilton. *Money, Prices, and Wages in Valencia, Aragon, and Navarre, 1351–1500*. Harvard University Press, Cambridge, MA, 1936.

[108] Roman Studer. *The Great Divergence Reconsidered: Europe, India, and the Rise to Global Economic Power*. Cambridge University Press, Cambridge, 2015. doi: https://doi.org/10.1017/CBO9781139104234.

[109] Gunnar Olsen. Studier i Danmarks Kornavl og Kornhandelspolitik i Tiden 1610–60. *Historisk Tidsskrift*, 10:428–484, 1942–1944.

[110] Joseph Goy. Dîmes, rendements, états des récoltes et revenu agricole réel. In *Les fluctuations du produit de la dîme: Conjoncture décimale et domaniale de la fin du Moyen Âge au XVIIIè siècle*, page 393. Mouton & Co, Paris, 1972.

[111] Emmanuel Le Roy Ladurie. *Les paysans de Languedoc*. Mouton & Co., Paris: The Hague, 1966.

[112] B. Veyrassat-Herren. Dîmes alsaciennes. In Joseph Goy and Emmanuel Le Roy Ladurie, editors, *Les fluctuations du produit de la dîme: Conjoncture décimale et domaniale de la fin du Moyen Âge au 18. siècle*, pages 83–102. École pratique des hautes études, Paris, 1972.

[113] Joseph Goy. Les rendements du blé au pays d'Arles, XVIè–XVIIIè siècles. In Joseph Goy and Emmanuel Le Roy Ladurie, editors, *Les fluctuations du produit de la dîme: Conjoncture décimale et domaniale de la fin du Moyen Âge au 18. siècle*. École pratique des hautes études, Paris, 1972.

[114] Hugues Neveux. La production céréalière dans une région frontalière: le Cambrésis du XVe au XVIIIe siècle. In *Les fluctuations du produit de la dîme: Conjoncture décimale et domaniale de la fin du Moyen Âge au XVIIIe siècle*, pages 63–64. Mouton & Co, Paris, 1972. doi: 10.1515/9783111413822-004.

[115] Albert Silbert. La production des céréales à Beaune d'après les dîmes, XVIe–XVIIIe siècles. In *Les fluctuations du produit de la dîme: Conjoncture décimale et domaniale de la fin du Moyen Âge au XVIIIe siècle*, pages 151–152. Mouton & Co, Paris, 1972. doi: 10.1515/9783111413822-008.

[116] I. Hunyadi. Production agricole dans le diocèse de Györ au XVIe siècle: Bilan provisoire. In *Prestations paysannes: Dîmes, rente foncière et mouvement de la production agricole à l'époque préindustrielle*, pages 75–92. Mouton éditeur, Paris, 1978. doi: 10.1515/9783112316047-006.

[117] R. Davico. Produzione agricola piemontese e gabelle siciliane: Due esempi. In *Prestations paysannes: Dîmes, rente foncière et mouvement de la production agricole à l'époque préindustrielle*. Mouton, Paris, 1978. doi: 10.1515/9783112316047-014.

[118] Jean-Marie Yante. Grains et vins des terroirs mosellans de Remich et Grevenmacher (XV^{e}–XVIII^{e} siècles). *Revue belge de Philologie et d'Histoire*, 63:273–309, 1985.

[119] Antonio Eiras Roel. Dîme et mouvement du produit agricole en Galice 1600–1837. In Joseph Goy and Emmanuel Le Roy Ladurie, editors, *Prestations paysannes, dîmes, rente foncière et mouvements de la production agricole à l'époque pré-industrielle*, pages 341–358. Paris: Mouton, 1982.

[120] José Manuel Latorre Ciria. La producción agraria en el sur de Aragón (1660–1827). *Hist. Agrar.*, 41: 3–30, 2007.

[121] Carlos Santiago-Caballero. Tithe series and grain production in central Spain, 1700–1800. *Rural History*, 25:15–37, 2014. doi: 10.1017/S0956793313000186.

[122] Pierre Ponsot. En Andalousie occidentale: Les fluctuations de la production du blé sous l'Ancien Régime. *Études rurales*, 34:97–112, 1969.

[123] P. Ponsot. Malthus n'était-il pas prophète en Andalousie? Les rendements des céréales en Basse Andalousie, XVIIè–XIXè siècles. In *Prestations paysannes: Dîmes, rente foncière et mouvement de la production agricole à l'époque préindustrielle*. Mouton, Paris, 1978. doi: 10.1515/9783112316047-030.

[124] J. J. Vidal. La evolución de la producción agrícola en Mallorca durante la Edad Moderna. Fuentes y problemas de su estudio. *Moneda y Crédito*, (145):93–99, 1978.

[125] M. K. Skoglund. Farming at the margin: Climatic impacts on harvest yields and agricultural practices in Central Scandinavia, c. 1560–1920. *Agricultural History Review*, 71:203–233, 2023.

[126] Lotta Leijonhufvud. *Grain Tithes and Manorial Yields in Early Modern Sweden: Trends and Patterns of Production and Productivity c. 1540–1680*. PhD thesis, Swedish University of Agricultural Sciences, Ulltuna, 2001.

[127] Erik Hallberg, Lotta Leijonhufvud, Martin Linde, and Lennart Andersson Palm. *Skördar i Sverige före agrarrevolutionen: Statistisk undersökning av det rörliga tiondet fr.o.m. 1665: Introduktion till databaser*. Department of Historical Studies, University of Gothenburg, Gothenburg, 2016.

[128] Christian Pfister. *Klimageschichte der Schweiz 1525–1860. Das Klima der Schweiz und seine Bedeutung in der Geschichte von Bevölkerung und Landwirtschaft*, volume 2. Verlag Paul Haupt, Bern, 1984.

[129] Anne-Lise Head-Köenig and Béatrice Veyrassat-Herren. Les revenus décimaux à Genève de 1540 à 1783. In Joseph Goy and Emmanuel Le Roy Ladurie, editors, *Les fluctuations du produit de la dîme:*

Conjoncture décimale et domaniale de la fin du Moyen Age au 18. siècle, pages 165–179. Paris: École pratique des hautes études, 1972.

[130] Anne-Lise Head-Köenig. Les fluctuations des rendements et du produit décimal céréaliers dans quelques régions du plateau suisse (1500–1800). *Revue Suisse d'histoire*, 29:575–604, 1979.

[131] Poul Holm, John Nicholls, Patrick W. Hayes, Josh Ivinson, and Bernard Allaire. Accelerated extractions of North Atlantic cod and herring 1520–1790. *Fish and Fisheries*, 23:54–72, 2021. doi: 10.1111/faf.12532.

[132] John Nicholls, Poul Holm, Patrick Hayes, Josh Ivinson, and Bernard Allaire. Norfish data collection, 2021.

[133] P. Ortega, F. Lehner, D. Swingedouw, J. Masson-Delmotte, J. Yiou, J. C. Raible, R. Neukom, M. V. Khodri, C. Mignot, and E. Zorita. A model-tested North Atlantic Oscillation reconstruction for the past millennium. *Nature*, 523(7558):71–74, 2015. doi: 10.1038/nature14518.

[134] Bianca Mezzina, Javier García-Serrano, Ileana Bladé, and Fred Kucharski. Dynamics of the ENSO teleconnection and NAO variability in the North Atlantic–European late winter. *Journal of Climate*, 33 (3):907–923, 2020. doi: 10.1175/JCLI-D-19-0192.1.

[135] L.S Parsons and W.H Lear. Climate variability and marine ecosystem impacts: a North Atlantic perspective. *Progress in Oceanography*, 49(1):167–188, 2001. doi: https://doi.org/10.1016/S0079-6611(01)00021-0.

[136] Maria Waldinger. The economic effects of long-term climate change: Evidence from the Little Ice Age. *Journal of Political Economy*, 130(9):2275–2314, 2022. doi: 10.1086/720393.

[137] R. Young and Solomon Hsiang. Mortality caused by tropical cyclones in the United States. *Nature*, 635:121–128, 2024. doi: 10.1038/s41586-024-07945-5.

[138] Timothy G Conley. Spatial econometrics. In *Microeconometrics*, pages 303–313. Springer, 2010. doi: 10.1057/9780230280816_33.

Supplementary

Table of contents below provides page numbers for both main text and Supplementary sections

Contents

A Grain Prices and Harvest Data References

Here we present tables with references to all grain price and grain harvest data. The grain price data has been collected by Ljungqvist and Seim [10], while some of the grain harvest data have been published in Ljungqvist et al. [39].

Table 2: The dataset of 69 annual grain price series from Ljungqvist and Seim [10] with information about location (city), the covered period, missing values ('gaps') within the covered period (in percent), mean price (g Ag/l) for the covered period, coefficient of variation (CV) of the price for the covered period, the auto-correlation (AR1) value of the grain prices, and original data source(s). Only price series covering at least the common period 1590–1700, and with a maximum of 35% data gaps, are included.

City	Coverage	Gaps	Mean price	CV	AR1	Reference(s)
Barley (11 series)						
Augsburg	1500–1800	2%	0.35	0.66	0.70	Elsas [82]
Coimbra	1515–1800	14.74%	0.45	0.38	0.52	Palma and Reis [83]
England	1500–1800	0.33%	0.29	0.47	0.86	Rogers [84]
Gdansk	1501–1800	23%	0.27	0.42	0.82	Furtak [85]
Lisbon	1511–1800	18.69%	0.46	0.35	0.57	Palma and Reis [83]
New Castile	1504–1750	15.85%	0.33	0.56	0.74	Hamilton [86]
Paris	1520–1800	3.93%	0.32	0.50	0.52	Hoffman [87]
Speyer	1514–1799	32.84%	0.32	0.49	0.59	Elsas [82]
Strasbourg	1500–1800	5.36%	0.27	0.67	0.82	Hanauer [88]
Vienna	1526–1800	17%	0.23	0.55	0.69	Pribram [89]
Wels	1501–1768	17.52%	0.24	0.42	0.68	Pribram [89]
Oats (6 series) Augsburg	1500–1800	1.67%	0.21	0.60	0.65	Elsas [82]
Paris	1528–1788	0.37%	0.26	0.40	0.68	Hoffman [87]
Pisa	1553–1800	6.07%	0.16	0.31	0.62	Malanima [90]
Southern England	1500–1702	2.48%	0.19	0.56	0.90	Rogers [84]
Speyer	1517–1799	31.21%	0.25	0.59	0.63	Elsas [82]
Strasbourg	1500–1800	9.33%	0.19	0.66	0.87	Hanauer [88]
Rye (20 series)						
Aachen	1531–1800	12.27%	0.40	0.37	0.51	Rahlf [91]
Augsburg	1500–1800	4.33%	0.40	0.50	0.77	Elsas [82]
Basle	1501–1797	23.31%	0.36	0.60	0.84	Hanauer [88]
Brussels	1575–1795	—	0.38	0.46	0.67	Jacks [92]
Coimbra	1517–1800	14.34%	0.53	0.42	0.57	Palma and Reis [83]
Cologne	1531–1797	0.75%	0.42	0.36	0.71	Metz [93]
Düren	1570–1783	—	0.44	0.32	0.57	Rahlf [91]
Frankfurt	1500–1800	41.31%	0.36	0.48	0.58	Elsas [82]
Gdansk	1538–1800	3.67%	0.28	0.41	0.75	Furtak [85], Pelc [94]
Ghent	1500–1795	—	0.51	0.57	0.73	Jacks [92]
Grenoble	1501–1781	1.69%	0.43	0.50	0.67	Hauser [95]
Leipzig	1572–1800	7.09%	0.35	0.47	0.51	Elsas [82]
Munich	1500–1773	17.60%	0.35	0.52	0.70	Elsas [82]
Paris	1520–1788	6.72%	0.39	0.64	0.43	Hoffman [87]
Pisa	1550–1800	2.61%	0.32	0.77	0.73	Malanima [90]
Speyer	1516–1800	22.40%	0.33	0.39	0.61	Elsas [82]
Strasbourg	1500–1800	4.23%	0.34	0.50	0.76	Hanauer [88]
Toulouse	1512–1792	0.67%	0.35	0.45	0.70	Frêche and Frêche [96]
Würzburg	1500–1799	7.86%	0.38	0.49	0.71	Elsas [82]
Xanten	1500–1800	—	0.31	0.46	0.70	Rahlf [91]
Wheat (32 series)						
Amsterdam	1500–1800	14.00%	0.56	0.34	0.74	Allen and Unger [72]

Table 2: Continued on next page

Table 2: continued from previous page

City	Coverage	Gaps	Mean price	CV	AR1	Reference(s)
Angers	1580–1789	—	0.56	0.37	0.66	Hauser [95]
Arnhem	1568–1800	—	0.66	0.33	0.66	Verrijn Stuart [97]
Avignon	1570–1789	0.46%	0.86	0.27	0.66	Baehrel [98]
Barcelona	1501–1800	3.01%	0.83	0.34	0.84	Feliu [99]
Bassano del Grappa	1501–1800	21.07%	0.89	0.36	0.73	Lombardini [100]
Brussels	1501–1796	2.71%	0.57	0.50	0.83	Jacks [92]
Cambridge	1500–1799	3.39%	0.55	0.57	0.70	Jacks [92]
Coimbra	1504–1800	12.71%	0.82	0.35	0.67	Palma and Reis [83]
Cologne	1531–1796	4.73%	0.49	0.25	0.74	Ebeling and Irsigler [101]
Douai	1500–1800	0.75%	0.45	0.68	0.73	Hauser [95]
Évora	1506–1800	21.67%	0.77	0.39	0.59	Palma and Reis [83]
Exeter	1500–1800	8.84%	0.64	0.48	0.79	Mitchell [102]
Grenoble	1501–1800	2.00%	0.60	0.45	0.73	Hauser [95]
Leiden	1500–1792	23.41%	0.69	0.35	0.77	Posthumus [103]
Leipzig	1564–1800	3.42%	0.44	0.44	0.65	Elsas [82]
Lisbon	1500–1800	36.11%	0.85	0.43	0.59	Palma and Reis [83]
London	1500–1800	—	0.63	0.56	0.78	Rogers [84]
Madrid	1501–1799	8.67%	0.68	0.50	0.79	Hamilton [86]
Naples	1500–1800	10.60%	0.61	0.37	0.65	Faraglia [104]
Oxford	1559–1799	—	0.68	0.38	0.65	Jacks [92]
Paris	—	2.50%	0.66	0.53	0.79	Hoffman [87]
Pisa	1548–1800	2.00%	0.43	0.33	0.71	Malanima [90]
Siena	1546–1765	—	0.69	0.34	0.74	Parenti [105]
Strasbourg	1500–1800	5.00%	0.48	0.61	0.79	Hanauer [88]
Toulouse	1500–1792	—	0.53	0.44	0.76	Frêche and Frêche [96]
Tours	1500–1788	2.74%	0.70	0.52	0.77	Hauser [95]
Utrecht	1500–1800	12.00%	0.57	0.33	0.78	Sillem [106]
Valencia	1500–1789	0.67%	0.94	0.37	0.91	Hamilton [107]
Vienna	1531–1800	21.80%	0.41	0.61	0.74	Pribram [89]
Würzburg	1500–1799	28.33%	0.48	0.49	0.64	Elsas [82]
Zürich	1540–1800	—	0.80	0.48	0.61	Studer [108]

Table 2: It ends from the previous page.

Table 3: Grain harvest records, including tithe, yield ratio and yield per unit records, with information about location, period covered, grain types, and reference(s). Abbreviations as follows for the grain types: B = barley; R = rye; O = oats; W = wheat; S = spelt; M = maize; Ri = Rice; B/R = barley/rye mixture; R/W = rye/wheat mixture.

Location	Period	Record Type	Grain Type(s)	Reference(s)
Denmark				
Zealand	1610–1659	Yield ratio	B, R	Olsen [109]
France				
Provence	1731–1788	Yield ratio	Mixed	Goy [110]
Agde	1593–1734	Tithe	Mixed	Ladurie [111]
Strasbourg	1484–1790	Tithe	Mixed	Veyrassat-Herren [112]
Beaume	1597–1788	Tithe	Mixed	Goy [113]
Beziers	1560–1764	Tithe	Mixed	Ladurie [111]
Cambresis	1402–1599	Tithe	O, W	Neveux [114]
St Trophime	1662–1788	Tithe	W	Goy [110]
Burgundy	1509–1788	Tithe	Mixed	Silbert [115]
Hungary				
Sopron	1429–1630	Tithe	Mixed	Hunyadi [116]
Italy				
Piemonte	1746–1797	Yield per unit	B, R, Ri, M, O, W	Davico [117]
Siena	1546–1667	Yield per unit	Mixed	Parenti [105]
Luxembourg				
Grevenmacher	1444-1680	Tithe	Mixed	Yante [118]
Remich	1444–1746	Tithe	Mixed	Yante [118]
Spain				
Mondoñedo	1595–1800	Tithe	Mixed	Eiras Roel [119]
Santiago	1606–1799	Tithe	Mixed	Eiras Roel [119]
Galice	1595–1800	Tithe	Mixed	Eiras Roel [119]
Orense	1598–1800	Tithe	Mixed	Eiras Roel [119]
Aragon	1660–1827	Tithe	W	Ciria [120]
Guadalajara	1700–1800	Tithe	B, R, O, W	Santiago-Caballero [121]
Calañas	1563–1835	Tithe	W	Ponsot [122]
Puebla de Guzman	1563–1835	Tithe	W	Ponsot [122]
Lucena	1563–1835	Tithe	W	Ponsot [122]
Bollullos	1563–1835	Tithe	W	Ponsot [122]
El Rincón farm	1699–1781	Yield ratio	W	Llopis et al. [81]
La Burguilla farm	1699–1781	Yield ratio	W	Llopis et al. [81]
Madrigalejo farm	1699–1781	Yield ratio	W	Llopis et al. [81]
La Vega farm	1699–1781	Yield ratio	W	Llopis et al. [81]
Quintanajuar farm	1699–1781	Yield ratio	W	Llopis et al. [81]
Panguia farm[a]	1695–1799	Yield per unit	W	Llopis et al. [81]
Farms of Matallana	1699–1781	Yield ratio	W	Llopis et al. [81]
Rinconada Alta farm[a]	1695–1799	Yield per unit	W	Llopis et al. [81]
Andalusia[a]	1616–1800	Yield per unit	B, W	Ponsot [123]

Continued on next page

Table 3 – *Continued from previous page*

Location	Period	Record Type	Grain Type(s)	Source(s)
Cortijo Pan Ximenez, Andalusia	1611–1800	Yield ratio	B, W	Ponsot [123]
El Alto Mijares	1680–1800	Tithe	Mixed	**?**]
El Camp de Morvedre	1680–1800	Tithe	Mixed	**?**]
El Camp de Túria	1680–1800	Tithe	Mixed	**?**]
El Comtat	1680–1800	Tithe	Mixed	**?**]
El Valle de Cofrentes	1680–1800	Tithe	Mixed	**?**]
L'Alcoià	1680–1800	Tithe	Mixed	**?**]
La Canal de Navarrés	1680–1800	Tithe	Mixed	**?**]
La Costera	1680–1800	Tithe	Mixed	**?**]
La Hoya de Buñol	1680–1800	Tithe	Mixed	**?**]
L'Horta	1680–1800	Tithe	Mixed	**?**]
La Marina Alta	1680–1800	Tithe	Mixed	**?**]
La Marina Baixa	1680–1800	Tithe	Mixed	**?**]
La Safor	1680–1800	Tithe	Mixed	**?**]
La Vall d'Albaida	1680–1800	Tithe	Mixed	**?**]
Les Riberes	1680–1800	Tithe	Mixed	**?**]
Los Serranos	1680–1800	Tithe	Mixed	**?**]
País Valenciano	1680–1800	Tithe	Mixed	**?**]
Mallorca	1466–1800	Tithe	B, O, W	Vidal [124]
Sweden				
Härjedalen	1582–1800	Tithe	Mixed	Skoglund [125]
Jämtland	1565–1800	Tithe	Mixed	Skoglund [125]
Kopparberg County	1572–1740	Tithe	B/R, O, W	Leijonhufvud [126], Hallberg et al. [127]
Örebro County	1665–1720	Tithe	B/R, O, W	Leijonhufvud [126], Hallberg et al. [127]
Östergötland County	1573–1680	Tithe	B/R, O, W	Leijonhufvud [126], Hallberg et al. [127]
Södermanland County	1572–1681	Tithe	B/R, O, W	Leijonhufvud [126], Hallberg et al. [127]
Stockholm County	1572–1730	Tithe	B/R, O, W	Leijonhufvud [126], Hallberg et al. [127]
Uppsala County	1572–1740	Tithe	B/R, O, W	Leijonhufvud [126], Hallberg et al. [127]
Värmland County	1575–1730	Tithe	B/R, O, W	Leijonhufvud [126], Hallberg et al. [127]
Västmanland County	1572–1740	Tithe	B/R, O, W	Leijonhufvud [126], Hallberg et al. [127]
Switzerland				
Burgdorf	1550–1825	Tithe	R/W	Pfister [128]
Cappelerhof	1531–1797	Tithe	R/W	Pfister [128]
Fraumünsteramt	1531–1797	Tithe	R/W	Pfister [128]
Frienisberg	1529–1797	Tithe	R/W	Pfister [128]
Geneva	1542–1780	Tithe	R/W	Head-Köenig and Veyrassat-Herren [129]
Gottstatt	1558–1825	Tithe	R/W	Pfister [128]
Königsfelden	1556–1797	Tithe	R/W	Pfister [128]
Köniz	1732–1825	Tithe	R/W	Pfister [128]
Lausanne	1538–1796	Tithe	R/W	Pfister [128]
Moudon	1564–1796	Tithe	R/W	Pfister [128]
Nidau	1535–1800	Tithe	R/W	Pfister [128]
Romainmôtier	1538–1796	Tithe	R/W	Pfister [128]
Spital	1700–1797	Tithe	R/W	Pfister [128]
Stift Bern	1529–1796	Tithe	R/W	Pfister [128]
Töss	1529–1797	Tithe	R/W	Pfister [128]
Trachselwald	1534–1797	Tithe	R/W	Pfister [128]
Wädenswil	1533–1797	Tithe	R/W	Pfister [128]
Wangen	1686–1800	Tithe	R/W	Pfister [128]

Continued on next page

Table 3 – *Continued from previous page*

Location	Period	Record Type	Grain Type(s)	Source(s)
Zofingen	1542–1797	Tithe	R/W	Pfister [128]
Basel	1500–1800	Yield ratio	R, S	Head-Köenig [130]
St. Gallen	1549–1799	Yield ratio	S	Head-Köenig [130]
Zurich	1501–1800	Yield ratio	R, S	Head-Köenig [130]
Winterthur	1536–1785	Yield ratio	R, S	Head-Köenig [130]

Table 4: Summary Statistics of Famine Episodes

	Region	mean	sd	min	max	N
duration	Central Europe	3.23	1.41	1.00	6.00	22
	France	2.44	1.62	1.00	6.00	18
	Great Britain	2.80	0.79	1.00	4.00	10
	Ireland	3.56	3.36	1.00	12.00	9
	Italy	3.13	2.01	1.00	11.00	23
	Low Countries	2.50	0.65	2.00	4.00	14
	Nordic Countries	3.18	1.62	1.00	8.00	22
	Russia/Ukraine	2.14	1.56	1.00	5.00	21
	Spain	3.29	1.90	1.00	8.00	21

B Summary Statistics and Spatial Coverage

We present here summary tables of our datasets for famine duration, grain harvests, grain prices, and fish prices. We show the spatial coverage of the harvest and price data in Figure 6.

(a) Grain Prices (b) Fish Prices (c) Grain Harvests

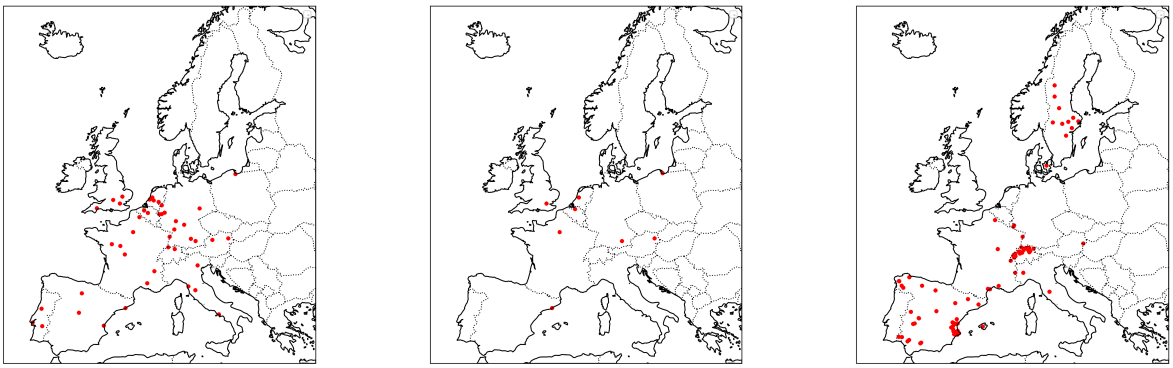

Figure 6: Spatial Coverage of Grain and Fish Prices and Harvest Series.

Table 5: Summary statistics for grain price data.

	Mean	SD	Min	Max	N
Price	0.54	0.31	0.04	3.99	11344
NINO3.4	0.05	0.67	−1.95	2.17	11344
scPDSI	−0.22	1.48	−6.73	5.17	11344
Temp. AMJJ	−0.15	0.60	−2.42	2.58	11344
Temp. NDJF	−0.22	0.77	−3.45	2.69	11344
Precip. AMJJ	0.97	9.34	−54.48	39.61	11344
Precip. NDJF	1.37	12.42	−82.20	68.30	11344
Ongoing wars	6.90	3.99	0.00	18.00	11344
Conflict deaths	69 916.78	103 485.59	0.00	446 412.37	11344

Table 6: Summary statistics for grain tithes data.

	Mean	SD	Min	Max	N
logyield	6.39	2.43	0.14	13.66	14915
NINO3.4	0.07	0.69	−1.95	2.17	14915
scPDSI	−0.19	1.44	−6.55	4.66	14915
Temp. AMJJ	−0.18	0.61	−2.42	2.58	14915
Temp. NDJF	−0.20	0.75	−3.38	2.81	14915
Precip. AMJJ	2.27	9.76	−54.48	40.77	14915
Precip. NDJF	3.42	13.48	−87.25	68.30	14915
Ongoing wars	6.29	3.96	0.00	18.00	14915
Conflict deaths	71 844.89	99 212.10	0.00	446 412.37	14915

Table 7: Summary statistics for yield ratio and yield per unit data.

	Mean	SD	Min	Max	N
logyield	3.08	3.29	−3.22	14.74	3934
NINO3.4	0.06	0.70	−1.95	2.17	3934
scPDSI	−0.19	1.47	−6.73	4.30	3934
Temp. AMJJ	−0.22	0.65	−2.42	2.58	3934
Temp. NDJF	−0.34	0.72	−3.38	2.17	3934
Precip. AMJJ	3.12	10.45	−47.83	39.61	3934
precip. NDJF	4.06	14.37	−69.30	65.24	3934
Ongoing wars	5.72	3.97	0.00	18.00	3934
Conflict deaths	75 013.27	102 854.78	0.00	446 412.37	3934

Table 8: Summary statistics for fish price data.

	Mean	SD	Min	Max	N
Price	53.62	166.35	0.00	2400.00	1451
NINO3.4	0.05	0.64	−1.95	2.17	1451
scPDSI	−0.19	1.37	−4.40	5.10	1451
Temp. AMJJ	−0.14	0.52	−2.03	1.73	1451
Temp. NDJF	−0.01	0.93	−3.64	2.36	1451
Precip. AMJJ	1.06	7.56	−23.91	25.70	1451
Precip. NDJF	2.86	8.85	−38.86	34.84	1451
Ongoing wars	7.26	3.90	0.00	18.00	1451
Conflict deaths	60 908.77	97 387.89	0.00	446 412.37	1451

C ENSO and the Onset of Famine periods

Causal Inference We provide here regression tables for our estimates of the regional impact of ENSO on the onset of famine periods (Table 9.) We regress a dummy of famine onset in Year t for Region r on the NINO3.4 index, controlling for local climate conditions (seasonal temperature, soil moisture, and precipitation) and broader measures of conflict across Europe. Using region fixed-effects as well as decade fixed-effects, we find a null effect of ENSO on the onset of famine periods overall but a very significant one for Central Europe, specifically when we interact our ENSO anomaly with each region. We estimate that a + 1° increase in NINO3.4 increased the probability that a famine would start in Central Europe by 7 percentage-points.

Machine Learning Attribution We report the estimated attribution of famine onsets in Central Europe using increasing subsets of predictors. For each specification, we present (A) observed and counterfactual famine onsets, (B) permutation feature importance, and (C) model performance.

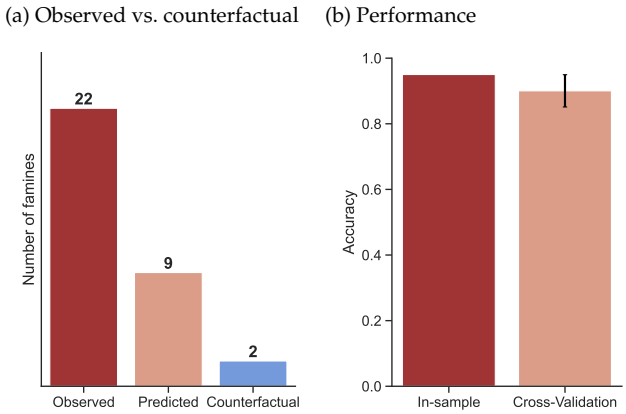

Figure 7: Attribution with NINO3.4 only.

Table 9: Effect of a 1°C Anomaly in the Nino 3.4 Index on the Probability of a Famine Start

Dependent Variable:	Famine Start					
Model:	(1)	(2)	(3)	(4)	(5)	(6)
	OLS	OLS	OLS	OLS	Logit	OLS
Variables						
Nino3.4 × RegionCentralEurope	0.0723***	0.0702***	0.0689***	0.0768***	1.538***	
	(0.0261)	(0.0265)	(0.0262)	(0.0282)	(0.4652)	
Nino3.4 × RegionFrance	0.0172	0.0150	0.0150	0.0157	0.4513	
	(0.0216)	(0.0210)	(0.0211)	(0.0208)	(0.4732)	
Nino3.4 × RegionGreatBritain	0.0093	0.0071	0.0101	0.0150	0.8692	
	(0.0124)	(0.0128)	(0.0120)	(0.0138)	(0.6711)	
Nino3.4 × RegionIreland	-0.0215	-0.0237	-0.0205	-0.0282*	-1.025	
	(0.0149)	(0.0153)	(0.0153)	(0.0154)	(0.9564)	
Nino3.4 × RegionItaly	-0.0134	-0.0156	-0.0177	-0.0194	-0.3218	
	(0.0219)	(0.0216)	(0.0214)	(0.0220)	(0.4716)	
Nino3.4 × RegionLowCountries	0.0129	0.0107	0.0122	0.0144	0.5977	
	(0.0202)	(0.0199)	(0.0199)	(0.0199)	(0.5476)	
Nino3.4 × RegionNordicCountries	-0.0054	-0.0076	-0.0093	-0.0107	-0.1889	
	(0.0256)	(0.0256)	(0.0258)	(0.0242)	(0.4728)	
Nino3.4 × RegionRussia/Ukraine	0.0130	0.0108	0.0096	0.0114	0.1626	
	(0.0219)	(0.0210)	(0.0210)	(0.0225)	(0.4210)	
Nino3.4 × RegionSpain	-0.0133	-0.0155	-0.0168	-0.0058	-0.2973	
	(0.0149)	(0.0156)	(0.0158)	(0.0160)	(0.5384)	
Nino3.4						0.0078
						(0.0073)
Decade FE	No	Yes	Yes	Yes	Yes	Yes
Region FE	No	No	Yes	Yes	Yes	Yes
Controls	No	No	No	Yes	Yes	Yes
Standard Errors	Newey-West	Newey-West	Driscoll-Kray	Driscoll-Kray	IID	IID
Fit statistics						
AIC	-137.65	-127.20	-125.30	-86.499	1,536.2	-120.53
BIC	-78.610	108.97	158.11	568.88	3,608.6	156.97
Observations	2,709	2,709	2,709	2,709	2,709	2,709
Squared Correlation	0.00602	0.02403	0.02910	0.05985	0.18110	0.02667

*Signif. Codes: ***: 0.01, **: 0.05, *: 0.1*

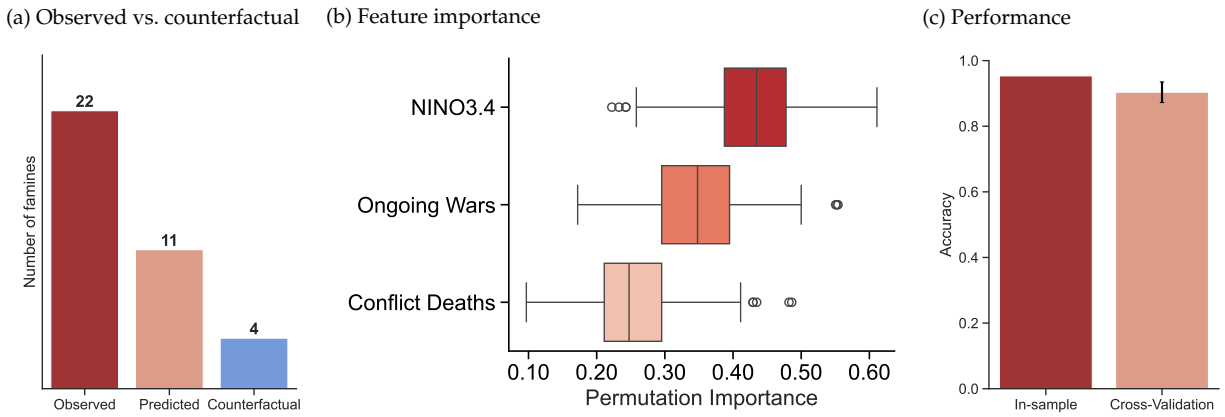

Figure 8: Attribution with NINO3.4, ongoing wars, and conflict deaths.

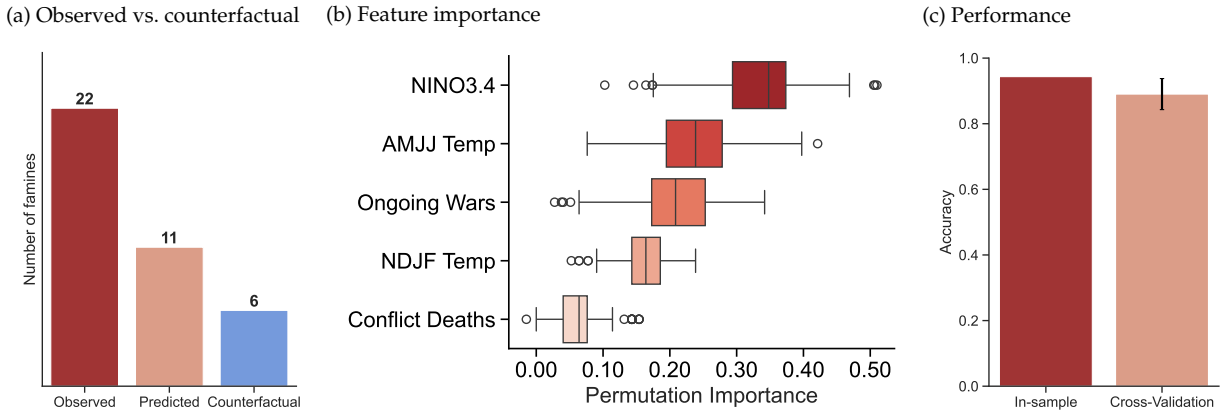

Figure 9: Attribution with NINO3.4, ongoing wars, estimated conflict deaths, NDJF and AMJJ temperatures.

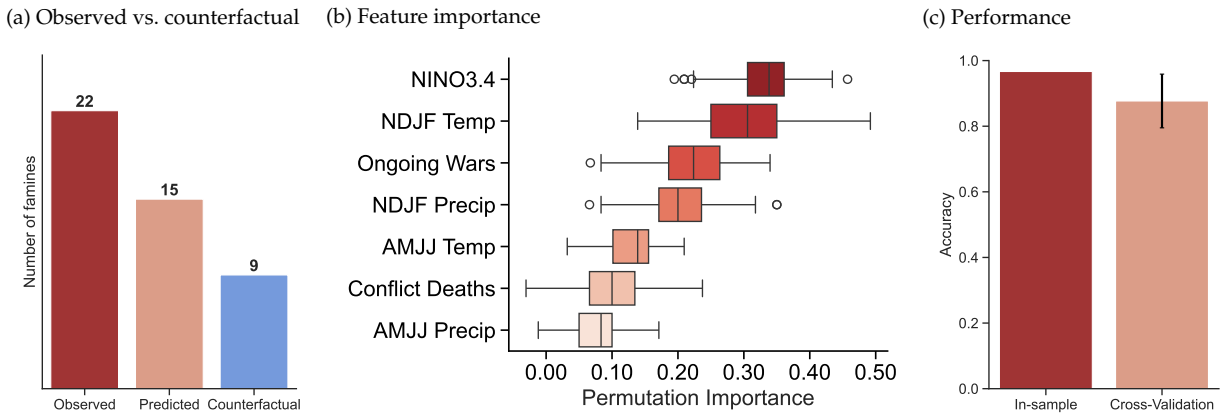

Figure 10: Attribution with NINO3.4, ongoing wars, estimated conflict deaths, NDJF and AMJJ temperatures, NDJF precipitation.

D Assessing ENSO Teleconnections to the Early Modern European Climate

We explore potential teleconnections between the ENSO index (NINO3.4) and our primary climate variables by calculating the grid-wise Pearson correlation between each pixel's time series in the climate reconstructions and the ENSO time series. Our results show that June–August soil moisture, and to a lesser extent, April–July precipitation, are the only variables significantly influenced by ENSO. This finding motivates our use of the self-calibrating Palmer Drought Severity Index (scPDSI) to classify a location's level of ENSO teleconnection.

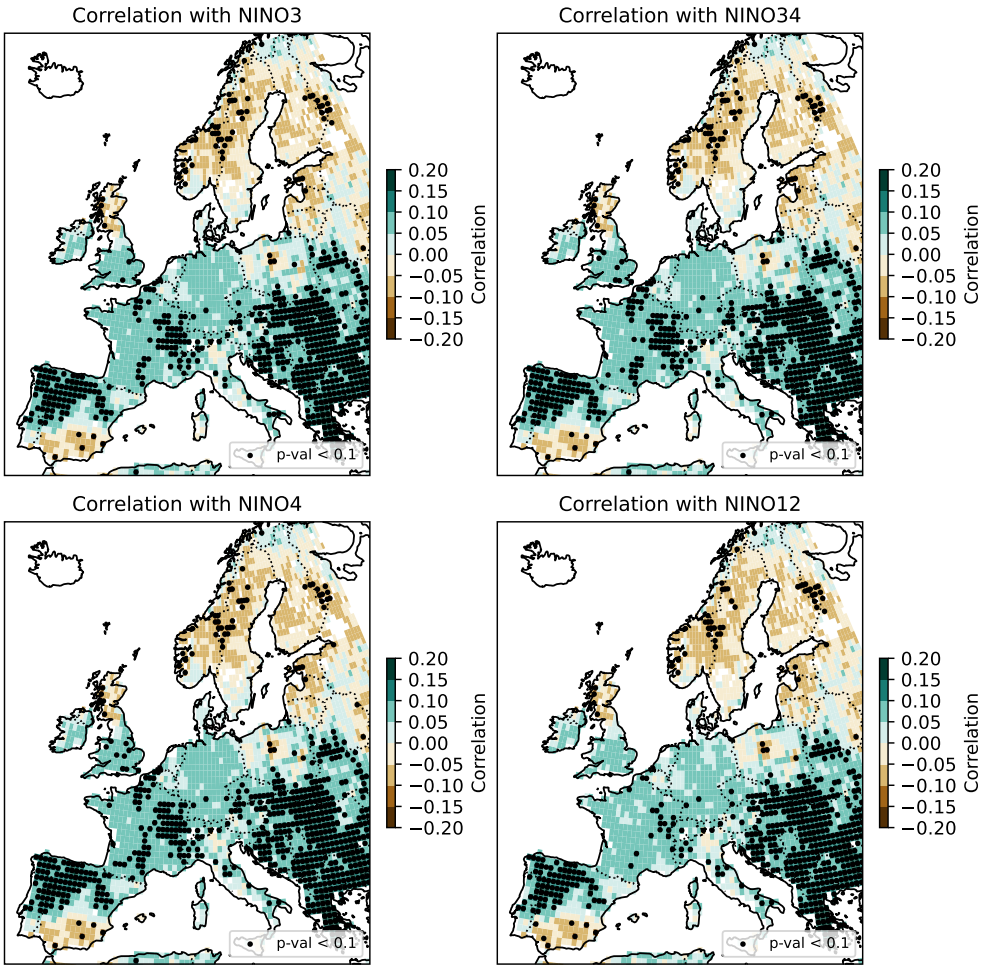

Figure 11: ENSO–scPDSI correlation maps. Dotted cells exhibit significant ($p < 0.1$) correlation to ENSO.

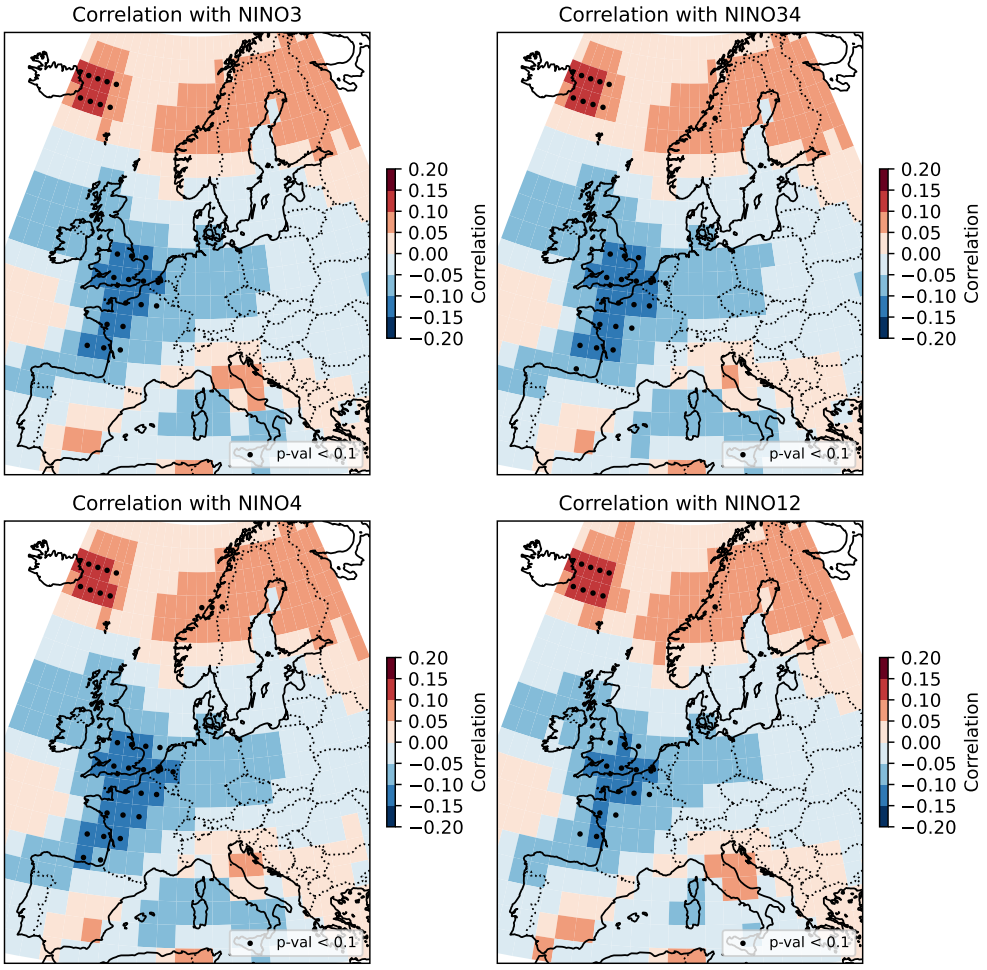

Figure 12: ENSO–AMJJ temperature correlation maps. Dotted cells mark significant ($p < 0.1$) correlations.

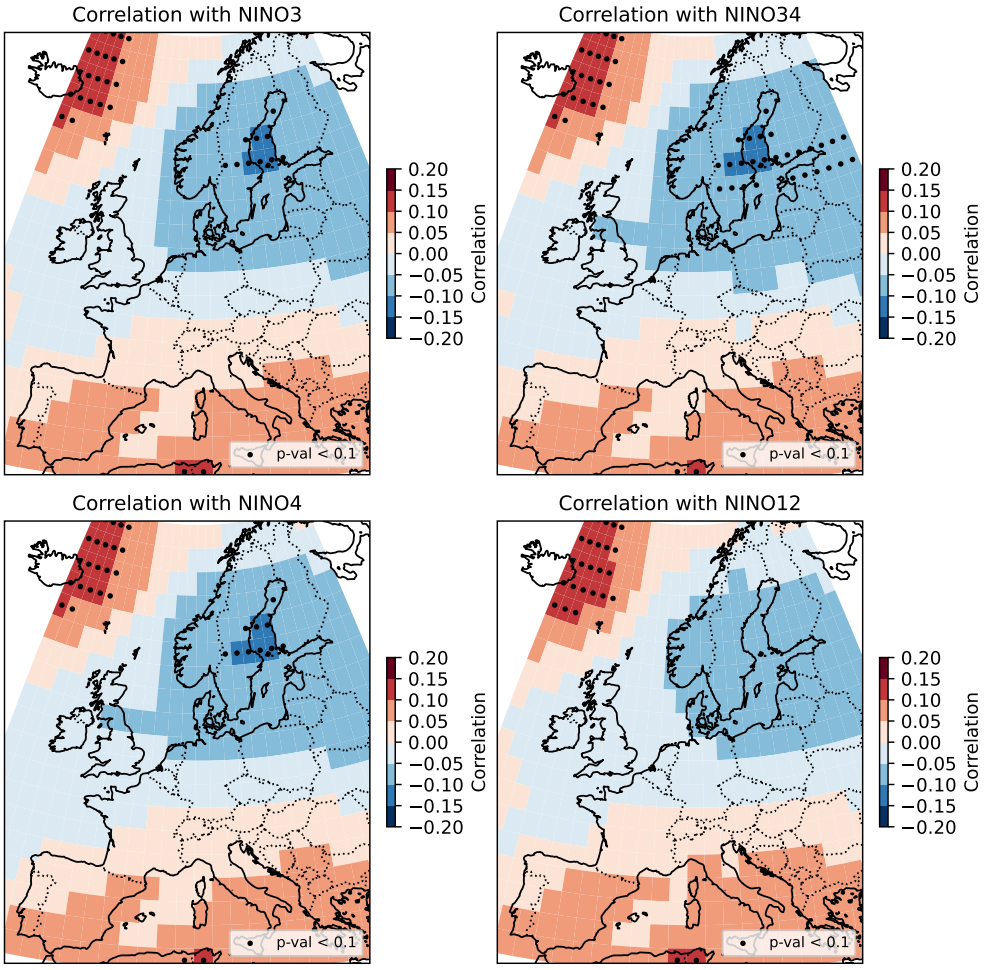

Figure 13: ENSO–NDJF temperature correlation maps. Dotted cells mark significant ($p < 0.1$) correlations.

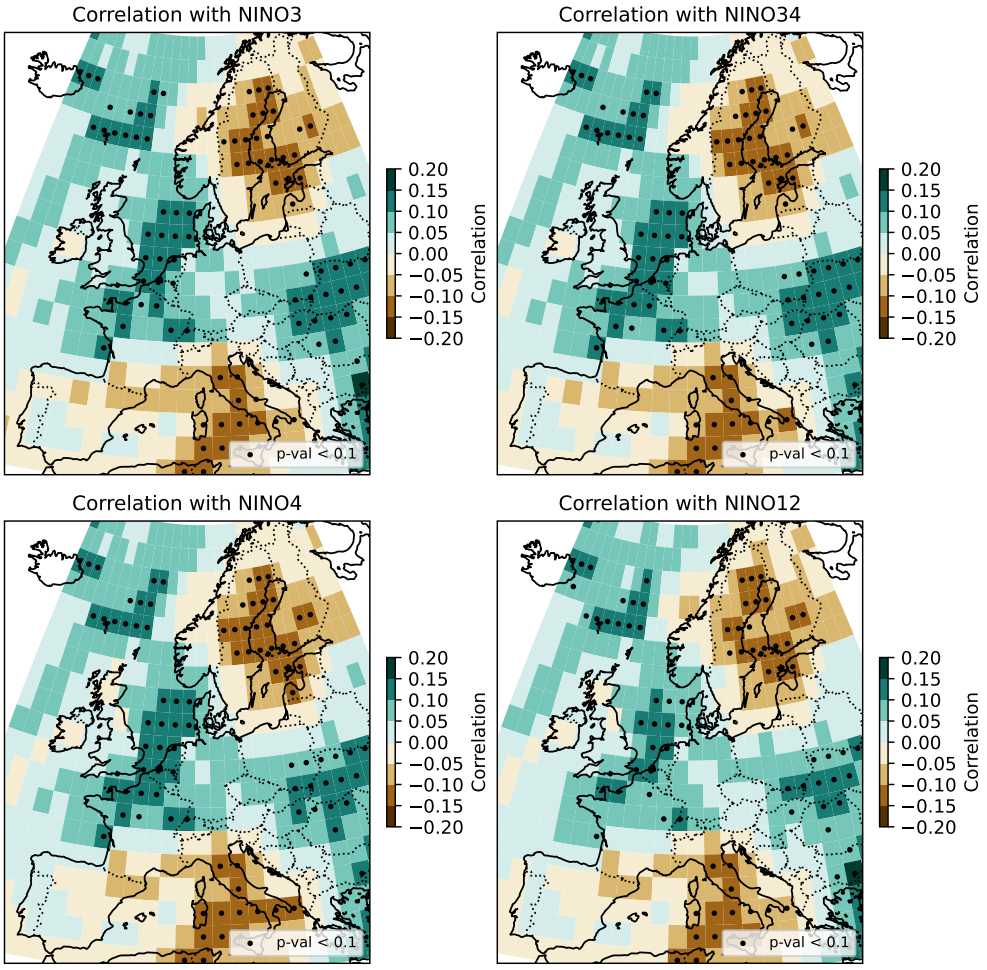

Figure 14: ENSO–AMJJ precipitation correlation maps. Dotted cells mark significant ($p < 0.1$) correlations.

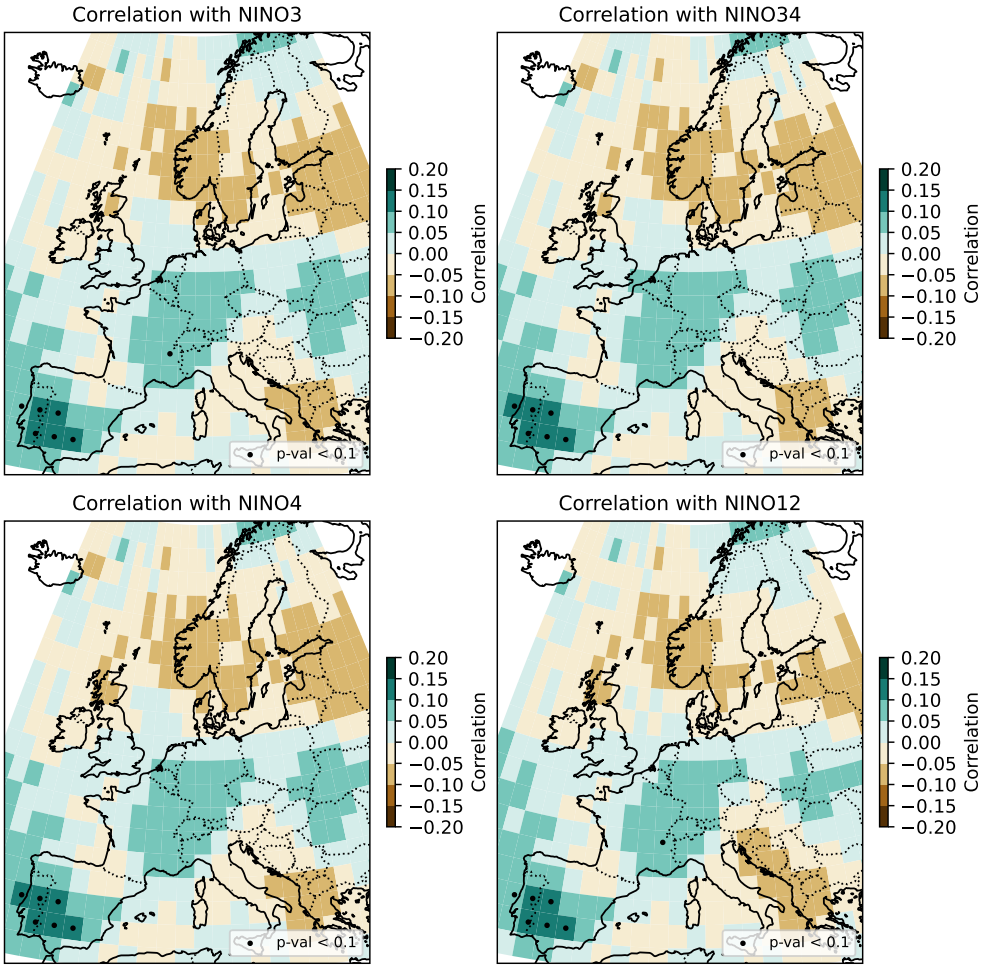

Figure 15: ENSO–NDJF precipitation correlation maps. Dotted cells mark significant ($p < 0.1$) correlations.

E Impact of ENSO on Harvests under Different Teleconnection Partitions

The main section presents the effect of a positive ENSO shock on harvests according to a teleconnection partition that uses soil moisture. Here we show additional results when using April–July and November–February precipitation and November–February temperature to assess ENSO teleconnections [1].

We obtain stronger results to the scPDSI-based partitioning when using AMJJ precipitation data for harvests, albeit with wider standard errors. Despite higher signal-to-noise ratios, we observe substantial effect sizes after one year for November–February temperature impacts on harvests, which we attribute to the memory embedded in grain tithes, which comprise the majority of our harvest records.

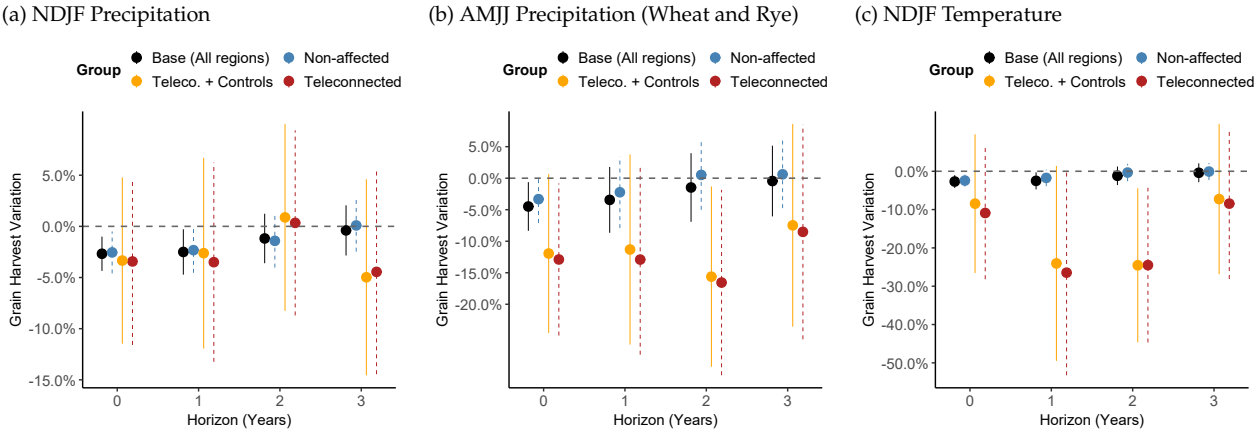

Figure 16: **Impulse responses to ENSO shocks for grain harvests** Each panel shows the impulse responses of a 1 °C ENSO shock on inter-annual variability in grain harvest records, while holding other factors constant. Teleconnection status is granted to locations whose local climate is significantly correlated at the 10% level to ENSO.

[1] No location in our harvest data compilation had teleconnected April–July temperature.

F Regional Heterogeneity in the Survival Analyses

We examine potential regional heterogeneity in the response to ENSO by including interaction terms between the NINO3.4 index and dummy region variables within a time-dependent Cox proportional hazards model. Additionally, we account for regional differences in baseline hazard functions through stratification by region. The results in 18 show an interesting tendency of Ireland to be more vulnerable to La Niña events (cooler NINO3.4 temperatures) than El Niño events.

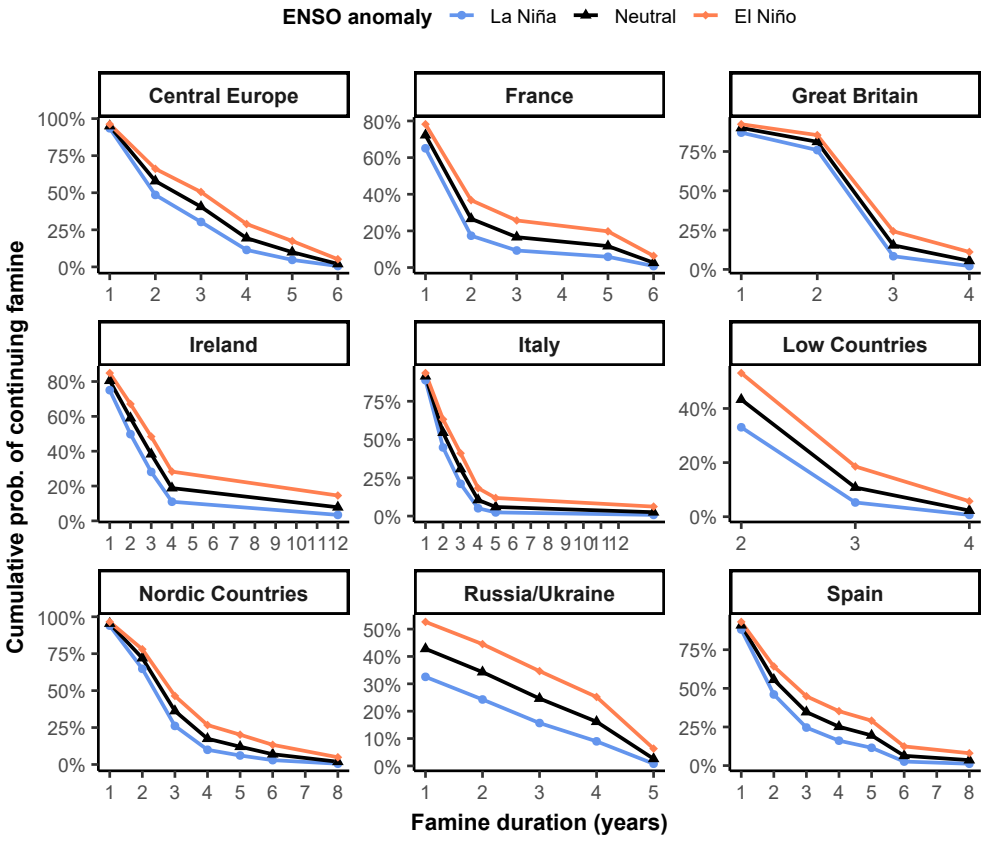

Figure 17: Survival Curves from Cox Regression with Region stratification.

We also report the results of our time-varying Cox Regression from the main section in Table 10.

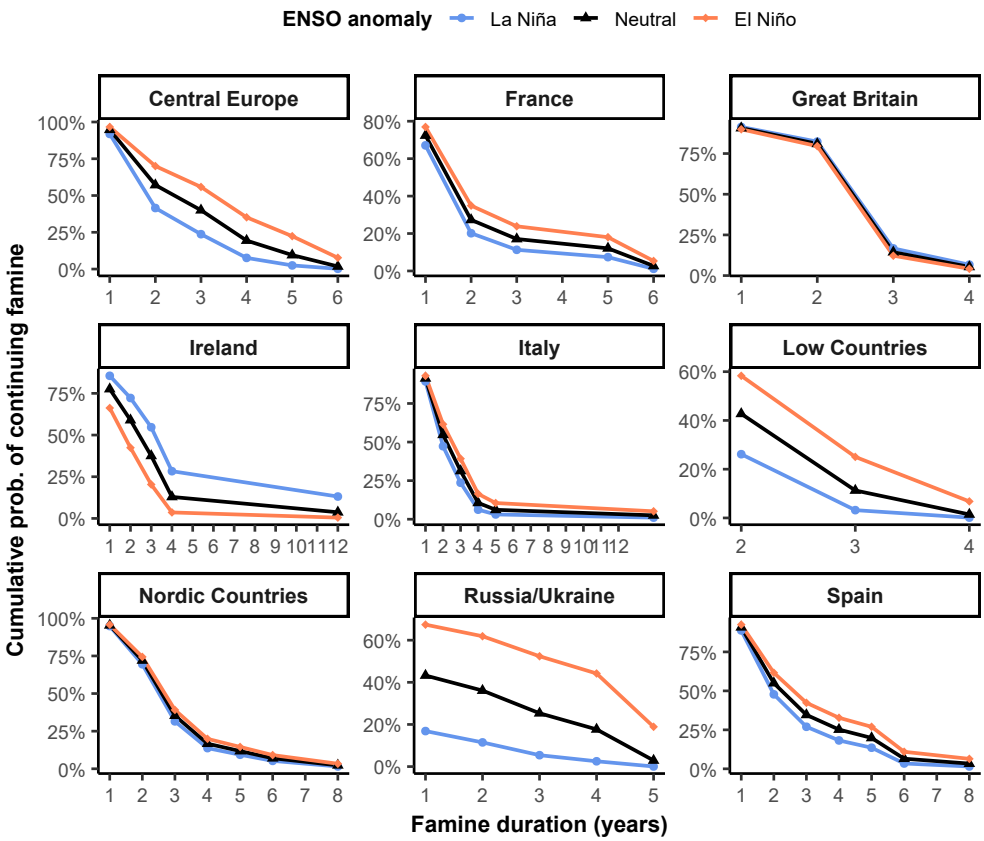

Figure 18: Survival Curves from Cox Regression with Region stratification and Region interaction for the ENSO hazard estimate.

Table 10: Log Hazard Ratio of Nino 3.4 on Famine Duration, Time-varying Cox Model

	(1)	(2)	(3)	(4)	(5)	(6)
nino34	−0.260**	−0.279**	−0.279**	−0.260**	−0.250**	−0.283*
	(0.124)	(0.140)	(0.140)	(0.124)	(0.127)	(0.145)
Clustered SEs	No	No	Yes	No	Yes	No
Strata by Region	No	Yes	Yes	No	No	Yes
Controls	No	No	No	No	Yes	Yes
Random Effects	No	No	No	Yes	No	No
Proportional Hazards p	0.939	0.648	0.648	-	0.795	0.366
Concordance Index	0.558	0.566	0.566	0.558	0.606	0.603
AIC	1288.2	643.1	643.1	1288.2	1289.9	646.1
BIC	1291.3	646.1	646.1	1291.3	1311.3	667.5

* p <0.1, ** p <0.05, *** p <0.01

G Machine Learning Survival Analyses

We demonstrate that ENSO, measured by the NINO3.4 index, possesses predictive power in modeling famine hazard. As outlined in the main text, cross-validation exercises highlight ENSO's explanatory power (see Figure 4). We further show that when models are overfit to the full sample, ENSO consistently emerges as a key predictor (see Figure 19).

We use the following hyper-parameters for the full-sample models:

1. **Random Survival Forest (RSF)**: Number of trees: 200; Maximum depth of each tree: 20
2. **Gradient Boosting Survival Analysis (GBSA)**: Number of boosting iterations: 200; Maximum depth of each tree: 3; Learning rate: 0.1
3. **Elastic-Net Cox (Coxnet)**: Regularization parameter α: 0.1; L1 ratio (Elastic-net mixing): 0.5; Maximum number of iterations: 10,000

The grids used for cross-validation tuning are described in table 11.

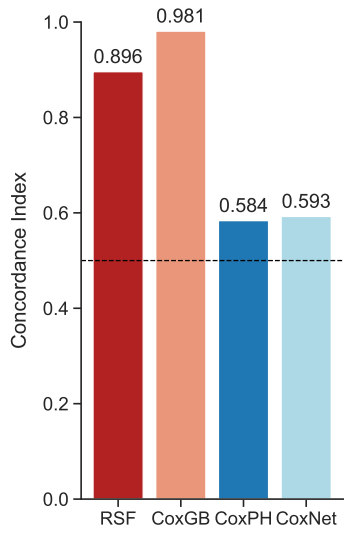

(a) CI (full sample)

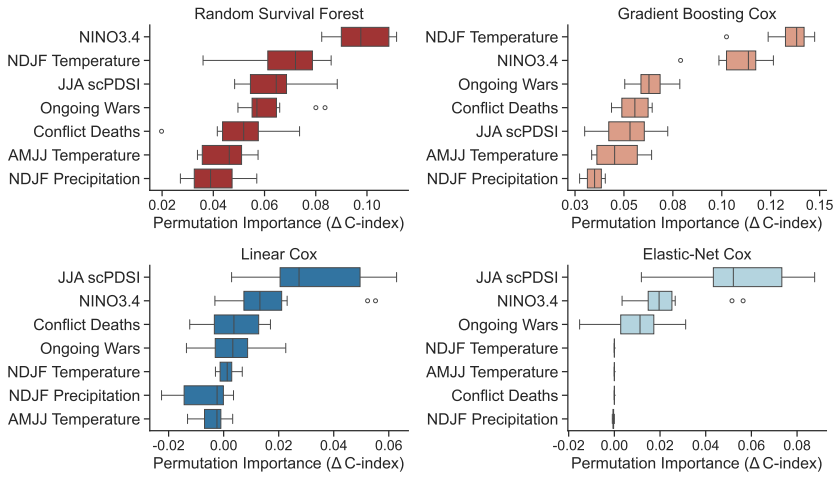

(b) Feature importance (full sample)

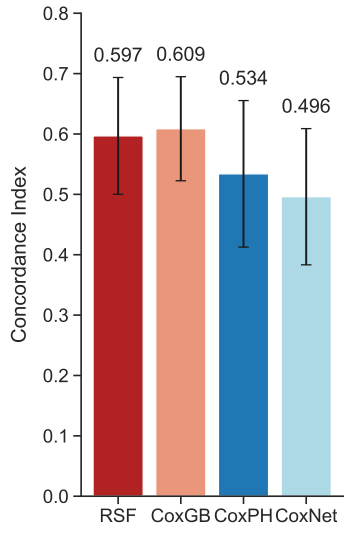

(c) CI (CV)

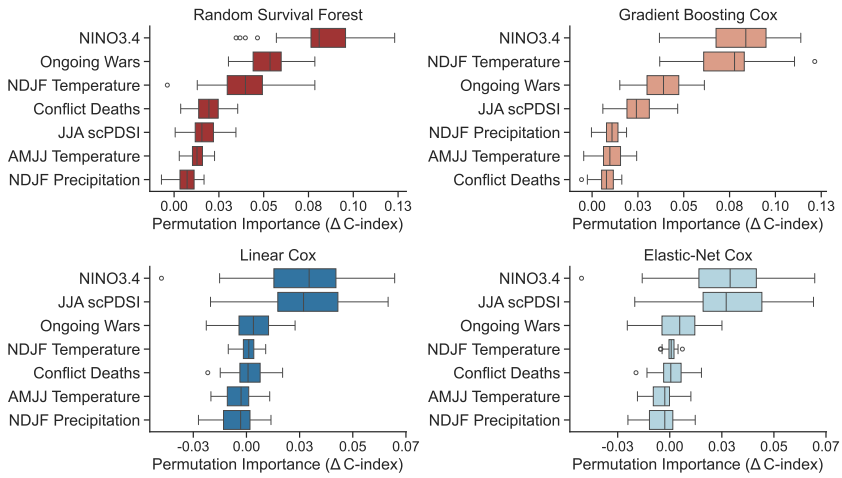

(d) Feature importance (CV)

Figure 19: **Model Performance and Feature Importance in Predicting Famine Duration** Model performance (concordance index, CI) and feature importance on the full sample and test set from each fine-tuned survival models – Random Survival Forest (RSF), Gradient Boosting Cox (CoxGB), standard Cox Proportional Hazards (CoxPH), and Cox regression with elastic net regularization (CoxNet). Panels **(a)** and **(b)** show full-sample results; panels **(c)** and **(d)** report out-of-sample results using nested cross-validation (CV) with error bars based on the 10 outer cross validation folds. Across both setups, the ENSO index consistently emerges as a key predictor of famine duration.

Table 11: Hyperparameter grids used for model tuning via cross-validation.

Model	Hyperparameters
CoxNet (CoxPH with ElasticNet)	`alphas` $\in \{0.001, 0.01, 0.1, 1, 10\}$ `l1_ratio` $\in \{0.01, 0.5, 1.0\}$
Random Survival Forest (RSF)	`n_estimators` $\in \{10, 20, 50\}$ `min_samples_split` $\in \{3, 5, 10\}$ `min_samples_leaf` $\in \{3, 5, 10\}$ `max_features` $\in \{\sqrt{}, 0.5\}$
Gradient Boosting Survival Analysis (GBSA)	`n_estimators` $\in \{10, 20, 50\}$ `learning_rate` $\in \{0.1, 0.5, 0.9\}$ `max_depth` $\in \{1, 3, 5\}$

H Null Effect of ENSO on Fish Catches

We use a compilation of fish catches of North Atlantic cod and herring spanning 1520–1790. The data on fish catches are published in Holm et al. [131] with supporting documentation published by Nicholls et al. [132].

Using a panel local projection with city-species and decade fixed-effects, we report a null effect of ENSO on fish catches for the early modern period in Figure 20, consistent with similar findings for the present day [49]. We use both the NINO3.4 index, and the North Atlantic Oscillation (NAO)[2], known for its connection to ENSO patterns [134] and its influence on marine ecosystems [135].

[2] using the calibrated reconstruction from [133]

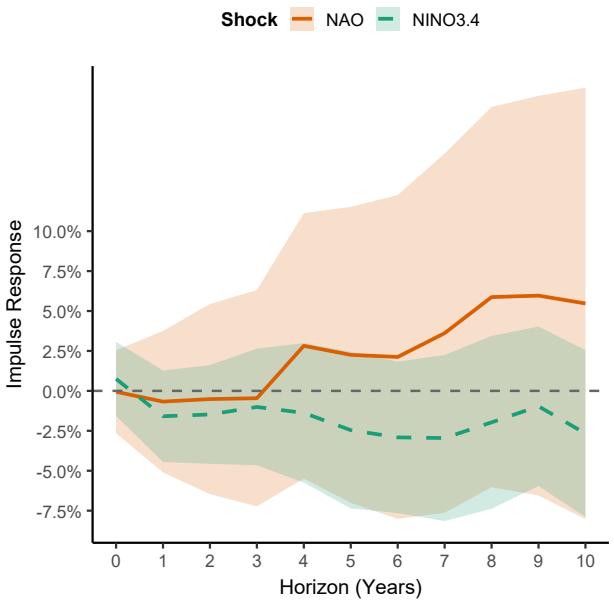

Figure 20: Impulse Responses of a 1 °C NINO3.4 shock and a 1 unit NAO shock on Fish Catches. Shaded area represents the 95% confidence interval from Driscoll-Kraay standard errors.

I Robustness Checks

We conduct an extensive battery of robustness checks for our main analyses, detailed below. Find their summary in Table 12.

I.1 Alternative Model Specifications

We report results under alternative model specification for the famine duration analyses, as well as the impact of the ENSO on prices and harvests.

I.1.1 Parametric Survival Models

We use parametric survival models with 3 distributions that enable use to use Region stratification, Weibull, log-logistic and Gaussian (Tobit model). Across all three choices of parametric modeling, we find that ENSO is significantly associated with longer famine periods.

Table 12: Summary of robustness checks.

Category	**Robustness Checks**
Data quality	Alternative grain price datasets: Federico et al. [46] and Allen [80] (I.2).
	Alternative harvest datasets: Slicher van Bath [41] compilation (I.2).
	Alternative ENSO indices: NINO1+2, NINO3, NINO4 (I.1).
Model specification	Parametric Survival Models I.1.1.
	Distributed-lag FE regressions: famine duration, prices, harvests (I.1).
Sample composition	Leave-one-out: drop each location or famine episode (I.5).
	Time-block exclusion: remove 20-year windows (I.6).
Inference	Alternative standard errors: Conley, two-way clustering (I.7).
Identification of a Causal Effect	Control for decade and location fixed-effects, as well as time and location-varying controls (done throughout Main and Supplementary I).
	Placebo/permutation tests: permute ENSO across and within locations (I.4).
Endogeneity	Granger causality test on time series: prices/yields do not Granger-cause ENSO anomalies (I.8).

Table 13: Parametric Survival Models of Famine Duration

	Dependent variable:		
	Duration		
	Weibull	*Log-logistic*	*Tobit*
	(1)	(2)	(3)
Nino34	0.205* (0.121)	0.231** (0.094)	0.485* (0.270)
Constant	1.126*** (0.042)	0.927*** (0.040)	2.706*** (0.116)
Observations	160	160	
Log Likelihood	−276.507	−267.186	−295.544
χ^2 (df = 1)	2.946*	5.559**	3.156*
Note:			*p<0.1; **p<0.05; ***p<0.01

I.1.2 Distributed Lags Fixed Effects Regressions

As an alternative to estimate the causal effect of the El Niño-Southern Oscillation (ENSO) on famine duration, grain harvests and prices, we employ a fixed-effects regression model with distributed lags. We model our variable of interest as a function of both contemporaneous and lagged values (up to three years) of the ENSO shock.

The estimating equations are given by:

$$\ln(\text{GrainPrice}_{i,t}) = \sum_{l=0}^{3} \beta_l^G \, \text{ENSO}_{t-l} + \alpha_i^G + \gamma^G_{\text{Decade}(t)} + \theta_i^G t + \epsilon^G_{i,t}, \tag{6}$$

$$\ln(\text{FishPrice}_{i,s,t}) = \sum_{l=0}^{3} \beta_l^F \, \text{ENSO}_{t-l} + \alpha_{i,s}^F + \gamma^F_{\text{Decade}(t)} + \theta_i^F t + \epsilon^F_{i,s,t}, \tag{7}$$

$$\ln(\text{GrainHarvest}_{i,g,r,t}) = \sum_{l=0}^{3} \beta_l^Y \, \text{ENSO}_{t-l} + \alpha_{i,g,r}^Y + \gamma^Y_{\text{Decade}(t)} + \theta_i^Y t + \epsilon^Y_{i,g,t}, \tag{8}$$

$$\text{Duration}_{R,t} = \beta^D \, \text{ENSO}_t + \alpha_R^D + \gamma^D_{\text{Decade}(t)} + \epsilon^D_{R,t}. \tag{9}$$

where i indexes locations (cities for prices and estates or districts for harvests), s denotes fish species, g represents grain-type, r harvest record type, and R indexes regions. Each specification includes location-/location-species/location-grain-record or region-specific fixed effects (α), decade fixed effects (γ), and a linear, location-specific time trend (θ). Because ENSO shocks do not vary by location or commodity, the error terms ϵ may exhibit serial and cross-sectional dependence. For inference, we employ Driscoll–Kraay standard errors [75], which are robust to both forms of dependence.

The resulting regression tables below are in agreement with the main section's findings. On the one hand we see a strong effect of a ENSO anomalies, both the average NINO3.4 value during the famine and the maximum value during its first two years, on the duration of famines (Tables 14 and 15). On the other hand we estimate a similar impact of a +1 °C ENSO shock on grain prices (6% with a similar lag of 1 year, see Table 16), fish prices (5% with a lag of 3 years, see Table 17), and grain yields (–5% on the scPDSI-teleconnected harvests), see Table 18).

Table 14: Effect of a 1°C Anomaly in the Average Nino 3.4 Index During a Famine on Its Duration

Dependent Variable:	Duration (years)					
Model:	(1)	(2)	(3)	(4)	(5)	(6)
	OLS	OLS	Poisson	Poisson	Neg. Bin.	Neg. Bin.
Variables						
Nino3.4	0.5060*	0.6102**	0.1862**	0.2252**	0.1862**	0.2252**
	(0.2589)	(0.2421)	(0.0940)	(0.0893)	(0.0942)	(0.0896)
Controls	No	Yes	No	Yes	No	Yes
Region Fixed Effects	Yes	Yes	Yes	Yes	Yes	Yes
Fit statistics						
AIC	638.24	641.77	601.82	605.60	601.82	605.60
BIC	668.99	687.90	632.57	651.72	632.57	651.73
Observations	160	160	160	160	160	160
Squared Correlation	0.07526	0.11193	0.07317	0.11766	0.07317	0.11766

Clustered (Region) standard-errors in parentheses

*Signif. Codes: ***: 0.01, **: 0.05, *: 0.1*

Table 15: Effect of a 1°C Anomaly in the Maximum Nino 3.4 Index During the Initial Two Years of Famine on Its Duration

Dependent Variable:	Duration (years)					
Model:	(1)	(2)	(3)	(4)	(5)	(6)
	OLS	OLS	Poisson	Poisson	Neg. Bin.	Neg. Bin.
Variables						
Max Nino34 (2y)	0.6035**	0.6431**	0.2094***	0.2244***	0.2094***	0.2244***
	(0.2151)	(0.2085)	(0.0806)	(0.0819)	(0.0809)	(0.0821)
Controls	No	Yes	No	Yes	No	Yes
Region Fixed Effects	Yes	Yes	Yes	Yes	Yes	Yes
Fit statistics						
AIC	633.29	636.58	597.18	600.96	597.18	600.96
BIC	664.04	682.71	627.93	647.08	627.93	647.09
Observations	160	160	160	160	160	160
Squared Correlation	0.10344	0.14025	0.09704	0.13973	0.09704	0.13973

Clustered (Region) standard-errors in parentheses

*Signif. Codes: ***: 0.01, **: 0.05, *: 0.1*

Table 16: Effect of a 1°C Anomaly in the Nino 3.4 Index on Grain Prices

Dependent Variable:	Log Grain Price			
Model:	(1)	(2)	(3)	(4)
Variables				
nino3.4 T	0.0147	0.0139	0.0159	0.0149
	(0.0143)	(0.0141)	(0.0145)	(0.0142)
nino3.4 T-1	0.0453***	0.0457***	0.0445***	0.0449***
	(0.0110)	(0.0110)	(0.0109)	(0.0109)
nino3.4 T-2	0.0352***	0.0339***	0.0358***	0.0343***
	(0.0110)	(0.0111)	(0.0109)	(0.0110)
nino3.4 T-3	0.0326***	0.0317***	0.0325***	0.0316***
	(0.0115)	(0.0112)	(0.0113)	(0.0109)
Decade Fixed Effects	Yes	Yes	Yes	Yes
Location Fixed Effects	Yes	Yes	Yes	Yes
Controls	No	Climate	Conflict	Climate+Conflict
Fit statistics				
AIC	5,112.8	5,064.4	5,100.6	5,058.5
BIC	5,995.8	5,983.6	5,998.1	5,992.2
Observations	10,278	10,278	10,278	10,278
R^2	0.72151	0.72309	0.72195	0.72335
Within R^2	0.53492	0.53755	0.53565	0.53800

Driscoll-Kraay (L=4) standard-errors in parentheses

*Signif. Codes: ***: 0.01, **: 0.05, *: 0.1*

Table 17: Effect of a 1°C Anomaly in the Nino 3.4 Index on Fish Prices

Dependent Variable:	Log Fish Price			
Model:	(1)	(2)	(3)	(4)
Variables				
nino3.4 T	-0.0440	-0.0449	-0.0426	-0.0431
	(0.0345)	(0.0338)	(0.0348)	(0.0343)
nino3.4 T-1	0.0176	0.0206	0.0168	0.0199
	(0.0334)	(0.0348)	(0.0348)	(0.0360)
nino3.4 T-2	0.0208	0.0214	0.0216	0.0225
	(0.0282)	(0.0278)	(0.0284)	(0.0279)
nino3.4 T-3	0.0631**	0.0644**	0.0642**	0.0661**
	(0.0282)	(0.0287)	(0.0285)	(0.0293)
Decade Fixed Effects	Yes	Yes	Yes	Yes
Location-Species Fixed Effects	Yes	Yes	Yes	Yes
Controls	No	Climate	Conflict	Climate+Conflict
Fit statistics				
AIC	2,575.1	2,584.7	2,578.2	2,587.7
BIC	2,811.3	2,845.0	2,824.0	2,857.6
Observations	916	916	916	916
R^2	0.87321	0.87327	0.87333	0.87340
Within R^2	0.50194	0.50219	0.50243	0.50271

Driscoll-Kraay (L=4) standard-errors in parentheses

*Signif. Codes: ***: 0.01, **: 0.05, *: 0.1*

Table 18: Effect of a 1°C Anomaly in the Nino 3.4 Index on Wheat and Rye Grain Harvests (Yields and Tithes).

Dependent Variable:	Log Grain Harvest			
Model:	(1)	(2)	(3)	(4)
Variables				
nino3.4 T × scPDSI Teleconnection = 0	-0.0495*	-0.0552**	-0.0503*	-0.0466*
	(0.0278)	(0.0280)	(0.0275)	(0.0265)
nino3.4 T × scPDSI Teleconnection = 1	-0.0447**	-0.0587***	-0.0447**	-0.0392**
	(0.0211)	(0.0219)	(0.0215)	(0.0199)
nino3.4 T-1 × scPDSI Teleconnection = 0	-0.0336	-0.0364	-0.0326	-0.0294
	(0.0251)	(0.0242)	(0.0255)	(0.0270)
nino3.4 T-1 × scPDSI Teleconnection = 1	-0.0150	-0.0200	-0.0139	-0.0084
	(0.0210)	(0.0205)	(0.0218)	(0.0213)
nino3.4 T-2 × scPDSI Teleconnection = 0	-0.0316	-0.0344	-0.0321	-0.0336
	(0.0244)	(0.0239)	(0.0240)	(0.0241)
nino3.4 T-2 × scPDSI Teleconnection = 1	-0.0056	-0.0114	-0.0058	0.0007
	(0.0161)	(0.0169)	(0.0165)	(0.0167)
nino3.4 T-3 × scPDSI Teleconnection = 0	0.0029	-0.0035	0.0037	0.0012
	(0.0293)	(0.0291)	(0.0291)	(0.0288)
nino3.4 T-3 × scPDSI Teleconnection = 1	-0.0509**	-0.0705***	-0.0505**	-0.0479**
	(0.0214)	(0.0214)	(0.0217)	(0.0208)
Decade Fixed Effects	Yes	Yes	Yes	Yes
Record-Location-Grain Fixed Effects	Yes	Yes	Yes	Yes
Controls	None	Climate	Conflict	Climate + Conflict
Fit statistics				
Observations	5,349	5,349	5,349	5,349
R^2	0.95618	0.95637	0.95620	0.96392
Within R^2	0.04596	0.04993	0.04630	0.21439

Driscoll-Kraay (L=4) standard-errors in parentheses

*Signif. Codes: ***: 0.01, **: 0.05, *: 0.1*

I.2 Different Data Sources

Grain Price Data We use alternative grain price datasets, namely Federico et al. [46] and Allen [80], the latter is accessed via the processed version provided by Waldinger [136]. Both grain price compilations have been extensively used in the literature, and both yield extremely close estimates of the ENSO impulse response, in agreement with the one of our main dataset by Ljungqvist and Seim [10].

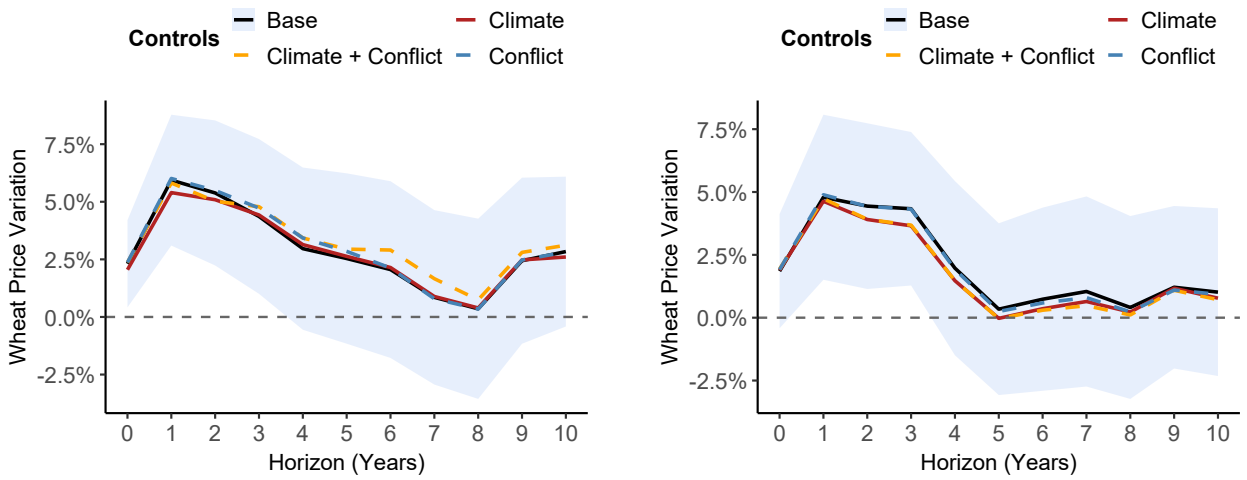

(a) IRF from a 1°C shock in ENSO on grain prices from the Federico et al. [46] dataset.

(b) IRF from a 1°C shock in ENSO on wheat prices from the Allen [80] dataset.

Figure 21: Impulse response functions (IRFs) of a 1°C shock in ENSO on historical grain prices.

Grain Harvest Data As an alternative measure of harvest outcomes, we use grain yield ratio data from Waldinger [136], based on the compilation by Slicher van Bath [41]. Yield ratio is the ratio of harvested grains to grains used for sowing. A higher yield ratio indicates higher per unit agricultural productivity. While yield ratio data are provided for between 1 and 200 years, the panel is unbalanced. For the majority of locations (346 out of 551), yield data are provided for 1 year only. In some cases, where yield ratios are provided for longer time periods, average yield ratios are provided covering between 2 and 50 years. We include only locations with at least 10 independent observations, following Waldinger [136]. The final yield data sample includes 12 cities in four present-day European countries: France, Germany, Poland, and Sweden.

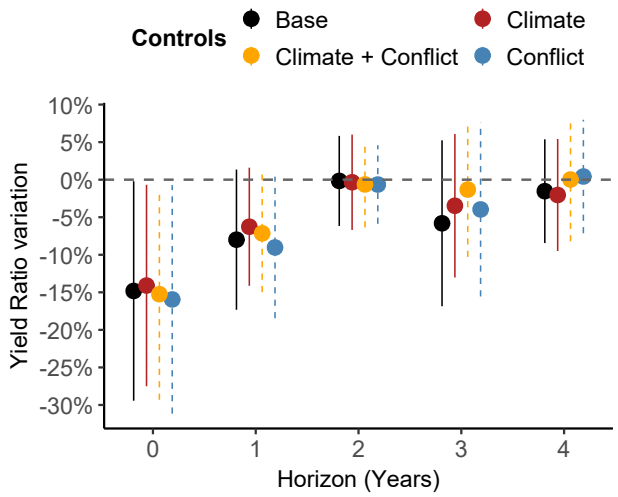

Figure 22: Impulse Response Function of grain yield ratios to a 1 °C anomaly in the NINO3.4 index, using yield ratio data from Slicher van Bath [41].

Our estimate of the immediate impact of an ENSO shock on harvests is now even stronger (–15% against –6.4% in our main harvest dataset), and is robust to different controls (see Figure 22). The stronger response is presumably due to a larger proportion of data from Central Europe in the smaller dataset by Slicher van Bath [41] than in our larger main harvest dataset.

I.3 Choice of ENSO index

We check that the estimated impulse response functions are robust to the choice of ENSO index in Figure 23.

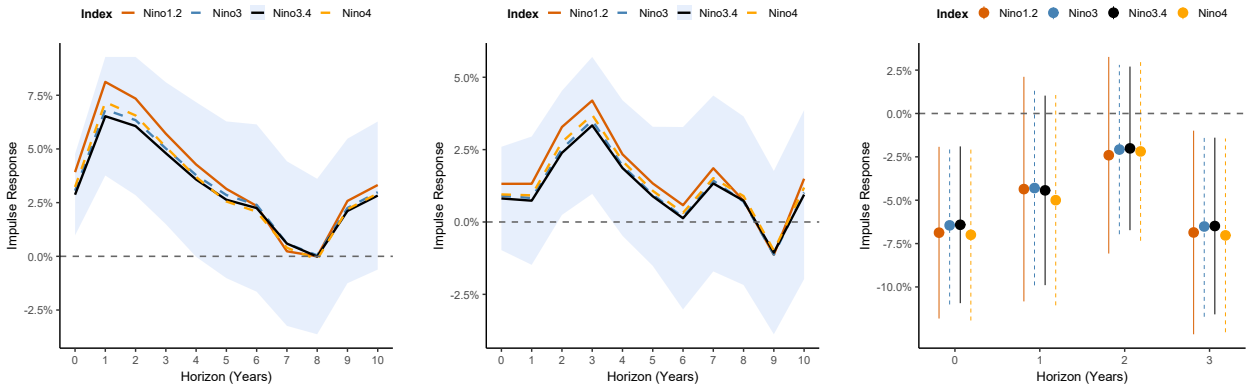

(a) Grain prices (b) Fish prices (c) Grain harvests

Figure 23: Impulse response to a 1°C ENSO shock, across multiple indices.

I.4 Permutation Check

We perform a standard permutation placebo test where we shuffle the NINO3.4 index across all samples and report the (null) estimated response functions across bootstraps, following Young and Hsiang [137] and others. We evaluate the robustness of our results using permutation tests for both the Linear Probability Model of famine onset and the Cox proportional hazards model for famine duration. For each model, we compare the baseline coefficient to the distribution of estimates obtained from $N = 10000$ random shuffles. We also perform analogous checks for price and yield local projections ($N = 500$ IRFs), reporting the baseline impulse response function alongside the 95% confidence interval of the placebo simulations. For the famine onset model, the probability of observing the baseline estimate by chance is below 1%, while for the Cox model it is approximately 1% (Figure 24). For the local projection models, we report that our baseline estimates of interest do not intersect with the 95% confidence interval of the placebo simulations (Figure 25), suggesting that the observed effects are statistically robust and unlikely to be driven by random variation.

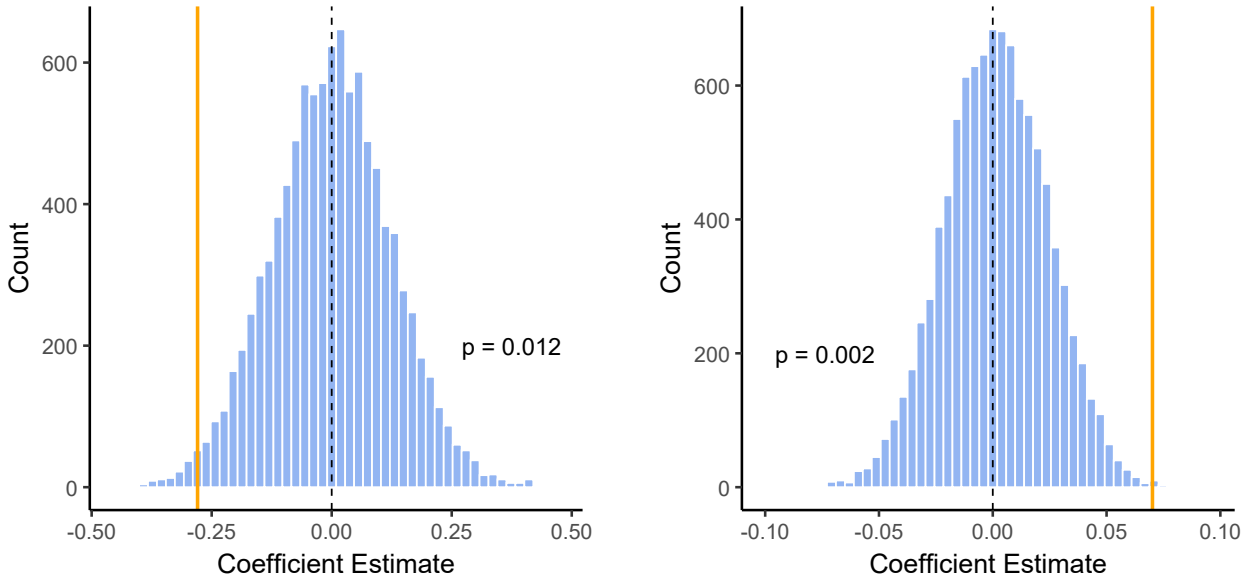

(a) Distribution of estimated log-hazard ratios of NINO3.4 on famine **hazard**, after random shuffling ($N = 10000$ simulations). The vertical line indicates the true estimate. The reported p-value is the probability of obtaining an estimate below the observed one.

(b) Distribution of estimated coefficients of NINO3.4 on famine **onset** in Central Europe after random shuffling ($N = 10000$ simulations). The vertical line indicates the true estimate. The reported p-value is the probability of obtaining an estimate above the observed one.

Figure 24: Permutation tests for the effect of NINO3.4 on famine dynamics. Panel (a) shows the effect on famine **duration** using a Cox proportional hazards model. Panel (b) shows the effect on famine **onset** in Central Europe using a linear probability model with interaction terms by Region.

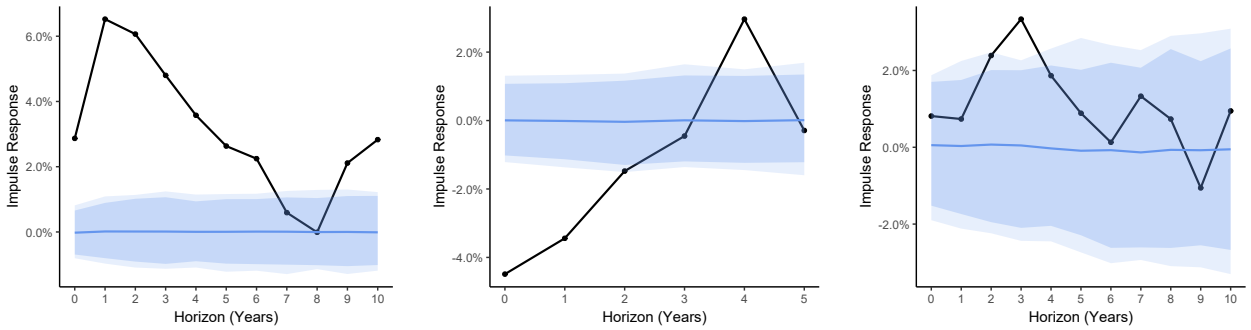

(a) Grain prices (b) Wheat and rye harvests (c) Fish prices

Figure 25: Estimated impulse responses to a 1°C ENSO shock. The black line shows the main specification, with shaded intervals denoting 90% and 95% confidence bands from $N = 500$ placebo shuffle tests.

I.5 Sensitivity of Famine Onset and Survival models to sample composition

To assess the sensitivity of our ENSO–famine estimates to individual events, we conduct a series of leave-one-out robustness checks. For the famine onset model, we re-estimate the linear probability specification after sequentially excluding each famine start in the Central Europe region, the subset that drives identification of the NINO3.4 interaction. The resulting coefficients remain clustered around the baseline estimate, suggesting that no single onset drives our findings.

For famine duration, we repeat the exercise by excluding one famine episode at a time and re-estimating the Cox proportional hazards model. The estimated log-hazard ratios again remain stable across exclusions, with baseline estimates lying well within the distribution of leave-one-out re-estimates. Taken together, these results demonstrate that our onset and duration findings are not driven by any single famine event, but rather reflect systematic ENSO effects across episodes (Fig. 26).

I.6 Sensitivity of Impulse Response Functions (IRFs) to sample composition

We show the panel local projection results are robust to estimating on the whole sample, leaving out one location at a time, in Figures 27, 28, 29. In the case of the yield ratio, we see the impact is even more pronounced when we leave out location identifier 327. Location 327 has the highest number of observations so it is indeed influential in the panel, but other panels show a consistent drop in yield as well, in line with the main result.

We then also show the panel local projection results are robust to estimating on the whole sample, leaving out 20-year blocks, on at a time, in order to detect potentially influential time periods, in Figures 30, 31, 32.

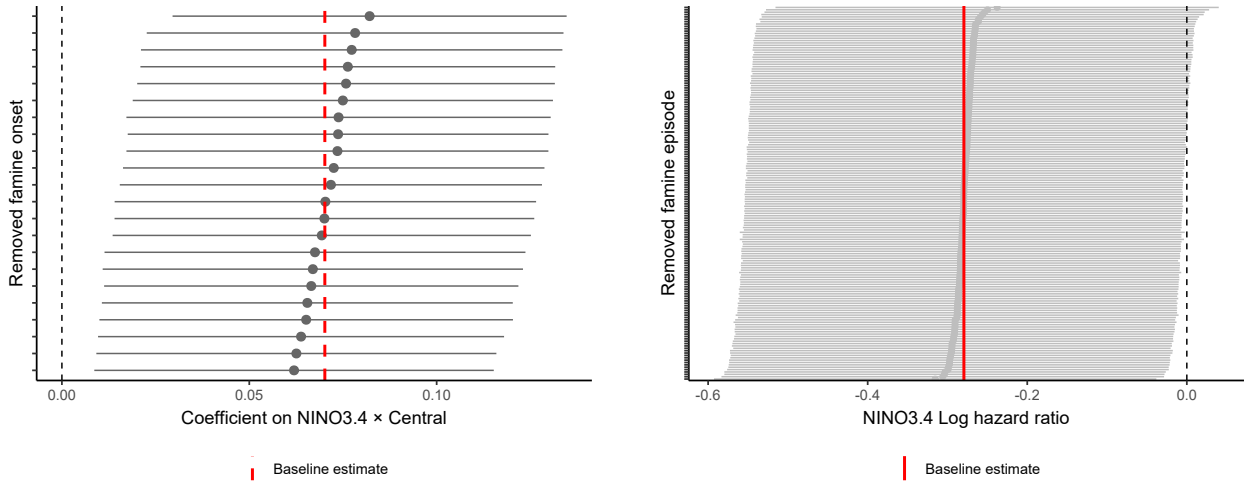

(a) Leave-one-famine-out estimates for famine onset (LPM, Central region).

(b) Leave-one-famine-out estimates for famine duration (Cox PH).

Figure 26: Sensitivity of famine–ENSO estimates to individual events. (a) Linear probability model of famine onset with NINO3.4 × Central Europe interaction. (b) Cox proportional hazards model of famine duration. Red dashed lines denote the baseline estimates; grey point-ranges indicate the coefficient estimates after dropping one famine at a time.

I.7 Robust Standard Errors

We check that our inference is robust to multiple choices of standard errors in the panel setting. We use Driscoll and Kraay [75] as our baseline, then compare with standard errors assuming both spatial and serial correlation (following Conley [138]) and two-way clustered standard errors at the location and year level.

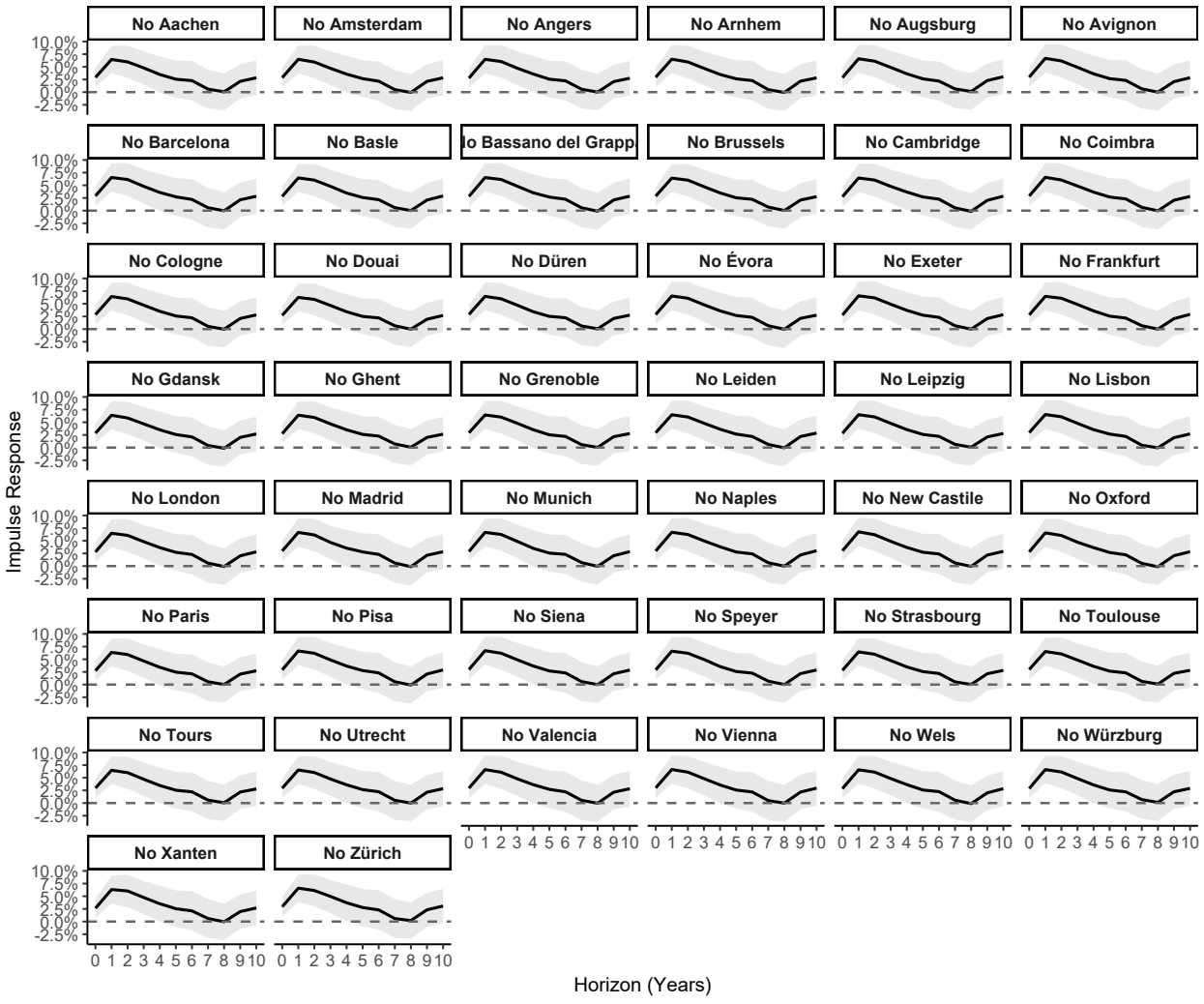

Figure 27: Estimated impulse response functions of grain prices to a 1 °C ENSO shock, removing one location at a time.

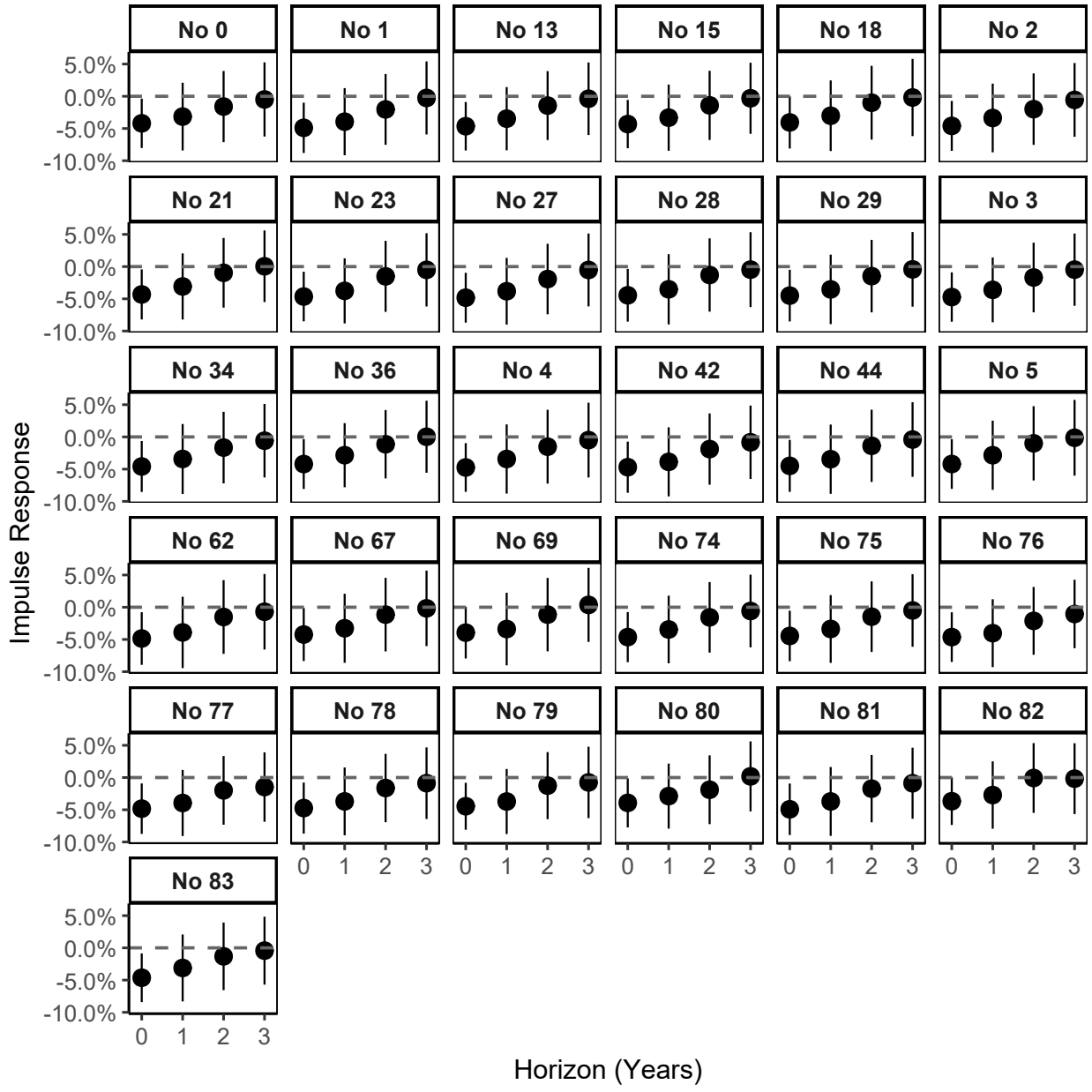

Figure 28: Estimated impulse response functions of grain harvests to a 1 °C ENSO shock, removing one location at a time.

Table 19: Effect of a 1°C Anomaly in the Nino 3.4 Index on Grain Prices under different Standard Errors

Dependent Variable:	Log Grain Price			
Model:	(1)	(2)	(3)	(4)
Variables				
nino 3.4 T	0.0147	0.0147***	0.0147*	0.0147
	(0.0143)	(0.0055)	(0.0083)	(0.0142)
nino 3.4 T-1	0.0453***	0.0453***	0.0453***	0.0453***
	(0.0110)	(0.0064)	(0.0088)	(0.0122)
nino 3.4 T-2	0.0352***	0.0352***	0.0352***	0.0352**
	(0.0110)	(0.0056)	(0.0072)	(0.0131)
nino 3.4 T-3	0.0326***	0.0326***	0.0326***	0.0326**
	(0.0115)	(0.0062)	(0.0088)	(0.0134)
Decade Fixed Effects	Yes	Yes	Yes	Yes
Location Fixed Effects	Yes	Yes	Yes	Yes
Standard Errors	Driscoll Kray (L=4)	Conley (200km)	Conley (500km)	Two-way Clustered
Fit statistics				
AIC	5,112.8	5,112.8	5,112.8	5,112.8
BIC	5,995.8	5,995.8	5,995.8	5,995.8
Observations	10,278	10,278	10,278	10,278
R^2	0.72151	0.72151	0.72151	0.72151
Within R^2	0.53492	0.53492	0.53492	0.53492

*Signif. Codes: ***: 0.01, **: 0.05, *: 0.1*

Notes: Two-way clustered standard errors at the Location and Year level

Table 20: Effect of a 1°C Anomaly in the Nino 3.4 Index on Grain Harvests (Rye and Barley) under different Standard Errors

Dependent Variable:	Log Grain Harvest			
Model:	(1)	(2)	(3)	(4)
Variables				
nino3.4 T × scPDSI Teleco. = 0	-0.0495*	-0.0495***	-0.0495***	-0.0495**
	(0.0278)	(0.0142)	(0.0168)	(0.0202)
nino3.4 T × scPDSI Teleco. = 1	-0.0447**	-0.0447***	-0.0447***	-0.0447***
	(0.0211)	(0.0116)	(0.0093)	(0.0137)
nino3.4 T-1 × scPDSI Teleco. = 0	-0.0336	-0.0336	-0.0336**	-0.0336
	(0.0251)	(0.0207)	(0.0133)	(0.0228)
nino3.4 T-1 × scPDSI Teleco. = 1	-0.0150	-0.0150	-0.0150	-0.0150
	(0.0210)	(0.0267)	(0.0145)	(0.0235)
nino3.4 T-2 × scPDSI Teleco. = 0	-0.0316	-0.0316*	-0.0316*	-0.0316
	(0.0244)	(0.0186)	(0.0172)	(0.0206)
nino3.4 T-2 × scPDSI Teleco. = 1	-0.0056	-0.0056	-0.0056	-0.0056
	(0.0161)	(0.0160)	(0.0090)	(0.0179)
nino3.4 T-3 × scPDSI Teleco. = 0	0.0029	0.0029	0.0029	0.0029
	(0.0293)	(0.0306)	(0.0395)	(0.0283)
nino3.4 T-3 × scPDSI Teleco. = 1	-0.0509**	-0.0509***	-0.0509***	-0.0509***
	(0.0214)	(0.0112)	(0.0043)	(0.0165)
Decade Fixed Effects	Yes	Yes	Yes	Yes
Record-Location-Grain Fixed Effects	Yes	Yes	Yes	Yes
Standard Errors	Driscoll-Kray (L=4)	Conley (200 km)	Conley (500 km)	Two-way Clustered
Fit statistics				
AIC	12,648.4	12,648.4	12,648.4	12,648.4
BIC	13,221.3	13,221.3	13,221.3	13,221.3
Observations	5,349	5,349	5,349	5,349
R^2	0.95618	0.95618	0.95618	0.95618
Within R^2	0.04596	0.04596	0.04596	0.04596

*Signif. Codes: ***: 0.01, **: 0.05, *: 0.1*

Two-way clustered standard errors at the Record-Location-Grain and Year level.

Table 21: Effect of a 1°C Anomaly in the Nino 3.4 Index on Fish Prices under different Standard Errors

Dependent Variable:	Log Fish Price			
Model:	(1)	(2)	(3)	(4)
Variables				
nino3.4 T	-0.0440	-0.0440	-0.0440**	-0.0440
	(0.0345)	(0.0278)	(0.0196)	(0.0327)
nino3.4 T-1	0.0176	0.0176	0.0176	0.0176
	(0.0334)	(0.0180)	(0.0196)	(0.0211)
nino3.4 T-2	0.0208	0.0208***	0.0208***	0.0208
	(0.0282)	(0.0057)	(0.0058)	(0.0143)
nino3.4 T-3	0.0631**	0.0631***	0.0631**	0.0631**
	(0.0282)	(0.0223)	(0.0269)	(0.0263)
Decade Fixed Effects	Yes	Yes	Yes	Yes
Location-Species Fixed Effects	Yes	Yes	Yes	Yes
Standard Errors	Driscoll Kray (L=4)	Conley (200km)	Conley (500km)	Two-way Clustered
Fit statistics				
AIC	2,575.1	2,575.1	2,575.1	2,575.1
BIC	2,811.3	2,811.3	2,811.3	2,811.3
Observations	916	916	916	916
R^2	0.87321	0.87321	0.87321	0.87321
Within R^2	0.50194	0.50194	0.50194	0.50194

*Signif. Codes: ***: 0.01, **: 0.05, *: 0.1*

Two-way clustered standard errors at the Location-Species and Year level.

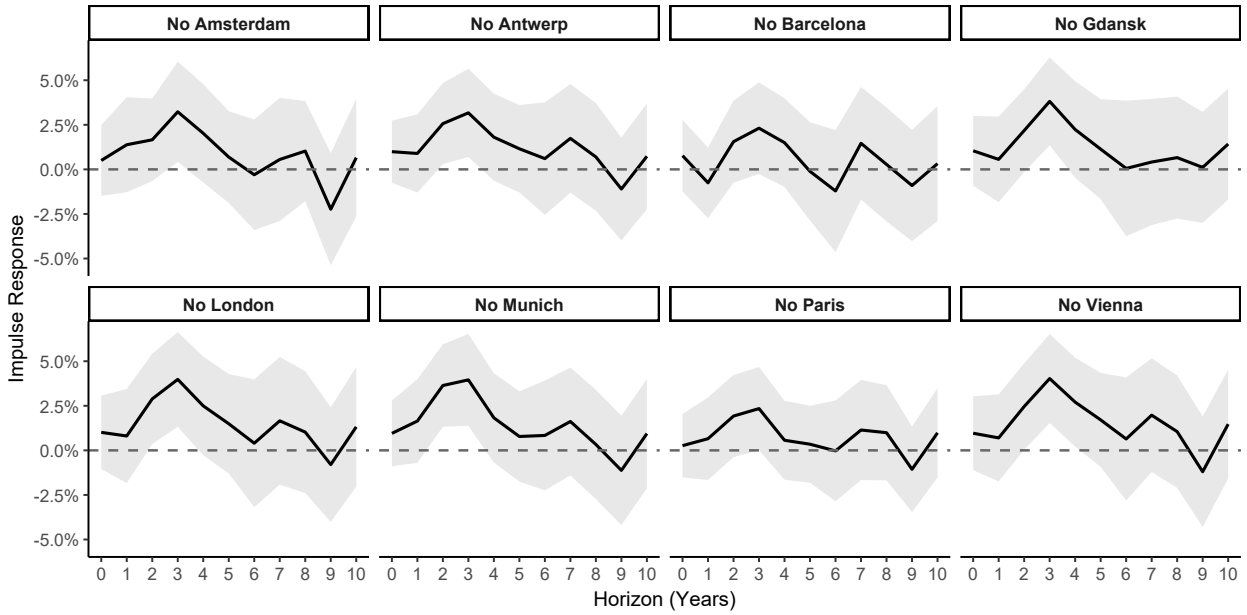

Figure 29: Estimated impulse response Functions of fish prices to a 1 °C ENSO shock, removing one location at a time.

Table 22: Granger causality tests for the relationship between ENSO (NINO3.4), prices and yields.

Variable	Direction	p-value
Grain Price (all cities)	Grain Price → NINO3.4	0.875
Grain Price (all cities)	NINO3.4 → Grain Price	0.001
Harvests (Teleconnected)	Harvest → NINO3.4	0.352
Harvests (Teleconnected)	NINO3.4 → Harvest	0.176
Fish Price (all cities)	Fish Price → NINO3.4	0.945
Fish Price (all cities)	NINO3.4 → Fish Price	0.088

I.8 Reverse Causality

Although it is highly unlikely, we now alleviate potential concerns about reverse causality of our impulse response estimates. We perform a series of Granger causality tests, summarized in Table 22. We use yearly-averaged time-series for all Granger-causality tests. The results show that NINO3.4 is not forecastable by past values of grain prices or harvests, confirming that reverse causality is not driving our findings. We allow for up to 10 lags when forecasting NINO3.4, and restrict to 1 lag when forecasting our outcome variables (harvests and prices). The lack of statistical significance for harvests likely reflects the fact that the impact of NINO3.4 is largely contemporaneous rather than lagged.

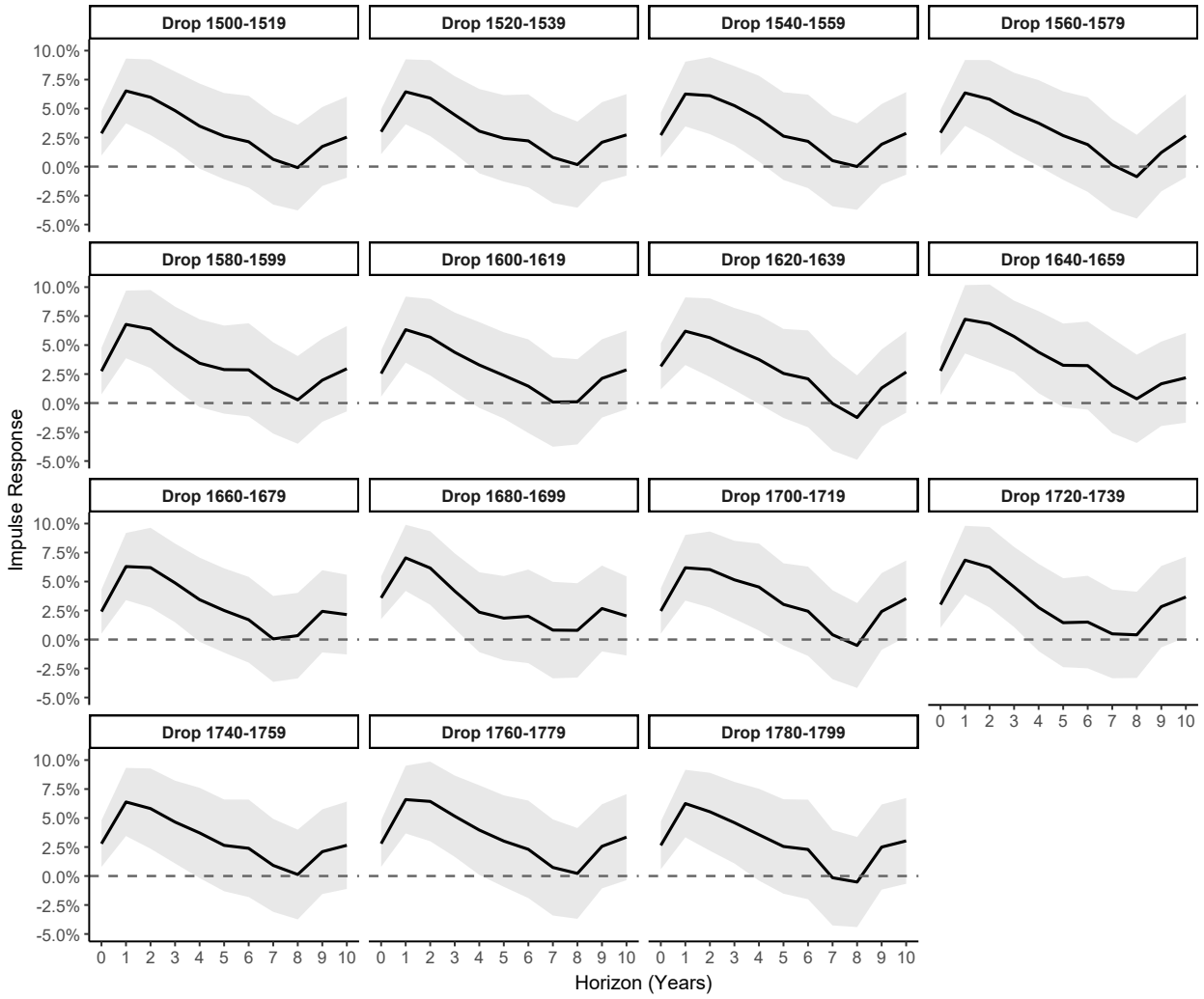

Figure 30: Estimated impulse response functions of grain prices to a 1 °C ENSO shock, removing 20 consecutive years at a time.

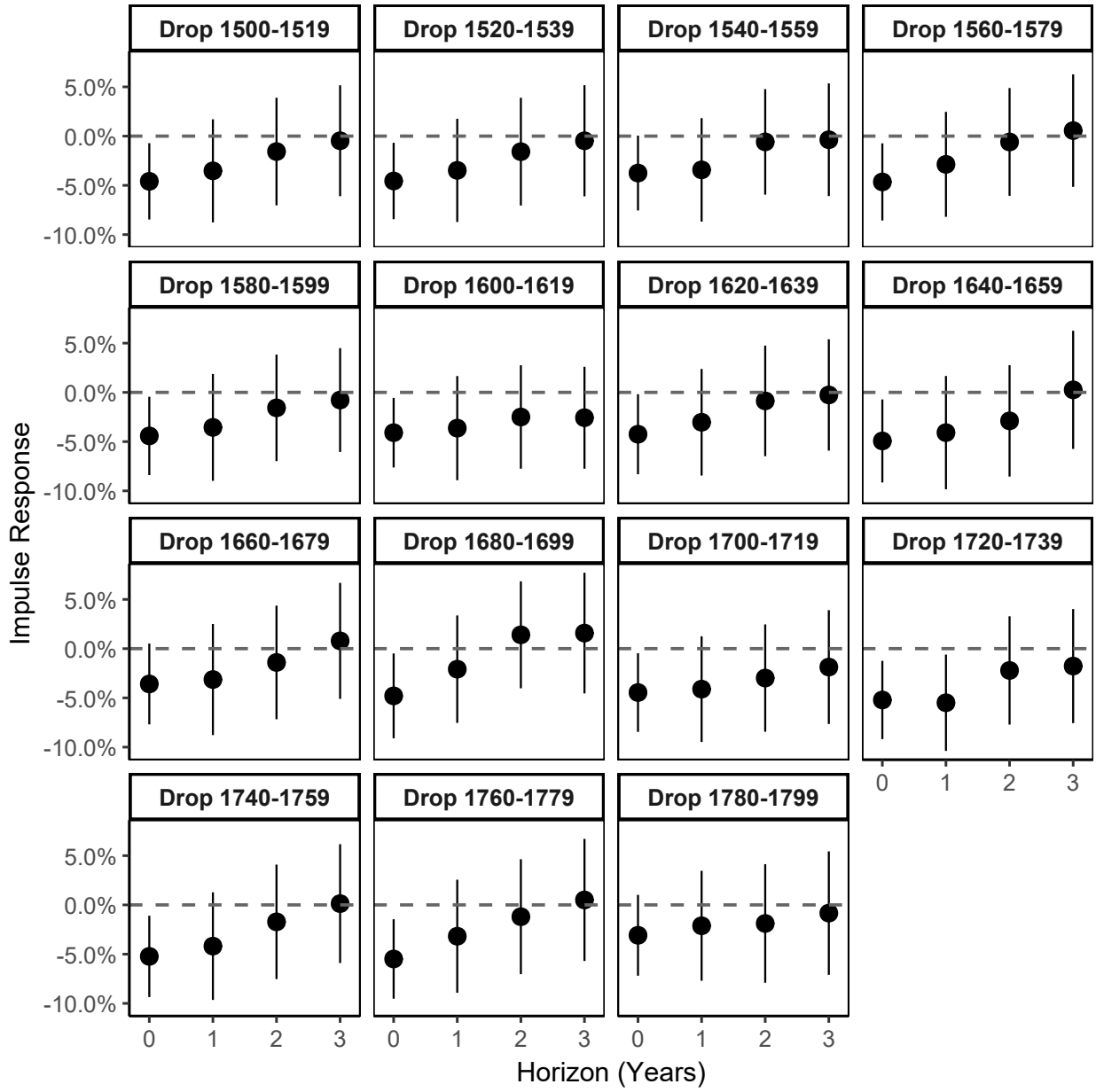

Figure 31: Estimated Impulse Response Functions of grain harvests to a 1 °C ENSO shock, removing 20 consecutive years at a time.

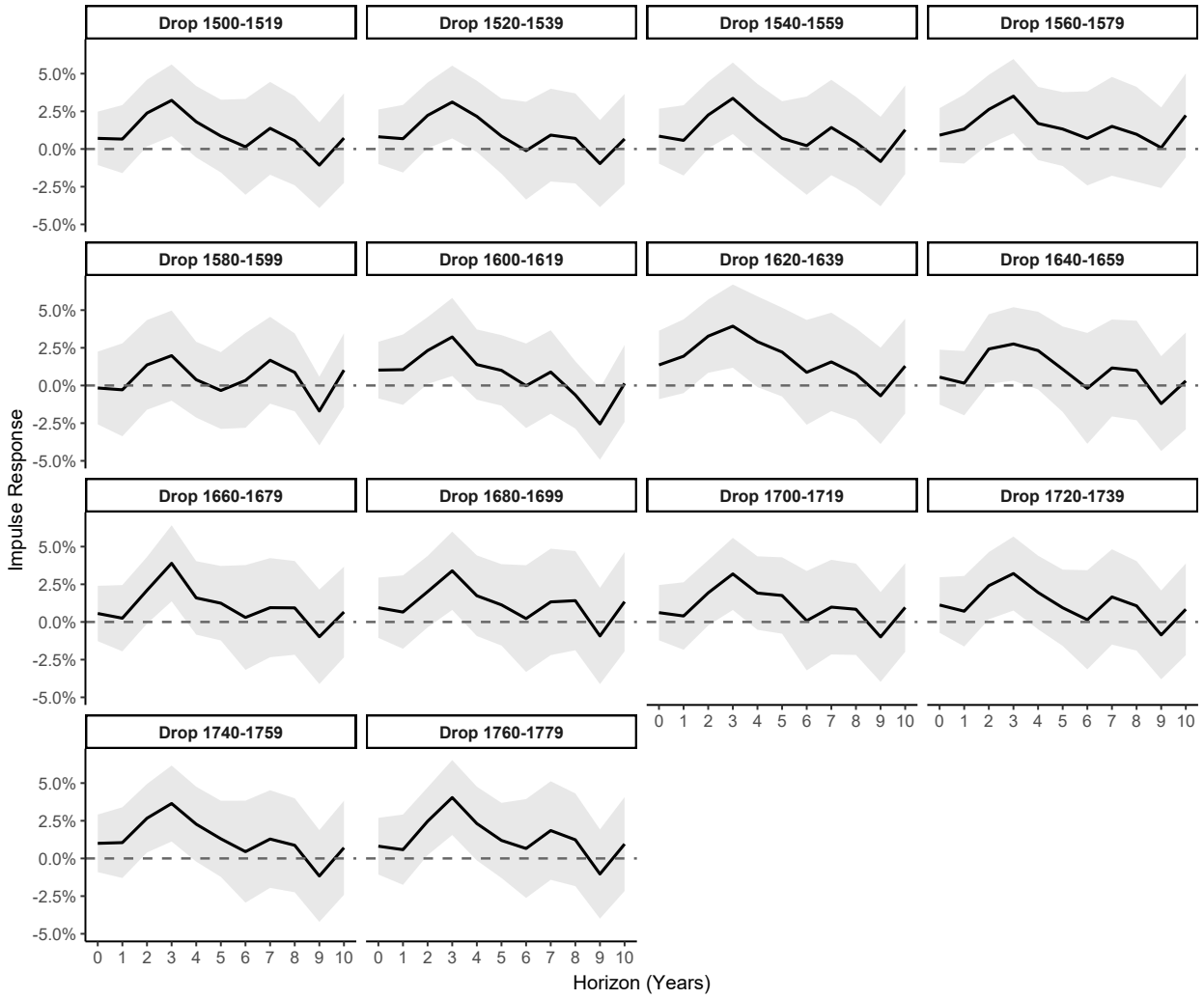

Figure 32: Estimated Impulse Response Functions of fish prices to a 1 °C ENSO shock, removing 20 consecutive years at a time.